Spectral Artifacts in Medical CT and Reduction Strategies

Marc Kachelrieß

German Cancer Research Center (DKFZ)
Heidelberg, Germany
www.dkfz.de/ct

GE Revolution CT

Philips IQon Spectral CT

Siemens Somatom Force

Toshiba Aquilion ONE Vision

What does CT Measure?

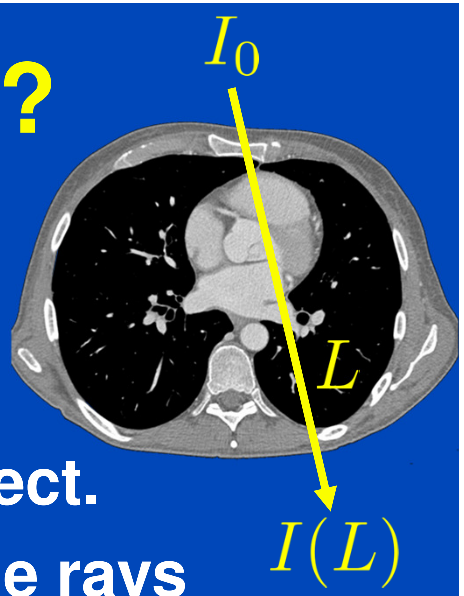

- **X-rays are generated in an x-ray tube.**
- **The polychromatic radiation is attenuated in the patient. X-ray photon attenuation is dominated by the photo and the Compton effect.**
- **Detectors measure the x-ray intensity after the rays have passed through the patient along several lines *L*.**
- **The log intensity is the so-called x-ray transform:**

$$q(L) = -\ln \frac{I(L)}{I_0} = -\ln \int dE\, w(E) e^{-\int dL \mu(\boldsymbol{r}, E)} + S$$

- **Often, the follwing monochromatic approximation is used:**

$$q(L) \approx p(L) = \int dL \mu(\boldsymbol{r}, E_{\text{eff}})$$

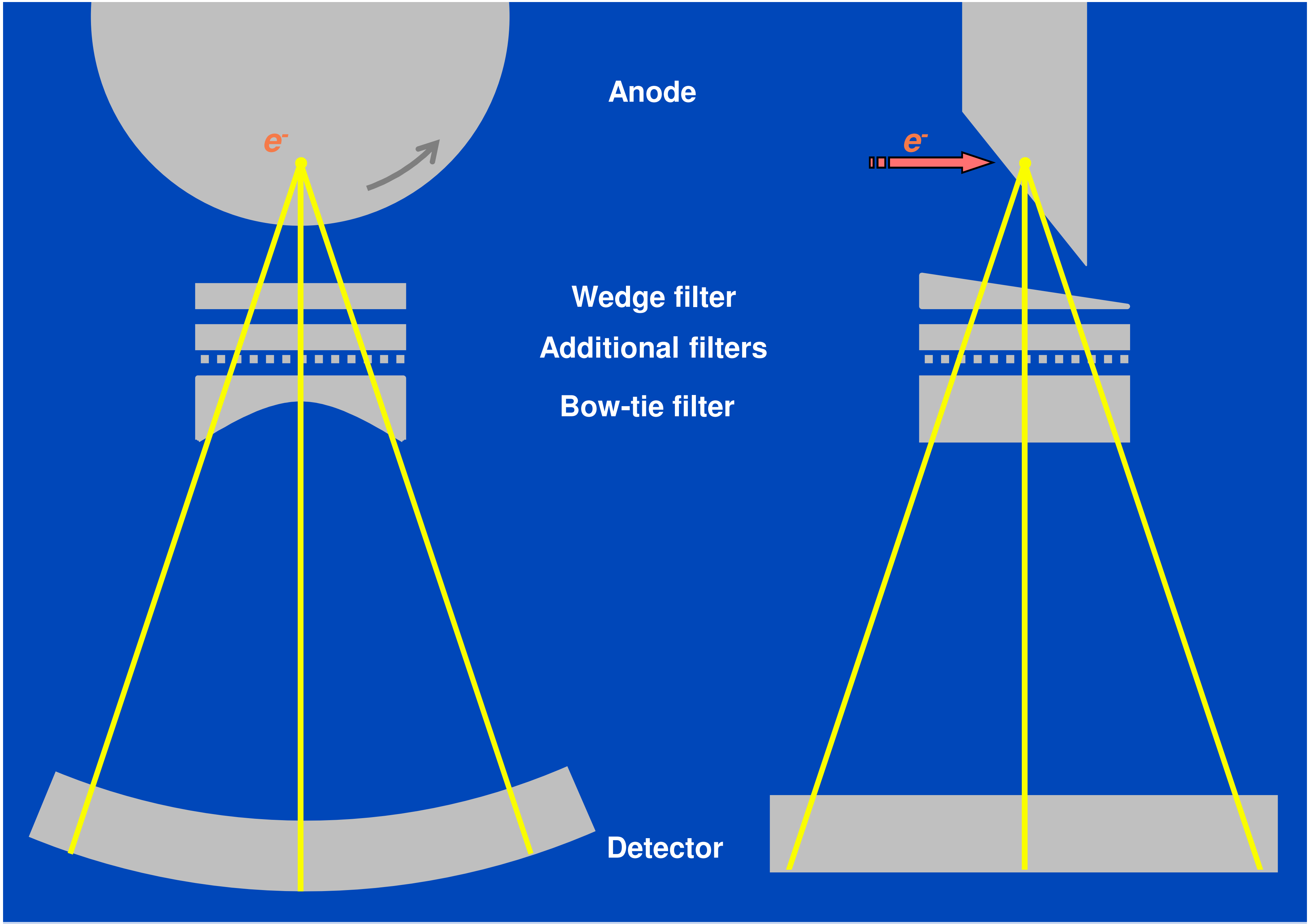

Figure not drawn to scale. Order of prefiltration may differ from scanner to scanner.

dkfz.

Basic Parameters
(best-of values typical for modern scanners)

- In-plane resolution: 0.4 … 0.7 mm
- Nominal slice thickness: S = 0.5 … 1.5 mm
- Effective slice thickness: S_{eff} = 0.5 … 10 mm
- Tube (max. values): 120 kW, 150 kV, 1300 mA
- Effective tube current: mAs_{eff} = 10 mAs … 1000 mAs
- Rotation time: T_{rot} = 0.25 … 0.5 s
- Simultaneously acquired slices: M = 16 … 320
- Table increment per rotation: d = 1 … 183 mm
- Pitch value: p = 0.1 … 1.5 (up to 3.2 for DSCT)
- Scan speed: up to 73 cm/s
- Temporal resolution: 50 … 250 ms

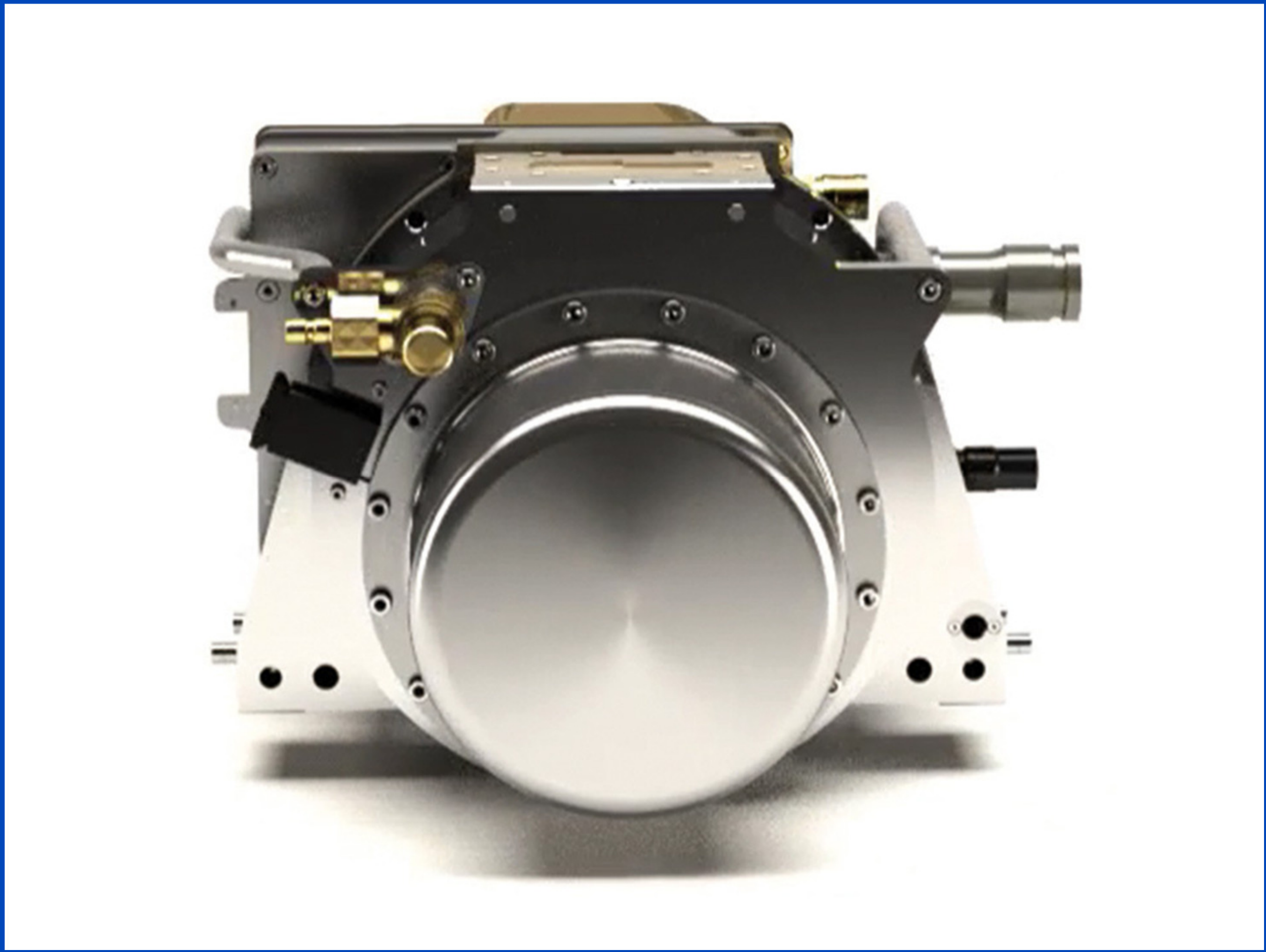

A directly cooled tube: The Siemens Vectron tube (Photo courtesy by Siemens)

Detector Technology

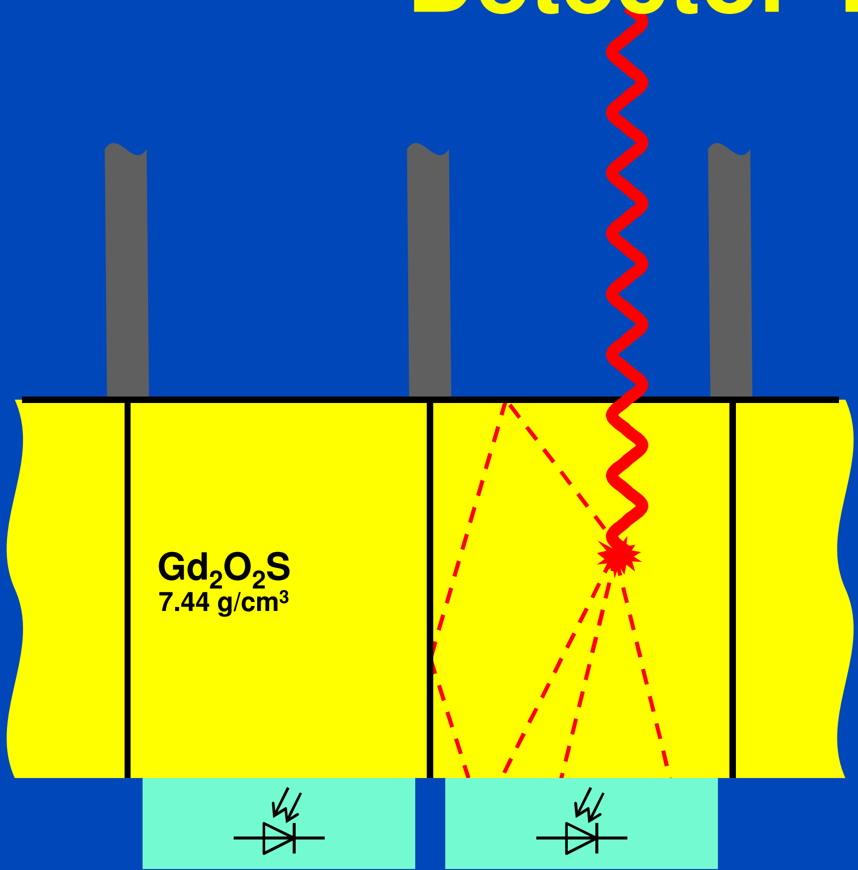

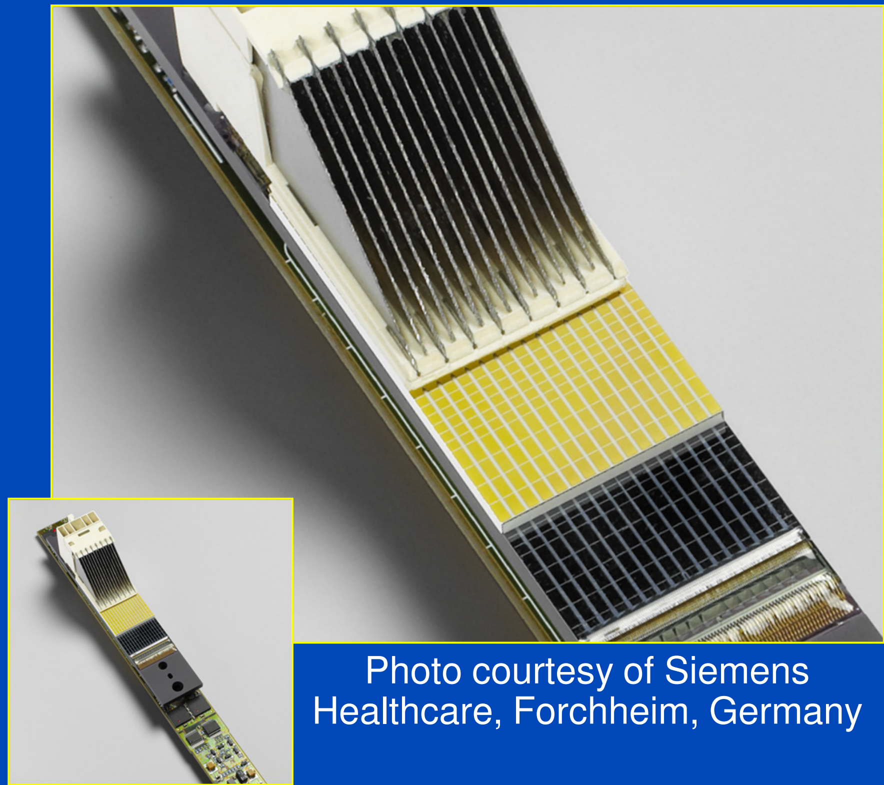

Photo courtesy of Siemens Healthcare, Forchheim, Germany

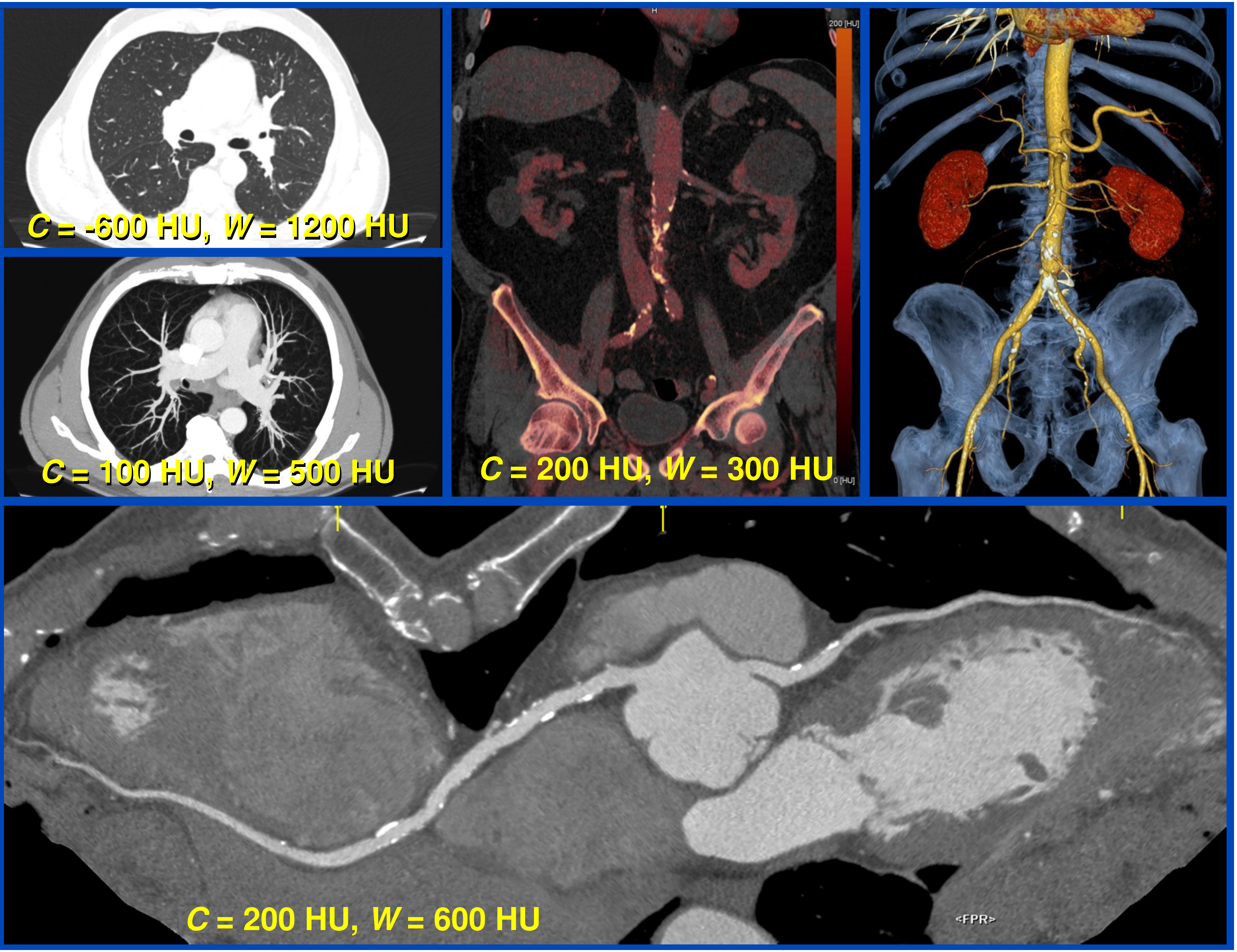

Image courtesy of University of Heidelberg and of University of Erlangen

Images of a 32 cm Water Phantom

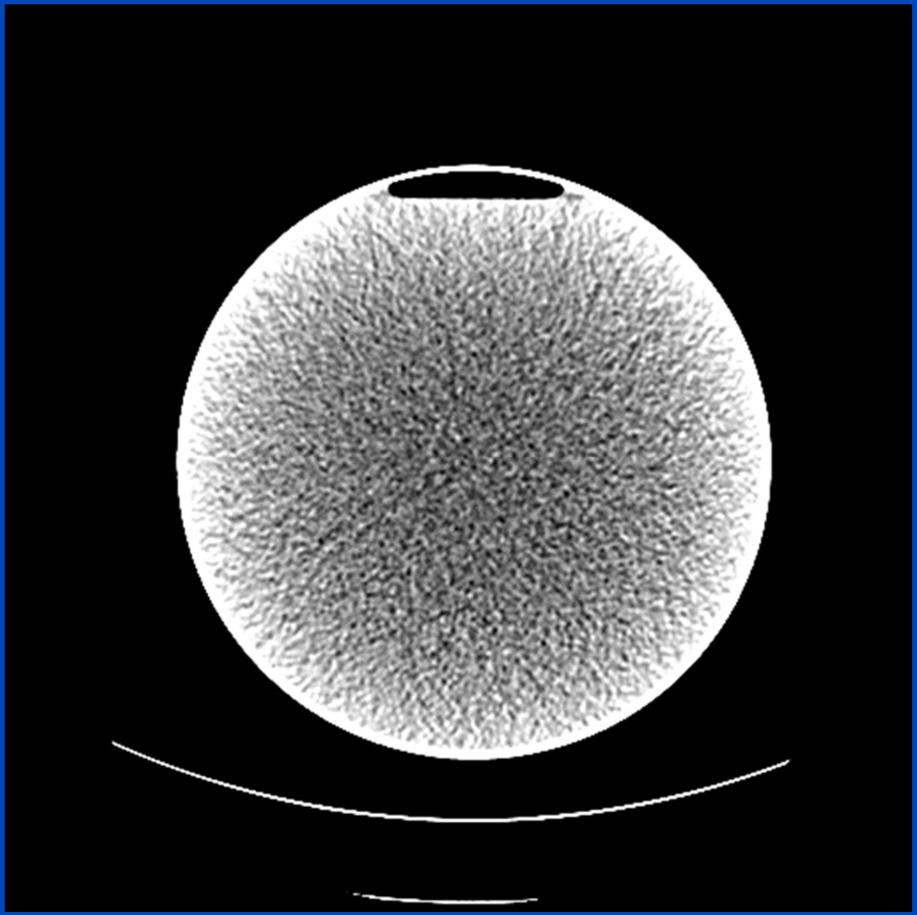

No water precorrection
(only accessible in service mode)

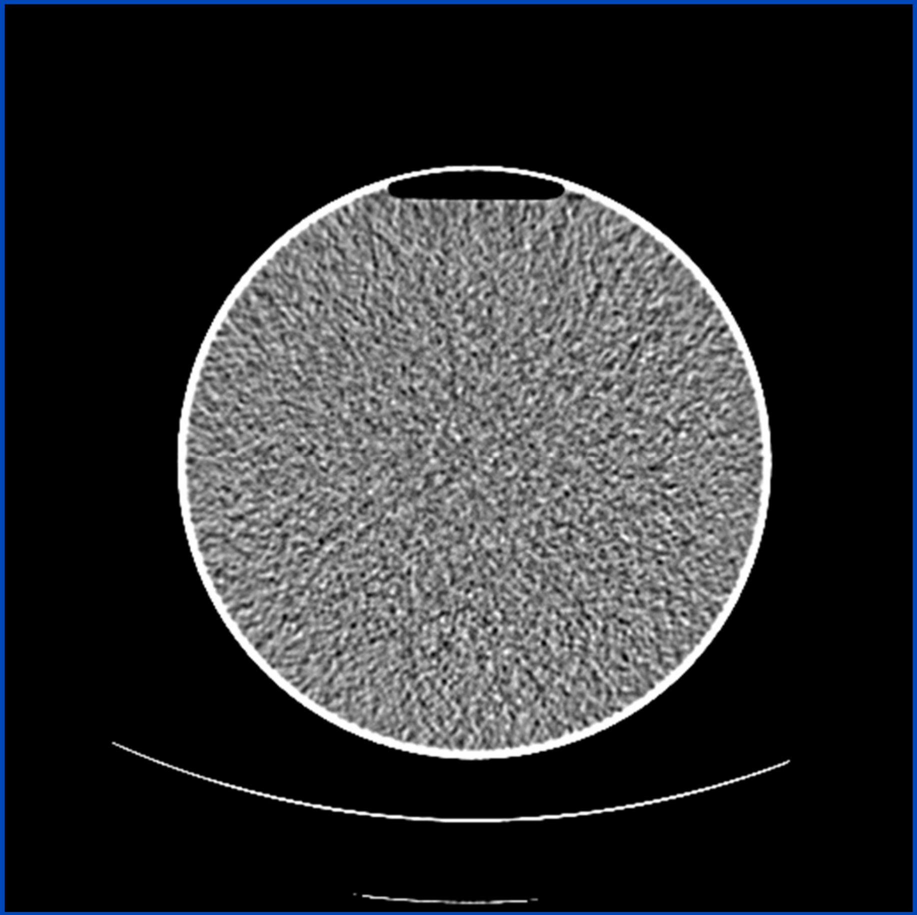

With water precorrection
(air = -1000 HU, water = 0 HU)

dkfz.

First Order Beam Hardening Correction

(Cupping Correction, Water Precorrection)

- Assumes the object to consist of only one energy dependency (one material)
- Often requires to know the spectral properties of all components involved
  - X-ray spectra
  - Pre patient filters
  - Attenuation properties of the assumed single material or shape and position of a calibration object
  - Absorption properties of detector

Empirical cupping correction: A first-order raw data precorrection for cone-beam computed tomography

Marc Kachelrieß,[a)] Katia Sourbelle, and Willi A. Kalender
Institute of Medical Physics, University of Erlangen-Nürnberg, Henkestraße 91, D-91052 Erlangen Germany

(Received 5 December 2005; revised 13 February 2006; accepted for publication 21 February 2006; published 19 April 2006)

We propose an empirical cupping correction (ECC) algorithm to correct for CT cupping artifacts that are induced by nonlinearities in the projection data. The method is raw data based, empirical, and requires neither knowledge of the x-ray spectrum nor of the attenuation coefficients. It aims at linearizing the attenuation data using a precorrection function of polynomial form. The coefficients of the polynomial are determined once using a calibration scan of a homogeneous phantom. Computing the coefficients is done in image domain by fitting a series of basis images to a template image. The template image is obtained directly from the uncorrected phantom image and no assumptions on the phantom size or of its positioning are made. Raw data are precorrected by passing them through the once-determined polynomial. As an example we demonstrate how ECC can be used to perform water precorrection for an *in vivo* micro-CT scanner (TomoScope 30 s, VAMP GmbH, Erlangen, Germany). For this particular case, practical considerations regarding the definition of the template image are given. ECC strives to remove the cupping artifacts and to obtain well-calibrated CT values. Although ECC is a first-order correction and cannot compete with iterative higher-order beam hardening or scatter correction algorithms, our *in vivo* mouse images show a significant reduction of bone-induced artifacts as well. A combination of ECC with analytical techniques yielding a hybrid cupping correction method is possible and allows for channel-dependent correction functions.
[DOI: 10.1118/1.2188076]

Key words: flat-panel detector CT, C-arm CT, micro-CT, artifacts, image quality

I. INTRODUCTION

Due to beam polychromacity in CT, the energy dependence of the attenuation coefficients, and scatter, the log-

know the calibration phantom shape, size, and position. Therefore, it has significant advantages over the other existing approaches that actually rely on this information.

ECC aims at linearizing the measurement using an opti-

M. Kachelrieß, K. Sourbelle, and W.A. Kalender, "Empirical cupping correction: A first-order raw data precorrection for cone-beam computed tomography," Med. Phys. 33(5):1269-1274, May 2006.

Motivation

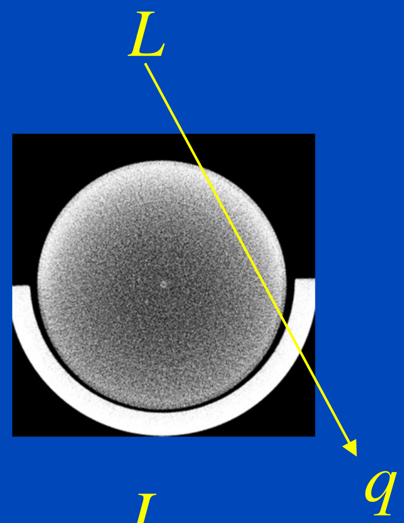

- **Measured projection value q**
  - **Detected spectrum w(L, E)**

$$q(L) = -\ln \int dE\, w(L,E)\, e^{-\int dL\, \mu(\boldsymbol{r}, E)}$$

  - **Scatter**
  - **Normalization**

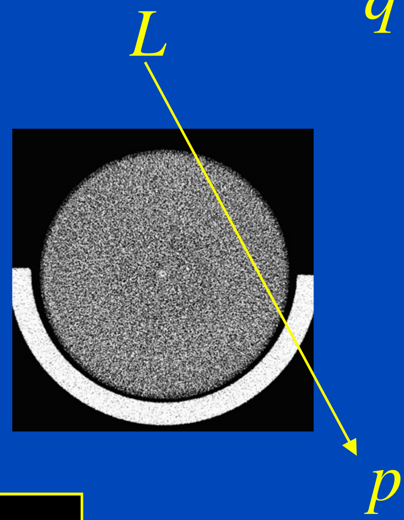

- **Ideal monochromatic projection value p**

$$p(L) = \int dL\, \mu(\boldsymbol{r}, E_0)$$

Determine a function *P* such that
***p*=*P*(*L*, *q*) corrects for the cupping.**

Analytical Cupping Correction

- **Know the detected spectrum**

detector material's attenuation × thickness

primary intensity

$$w(L,E) \propto E\, I(L,E)\,(1-e^{-\mu_D(E)d_D(L)})$$

energy weighting detectors

- **Assume the object to be decomposed as**

$$\boxed{\mu(\boldsymbol{r},E) = f(\boldsymbol{r})\psi(E)}$$

such that

$$q(L) = -\ln \int dE\, w(L,E)\, e^{-p\psi(E)}$$

- **Invert to get p**

$$p(L) = \int dL\, f(\mathbf{r})$$

$$\boxed{p = P(L,q)}$$

Empirical Cupping Correction (ECC)

- Series expansion of the precorrection function

$$p = P(q) = \sum_{n=0}^{N} c_n P_n(q) = \sum_{n=0}^{N} c_n q^n$$

- Go to image domain by reconstructing q^n

$$f_n(\boldsymbol{r}) = \mathsf{R}^{-1} P_n(q) = \mathsf{R}^{-1} q^n.$$

- Find coefficients from

$$f(\boldsymbol{r}) = \mathsf{R}^{-1} p = \mathsf{R}^{-1} P(q) = \sum_{n=0}^{N} c_n f_n(r)$$

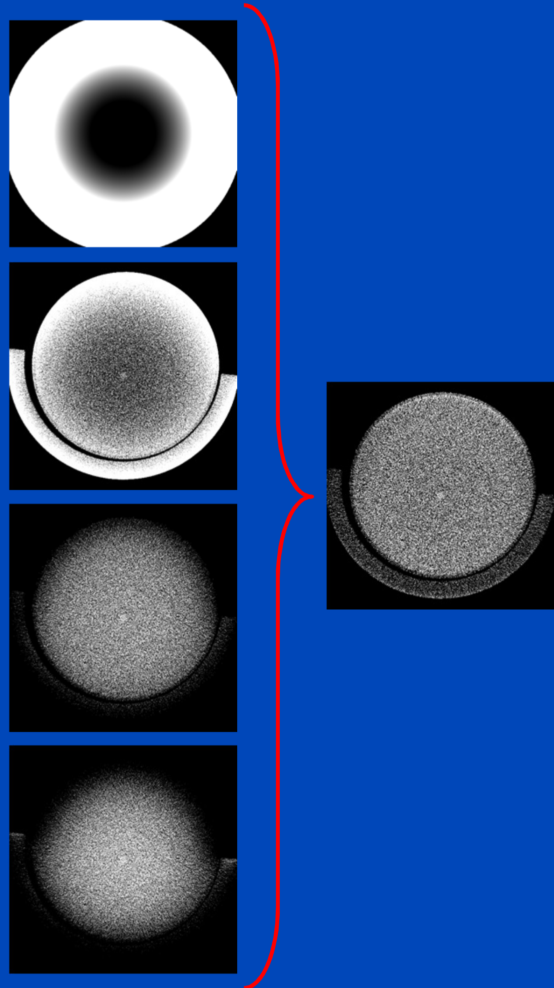

M. Kachelrieß, K. Sourbelle, and W.A. Kalender, "Empirical cupping correction: A first-order raw data precorrection for cone-beam computed tomography," Med. Phys. 33(5):1269-1274, May 2006.

ECC Template Image

$$\int d^2r\, w(\boldsymbol{r})\,(f(\boldsymbol{r})-t(\boldsymbol{r}))^2 = \min \quad \textbf{with} \quad f(\boldsymbol{r}) = \sum_{n=0}^{N} c_n f_n(r)$$

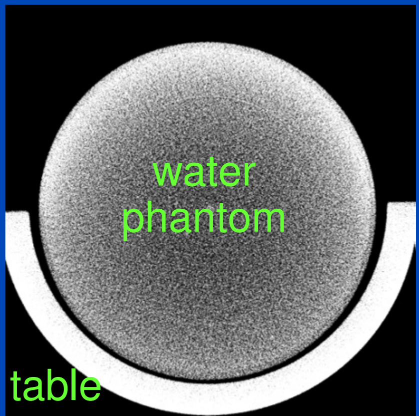

Original image

$f_1(\boldsymbol{r})$

segment and
specify CT-values

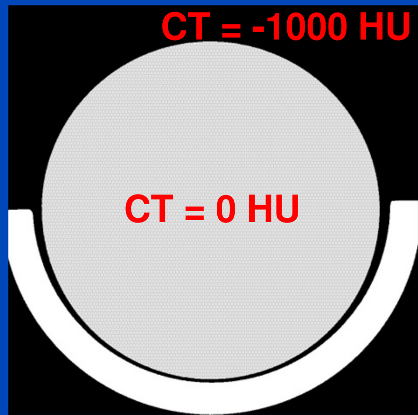

Template image

$t(\boldsymbol{r})$

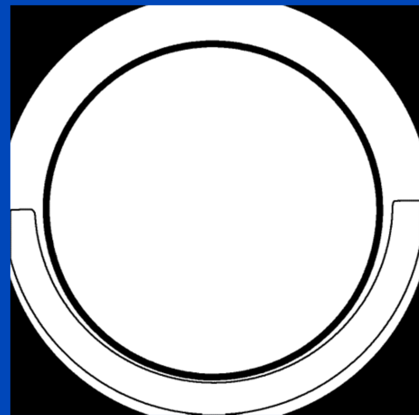

Weight image

$w(\boldsymbol{r})$

M. Kachelrieß, K. Sourbelle, and W.A. Kalender, “Empirical cupping correction: A first-order raw data precorrection for cone-beam computed tomography,” Med. Phys. 33(5):1269-1274, May 2006.

Results: Water Phantom

Orig (Mean±4Sigma)

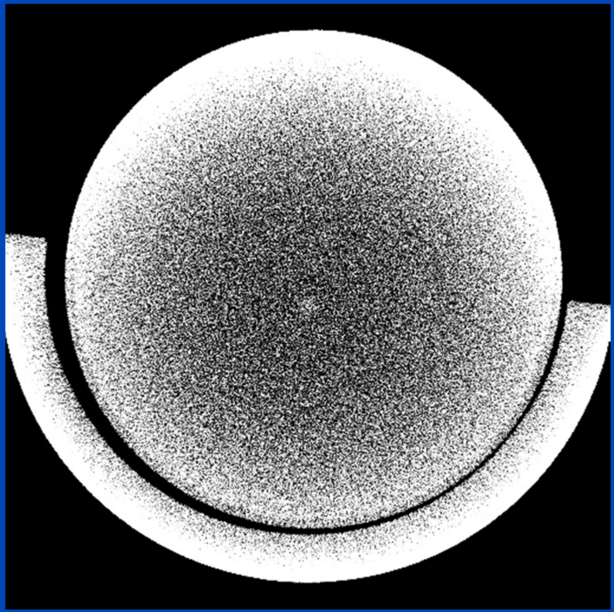

ECC (Mean±4Sigma)

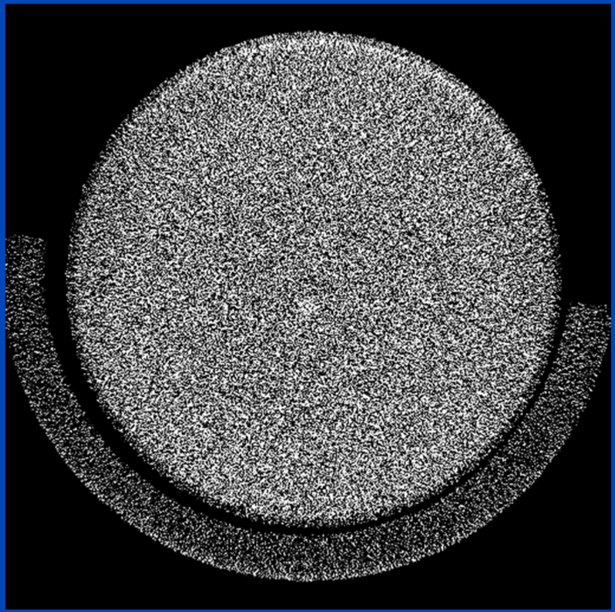

M. Kachelrieß, K. Sourbelle, and W.A. Kalender, "Empirical cupping correction: A first-order raw data precorrection for cone-beam computed tomography," Med. Phys. 33(5):1269-1274, May 2006.

Results: Mouse Scan

No correction (Mean±4Sigma)

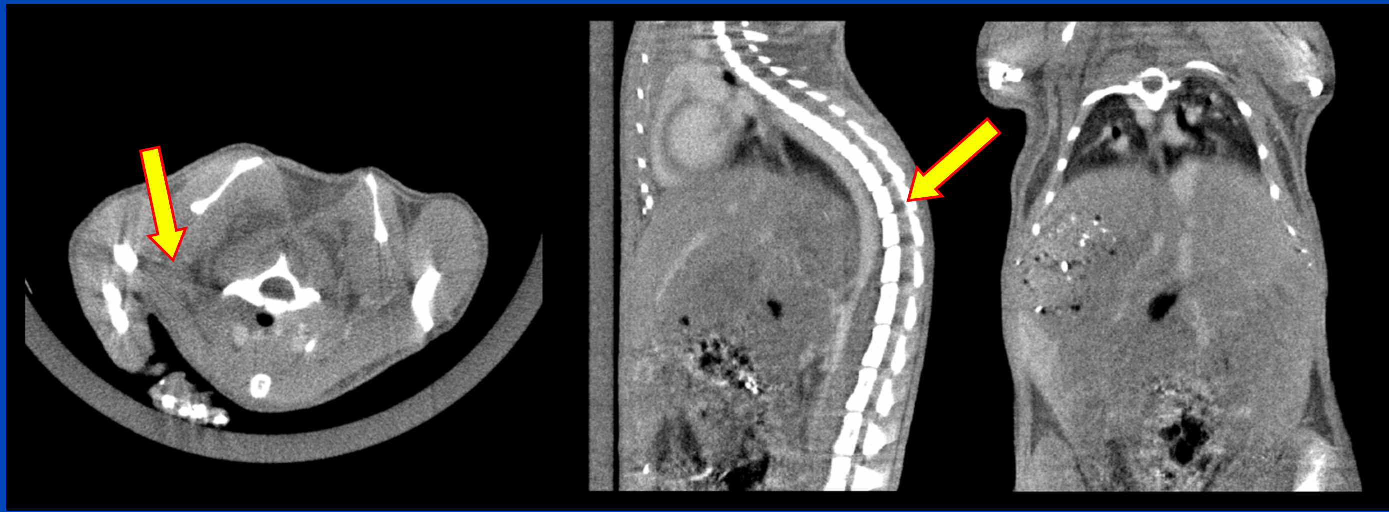

ECC (Mean±4Sigma)

M. Kachelrieß, K. Sourbelle, and W.A. Kalender, "Empirical cupping correction: A first-order raw data precorrection for cone-beam computed tomography," Med. Phys. 33(5):1269-1274, May 2006.

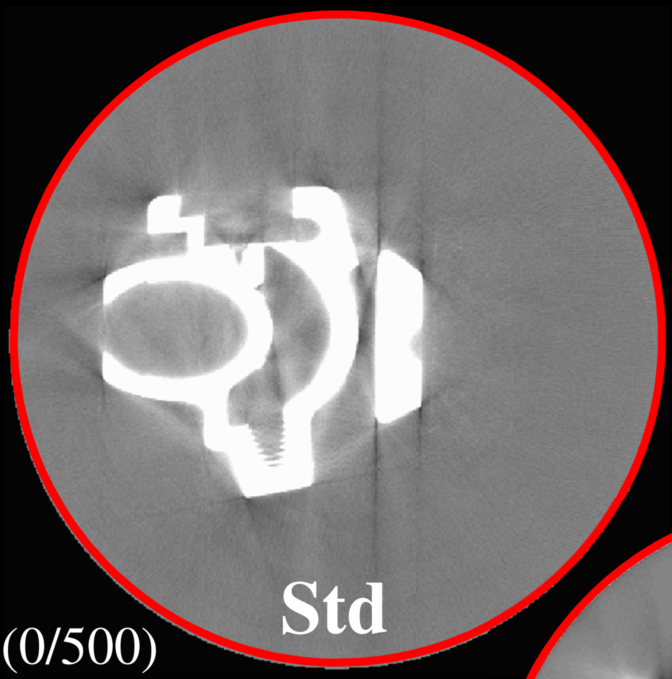

(0/500)

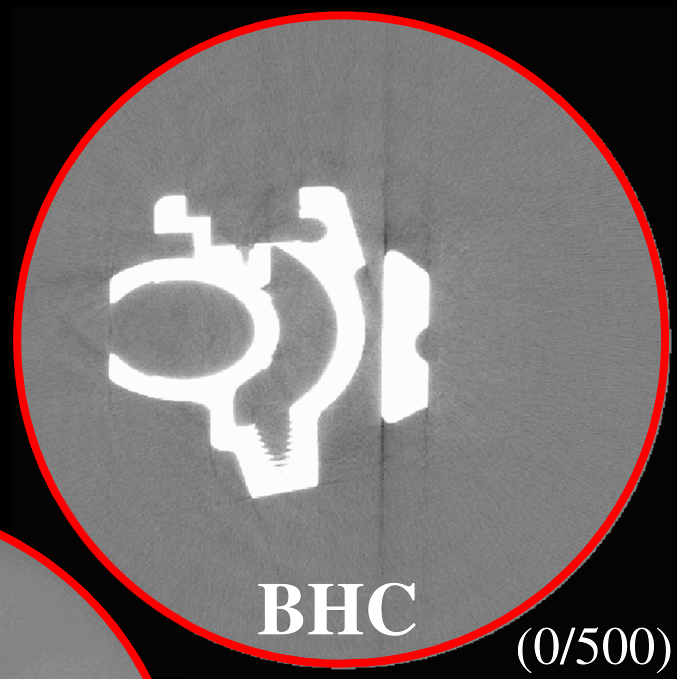

(0/500)

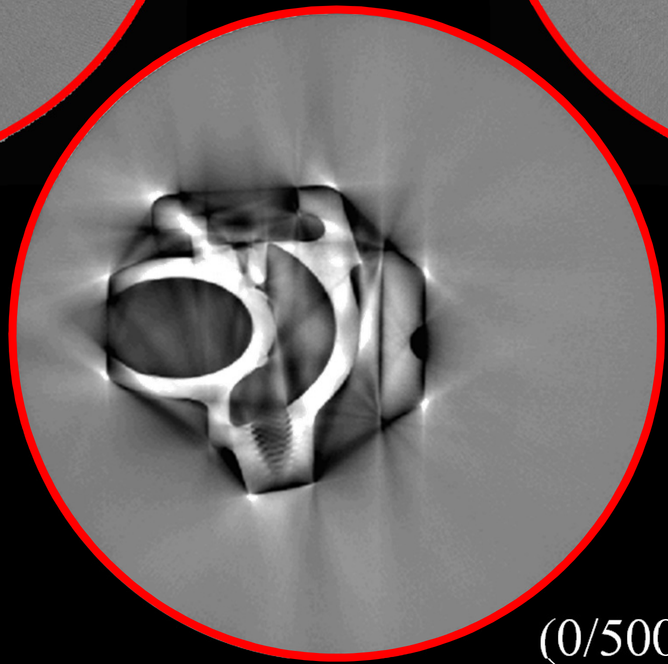
(0/500)

CT Metrology

M. Kachelrieß, K. Sourbelle, and W.A. Kalender, "Empirical cupping correction: A first-order raw data precorrection for cone-beam computed tomography," Med. Phys. 33(5):1269-1274, May 2006.

(1000/200)

(1000/200)

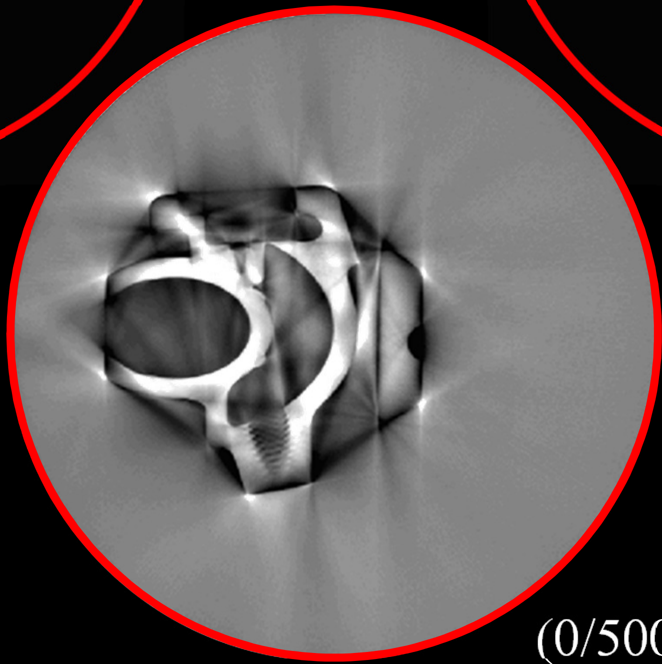

(0/500)

CT Metrology

M. Kachelrieß, K. Sourbelle, and W.A. Kalender, "Empirical cupping correction: A first-order raw data precorrection for cone-beam computed tomography," Med. Phys. 33(5):1269-1274, May 2006.

Higher Order Beam Hardening Correction

- Always requires to add a priori knowledge about the object
  - Segmentation into regions of constant energy dependencies
- Often requires to know the spectral properties of all components involved
  - X-ray spectra
  - Pre patient filters
  - Attenuation properties of materials abundant in humans
  - Absorption properties of detector

One Material
(needed for Water Precorrection)

energy dependence

spatial dependence

Assumption:

$$\mu(E,\boldsymbol{r}) = \psi(E) f(\boldsymbol{r})$$

$$q = \mathrm{R}_f f = -\ln \int dE\, w(E) e^{-\psi(E) p}$$

$$p = \mathrm{R} f = \int dL\, f(\boldsymbol{r})$$

All clinical CT images are corrected wrt a single material.

M. Kachelrieß, and W.A. Kalender, “Improving PET/CT attenuation correction with iterative CT beam hardening correction,” IEEE Medical Imaging Conference Program, M04-5, October 2005.

dkfz.

Many Materials
(required for iterative BHC)

sum over different materials

Assumption: $$\mu(E,\boldsymbol{r}) = \sum_i \psi_i(E) g_i(\boldsymbol{r}) = \boldsymbol{\psi}(E)\cdot \boldsymbol{g}(\boldsymbol{r})$$

$$q = \mathrm{R}_g g = -\ln \int dE\, w(E) e^{-\boldsymbol{\psi}(E)\cdot \boldsymbol{p}}$$

$$\boldsymbol{p} = \mathrm{R}\,\boldsymbol{g} = \int dL\, \boldsymbol{g}(\boldsymbol{r})$$

For PET/CT attenuation correction we need to recover $g_i(\boldsymbol{r})$ for all materials present. Then we can convert to E_0 = 511 keV as

$$\mu(E_0,\boldsymbol{r}) = \sum_i \psi_i(E_0) g_i(\boldsymbol{r}) = \boldsymbol{\psi}(E_0)\cdot \boldsymbol{g}(\boldsymbol{r})$$

Today's scaling algorithms, in contrast, simply use $g_i(\mathbf{r}) = f(\mathbf{r})\, s_i(\mathbf{r})$.

M. Kachelrieß, and W.A. Kalender, "Improving PET/CT attenuation correction with iterative CT beam hardening correction," IEEE Medical Imaging Conference Program, M04-5, October 2005.

Empirical beam hardening correction (EBHC) for CT

Yiannis Kyriakou, Esther Meyer, Daniel Prell, and Marc Kachelrieß[a)]
Institute of Medical Physics, University of Erlangen–Nürnberg, 91052 Erlangen, Germany

(Received 19 May 2010; revised 1 July 2010; accepted for publication 13 July 2010; published 8 September 2010)

Purpose: Due to x-ray beam polychromaticity and scattered radiation, attenuation measurements tend to be underestimated. Cupping and beam hardening artifacts become apparent in the reconstructed CT images. If only one material such as water, for example, is present, these artifacts can be reduced by precorrecting the rawdata. Higher order beam hardening artifacts, as they result when a mixture of materials such as water and bone, or water and bone and iodine is present, require an iterative beam hardening correction where the image is segmented into different materials and those are forward projected to obtain new rawdata. Typically, the forward projection must correctly model the beam polychromaticity and account for all physical effects, including the energy dependence of the assumed materials in the patient, the detector response, and others. We propose a new algorithm that does not require any knowledge about spectra or attenuation coefficients and that does not need to be calibrated. The proposed method corrects beam hardening in single energy CT data.
Methods: The only *a priori* knowledge entering EBHC is the segmentation of the object into different materials. Materials other than water are segmented from the original image, e.g., by using simple thresholding. Then, a (monochromatic) forward projection of these other materials is performed. The measured rawdata and the forward projected material-specific rawdata are monomially combined (e.g., multiplied or squared) and reconstructed to yield a set of correction volumes. These are then linearly combined and added to the original volume. The combination weights are determined to maximize the flatness of the new and corrected volume. EBHC is evaluated using data acquired with a modern cone-beam dual-source spiral CT scanner (Somatom Definition Flash, Siemens Healthcare, Forchheim, Germany), with a modern dual-source micro-CT scanner (TomoScope Synergy Twin, CT Imaging GmbH, Erlangen, Germany), and with a modern C-arm CT scanner (Axiom Artis dTA, Siemens Healthcare, Forchheim, Germany). A large variety of phantom, small animal, and patient data were used to demonstrate the data and system independence of EBHC.
Results: Although no physics apart from the initial segmentation procedure enter the correction process, beam hardening artifacts were significantly reduced by EBHC. The image quality for clinical CT, micro-CT, and C-arm CT was highly improved. Only in the case of C-arm CT, where high scatter levels and calibration errors occur, the relative improvement was smaller.
Conclusions: The empirical beam hardening correction is an interesting alternative to conventional iterative higher order beam hardening correction algorithms. It does not tend to over- or undercorrect the data. Apart from the segmentation step, EBHC does not require assumptions on the spectra or on the type of material involved. Potentially, it can therefore be applied to any CT image. [DOI: 10.1118/1.3477088]

Key words: Computed tomography (CT), beam hardening correction, x-ray, scatter

Empirical Beam Hardening Correction (EBHC)

- **Requirements/Objectives**
  - Empirical correction of <u>higher order</u> beam hardening effects
  - No assumptions on attenuation coefficients, spectra, detector responses or other properties of the scanner
  - Image-based and system-independent method

- **Overview of correction steps**
  - Forward project segmented bone volume to obtain artificial rawdata
  - Pass the artificial rawdata through basis functions
  - Reconstruct the basis functions
  - Linearly combine the correction volumes and the original volume using flatness maximization

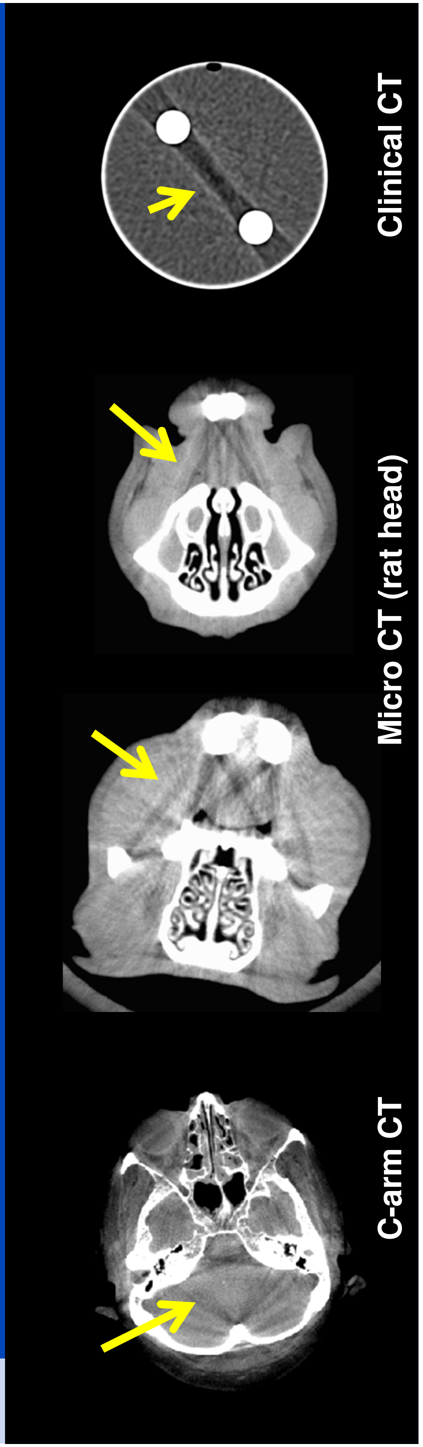

Y. Kyriakou, E. Meyer, D. Prell, and M. Kachelrieß, "Empirical beam hardening correction (EBHC) for CT," Med. Phys. 37(10):5179-5187, October 2010.

EBHC Details

- Decomposition into an effective water-equivalent density $\hat{f}_1(r)$ of the object and into an effective energy dependence $\hat{\psi}_2(E)$ of a second material, e.g. bone

$$\begin{aligned}\mu(\boldsymbol{r},E) &= f_1(\boldsymbol{r})\psi_1(E) + f_2(\boldsymbol{r})\psi_2(E)\\ &= \big(f_1(\boldsymbol{r}) + f_2(\boldsymbol{r})\big)\psi_1(E) + f_2(\boldsymbol{r})\big(\psi_2(E) - \psi_1(E)\big)\\ &= \hat{f}_1(\boldsymbol{r})\psi_1(E) + f_2(\boldsymbol{r})\hat{\psi}_2(E).\end{aligned}$$

- Assuming water-precorrected data gives

$$\int dE\, w(E) e^{-p_0\psi_0(E)} = \int dE\, w(E) e^{-\hat{p}_1\psi_1(E) - p_2\hat{\psi}_2(E)}$$

where $\hat{p}_1$ and p_2 are the line integrals through $\hat{f}_1(r)$ and $f_2(r)$

Y. Kyriakou, E. Meyer, D. Prell, and M. Kachelrieß, “Empirical beam hardening correction (EBHC) for CT,” Med. Phys. 37(10):5179-5187, October 2010.

EBHC Details

- We solve for $\hat{p}_1(r)$ using a series expansion

$$\hat{p}_1(p_0, p_2) = \sum_{ij} c_{ij} p_0^i p_2^j = p_0 + c_{01}p_2 + c_{11}p_0p_2 + c_{02}p_2^2 + \ldots$$

$\mathbf{R}^{-1}$ $\mathbf{R}^{-1}$ $\mathbf{R}^{-1}$

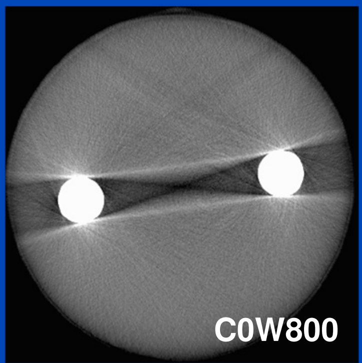

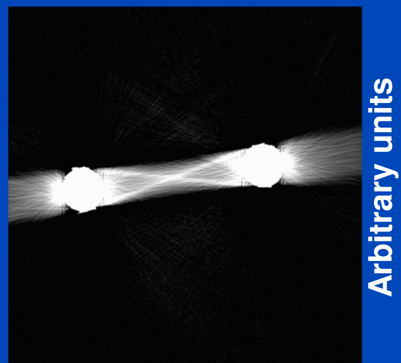

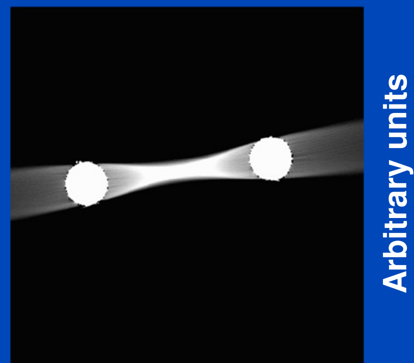

- Empirically find c_{11} and c_{02} to correct initial image by flatness maximization

Y. Kyriakou, E. Meyer, D. Prell, and M. Kachelrieß, "Empirical beam hardening correction (EBHC) for CT," Med. Phys. 37(10):5179-5187, October 2010.

dkfz.

EBHC for Clinical CT

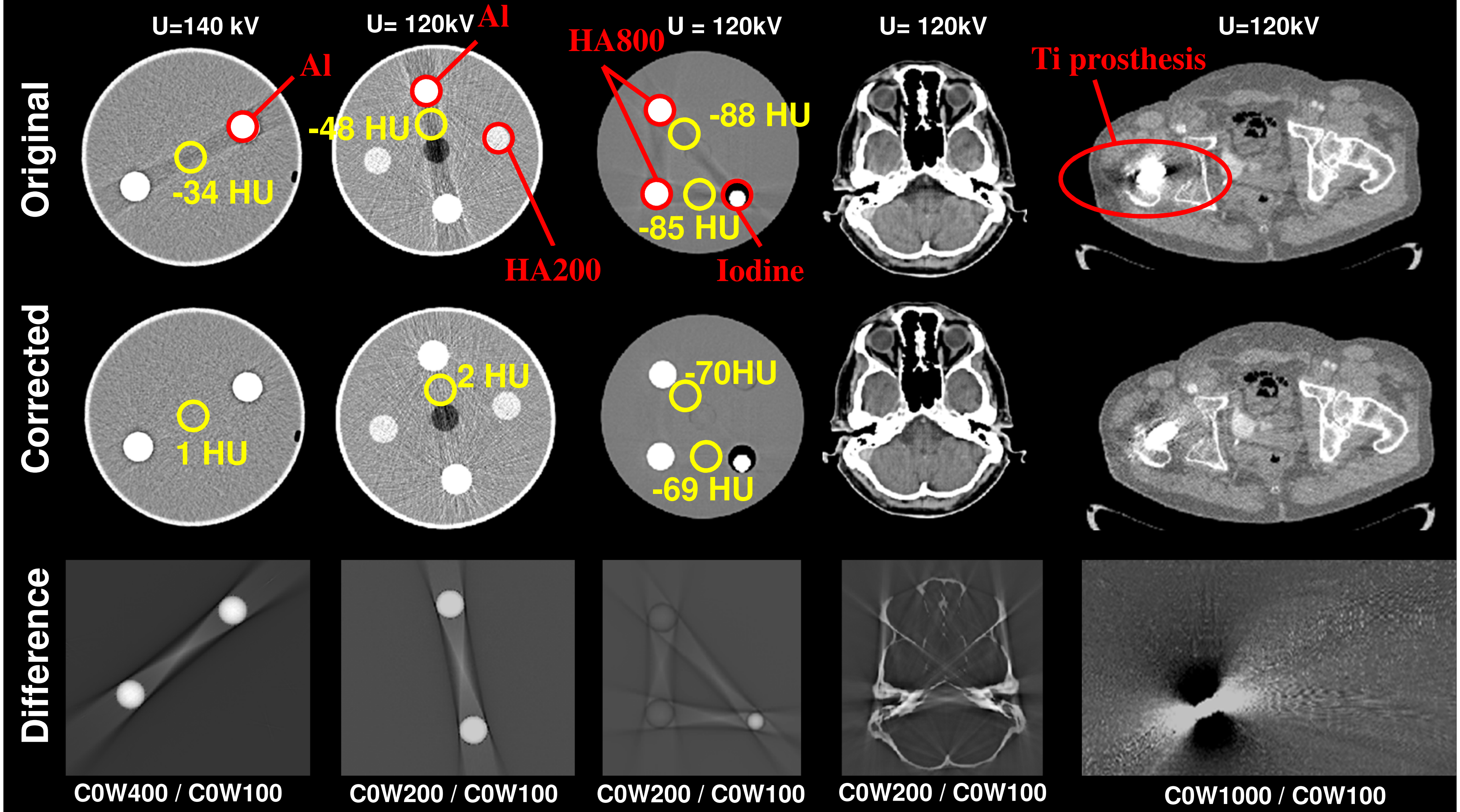

Y. Kyriakou, E. Meyer, D. Prell, and M. Kachelrieß, “Empirical beam hardening correction (EBHC) for CT,” Med. Phys. 37(10):5179-5187, October 2010.

EBHC for Micro CT

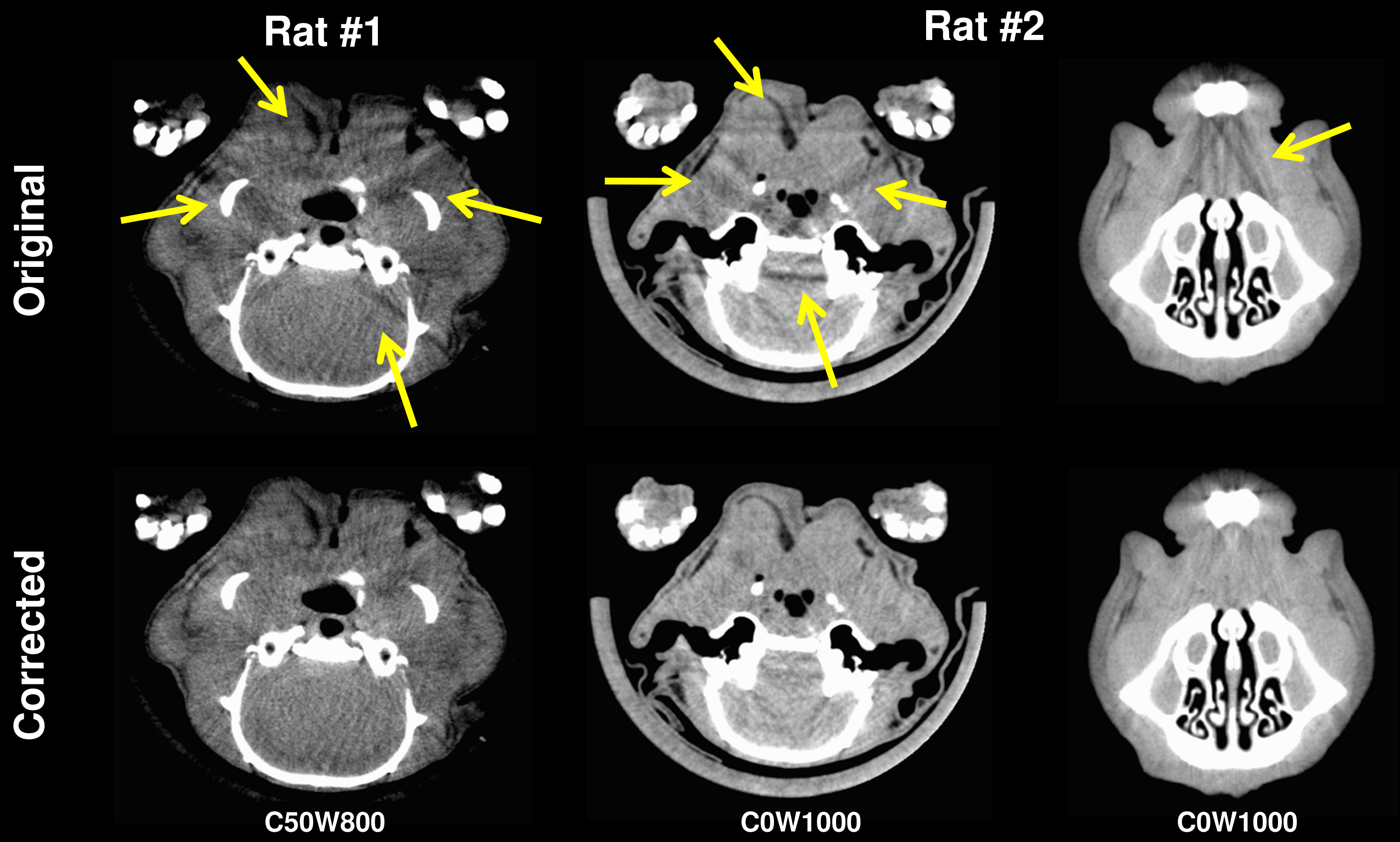

Y. Kyriakou, E. Meyer, D. Prell, and M. Kachelrieß, "Empirical beam hardening correction (EBHC) for CT," Med. Phys. 37(10):5179-5187, October 2010.

dkfz.

EBHC: Clinical CT vs. FD-CT

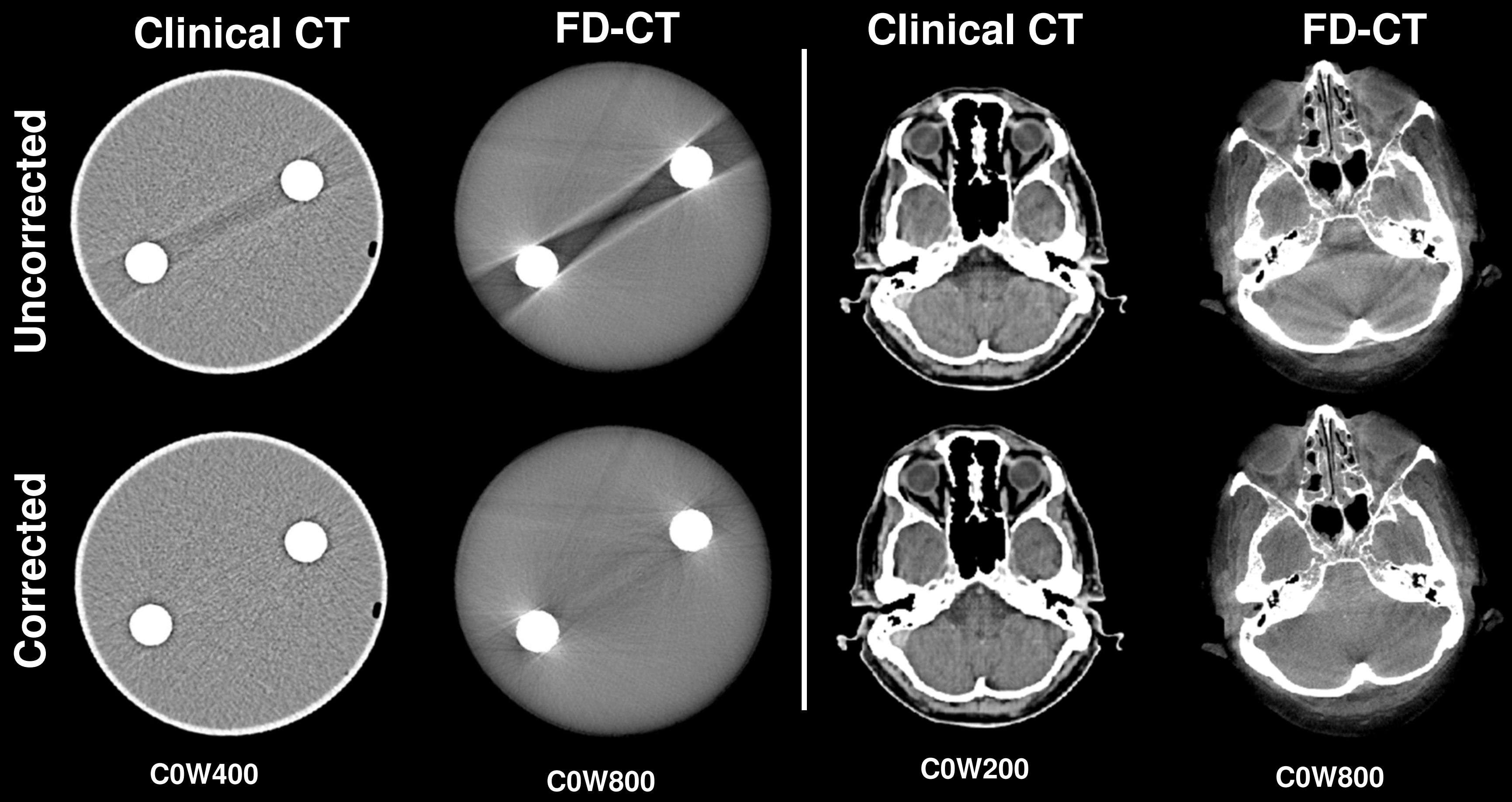

Y. Kyriakou, E. Meyer, D. Prell, and M. Kachelrieß, "Empirical beam hardening correction (EBHC) for CT," Med. Phys. 37(10):5179-5187, October 2010.

dkfz.

Conclusions on Empirical Cupping and Beam Hardening Corrections

- X-ray spectra need not necessarily be known
- Scatter is implicitly accounted for as well
- ECC and EBHC are robust methods that work well in clinical CT and that also have been applied to some industrial situations.

Scatter Correction

- **Remove or prevent scattered radiation (anti scatter grid, slit scan, large detector distance, …)**
- **Compute scatter to subtract it (convolution-based, Monte Carlo-based, …)**
- **Measure scatter distribution and subtract it (collimator shadow, beam blockers, primary modulators, …)**

- **Literature:**

- E.-P. Rührnschopf and K. Klingenbeck, *"A general framework and review of scatter correction methods in x–ray cone–beam computerized tomography. Part 1: Scatter compensation approaches,"* Med. Phys., vol. 38, pp. 4296–4311, July 2011.
- E.-P. Rührnschopf and K. Klingenbeck, *"A general framework and review of scatter correction methods in x–ray cone beam CT. Part 2: Scatter estimation approaches,"* Med. Phys., vol. 38, pp. 5186–5199, Sept. 2011.

Basis Images EBHC + ESC

Beam hardening basis images[1]

p : beam hardening-corrected projections

p_0 : water-precorrected projections of tissue

p_m : projections of metal

$$p(p_0, p_m) = \sum_{ij} c_n p_0^i p_m^j =$$

$$= p_0 + c_1 p_m + c_2 p_0 p_m + c_3 p_m^2 + \ \ldots$$

$\mathbf{R}^{-1}$ $\mathbf{R}^{-1}$ $\mathbf{R}^{-1}$

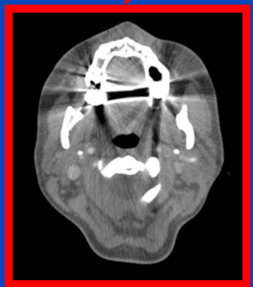
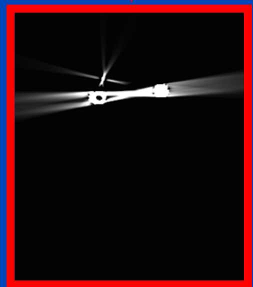
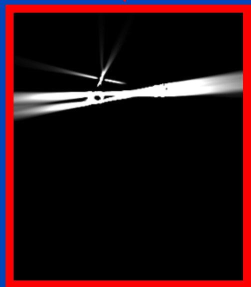

Scatter basis images[2]

I_S : scatter intensity

I_F : forward scatter intensity

K : scatter kernel

$$I_S(a,b,c) = I_F(a) * K(b,c)$$

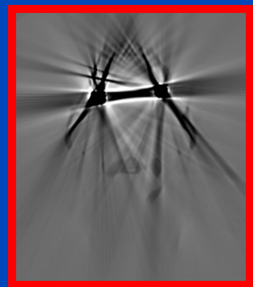
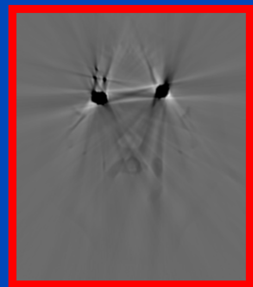

[1] Y. Kyriakou, E. Meyer, D. Prell, and M. Kachelrieß, “Empirical beam hardening correction for CT”, MedPhys 37: 5179-5187, 2010.
[2] B. Ohnesorge et al., “Efficient object scatter correction algorithm for third and fourth generation CT scanners”, EuRad 9:563-569, 1999.

EBHSC: Scheme

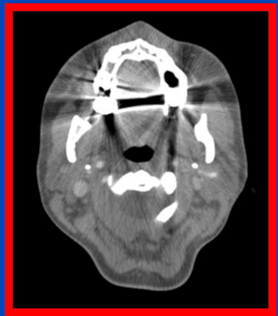 $+c_1\cdot$ 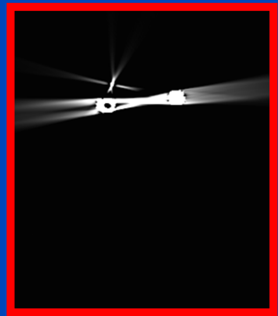 $+\ldots+c_N\cdot$ 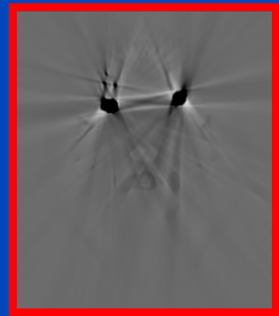 $=$ 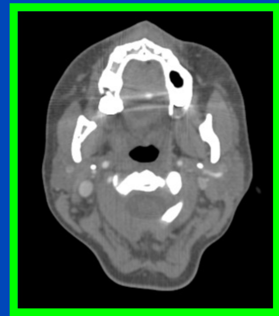

$$c_1 \ldots c_N = \underset{c_1 \ldots c_N}{\arg\min}\ \mathrm{f}_{\mathrm{cost}}\left(U - \sum_{i=1}^{N} c_i B_i\right)$$

E. Meyer, C. Maaß, M. Baer, R. Raupach, B. Schmidt, and M. Kachelrieß, "Empirical Scatter Correction (ESC) ", IEEE Medical Imaging Conference Record 2010:2036-2041, November 2010.

EBHSC: Results

Uncorrected image | EBHSC image

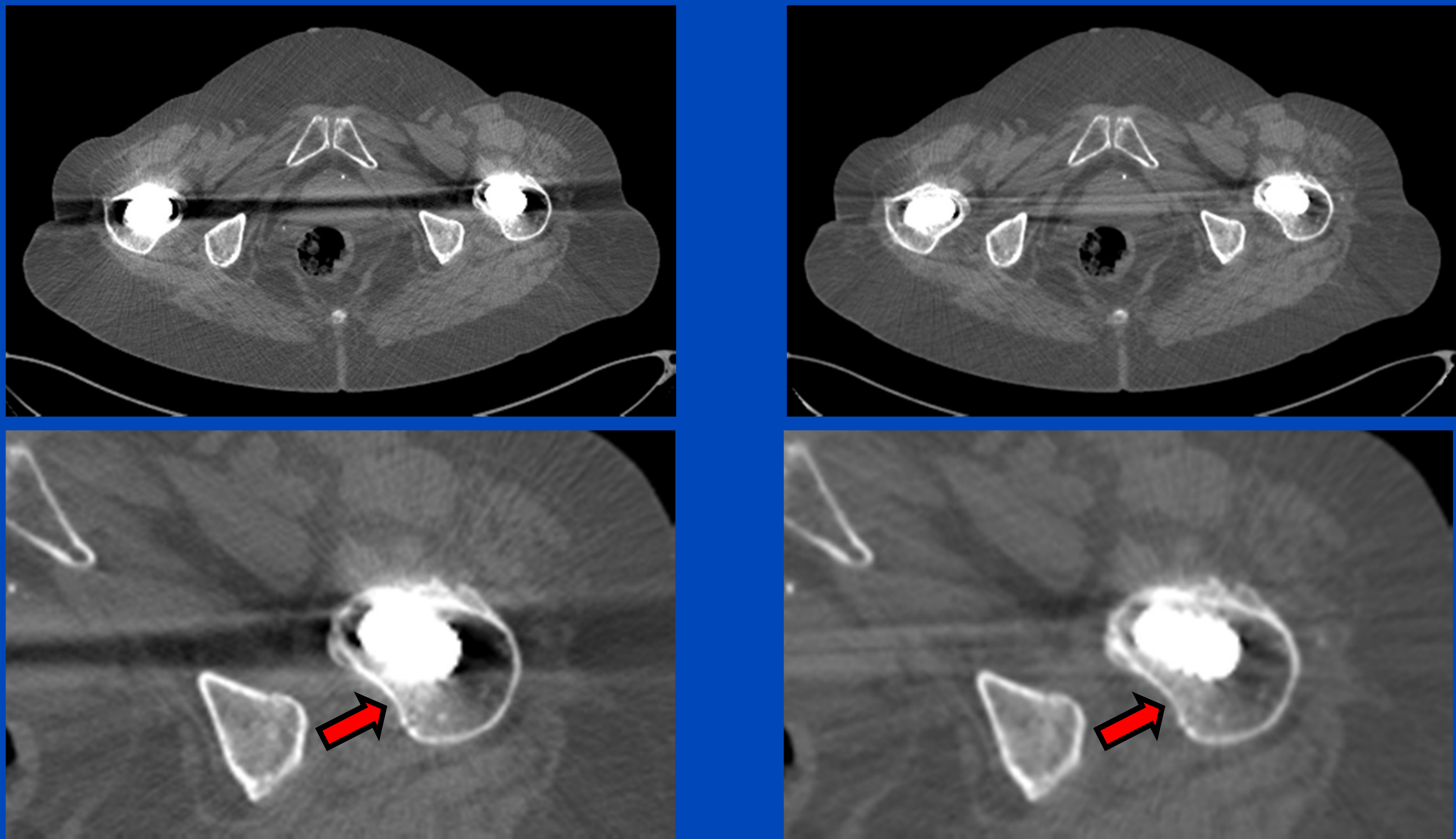

Patient with bilateral hip prosthesis, Siemens Somatom Definition (C=100/W=1000).

E. Meyer, C. Maaß, M. Baer, R. Raupach, B. Schmidt, and M. Kachelrieß, "Empirical Scatter Correction (ESC) ", IEEE Medical Imaging Conference Record 2010:2036-2041, November 2010.

Primary Modulation-based Scatter Estimation (PMSE)

- **Idea: Insert a high frequency modulation pattern between the source and the object scanned**

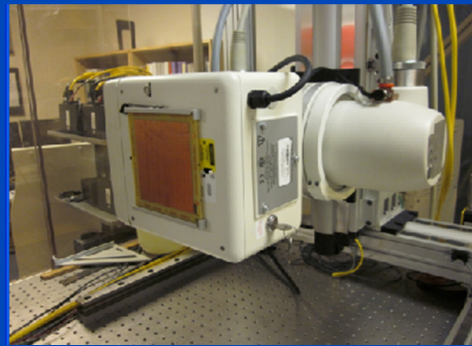

- **Rationale: The primary intensity is modulated. The scatter is created in the object and only consists of low frequency components.**

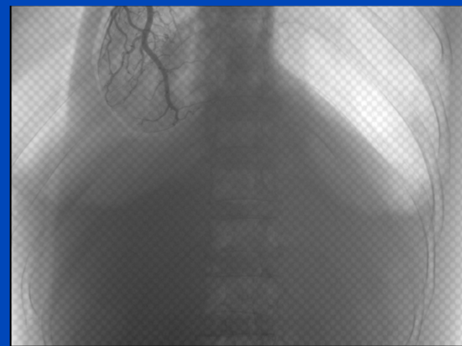

- **Method: Estimate low frequency primary without scatter by Fourier filtering techniques**

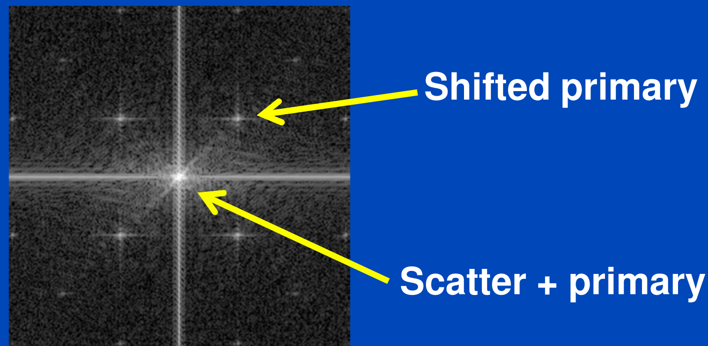

L. Zhu, R. N. Bennett, and R. Fahrig, “Scatter correction method for x–ray CT using primary modulation: Theory and preliminary results,” IEEE Transactions on Medical Imaging, vol. 25, pp. 1573–1587, Dec. 2006.

Primary Modulation-based Scatter Estimation (PMSE[1])

- **Advantages:**
  - Non-destructive measurement of the scatter distribution
  - Works with high accuracy on laboratory setups
  - Corrected projection data can be used for projective imaging (fluoroscopy) or for tomographic reconstruction
- **Drawbacks:**
  - Sensitive to non-linearities due to polychromaticity of x-rays. Ring artifacts are introduced[1]. Can be resolved using ECCP[2].
  - Requires exact rectangular pattern on the detector. Very sensitive to non-idealities of the projected modulation pattern (blurring, distortion, manufacturing errors of the modulator). Can be resolved using iPMSE[3].

[1]H. Gao, L. Zhu, and R. Fahrig. *Modulator design for x-ray scatter correction using primary modulation: Material selection.* Med. Phys. 37:4029–4037, 2010.
[2]R. Grimmer, R. Fahrig, W. Hinshaw, H. Gao, and M. Kachelrieß. *Empirical cupping correction for CT scanners with primary modulation (ECCP)*. Med. Phys. 39(2):825-831, February 2012.
[3]L. Ritschl, R. Fahrig, M. Knaup, J. Maier, and M. Kachelrieß, Robust primary modulation-based scatter estimation for cone-beam CT. Med. Phys. 42(1):469-478, January 2015.

Modulator

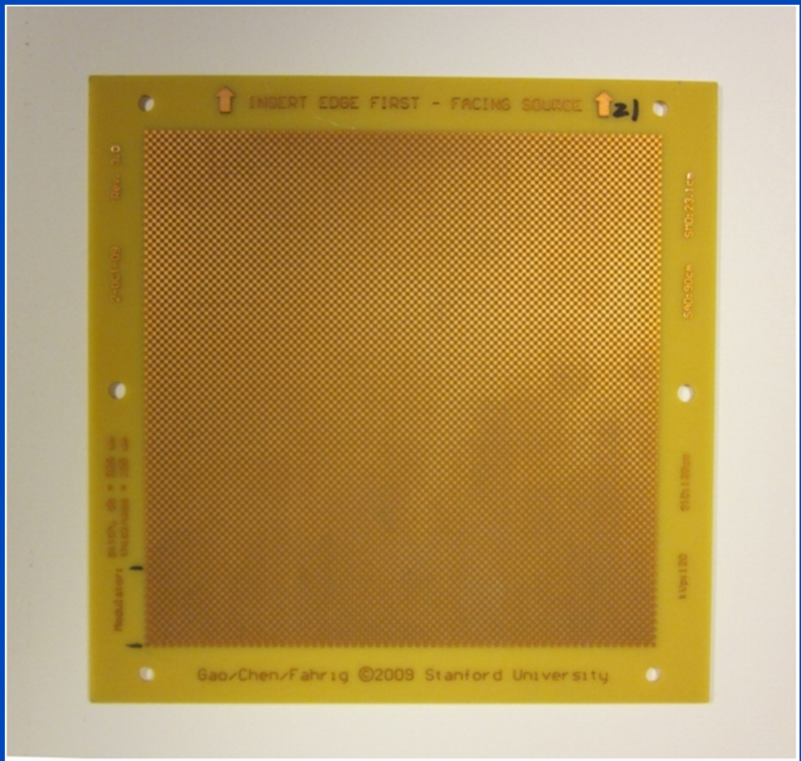

Photograph of the copper modulator

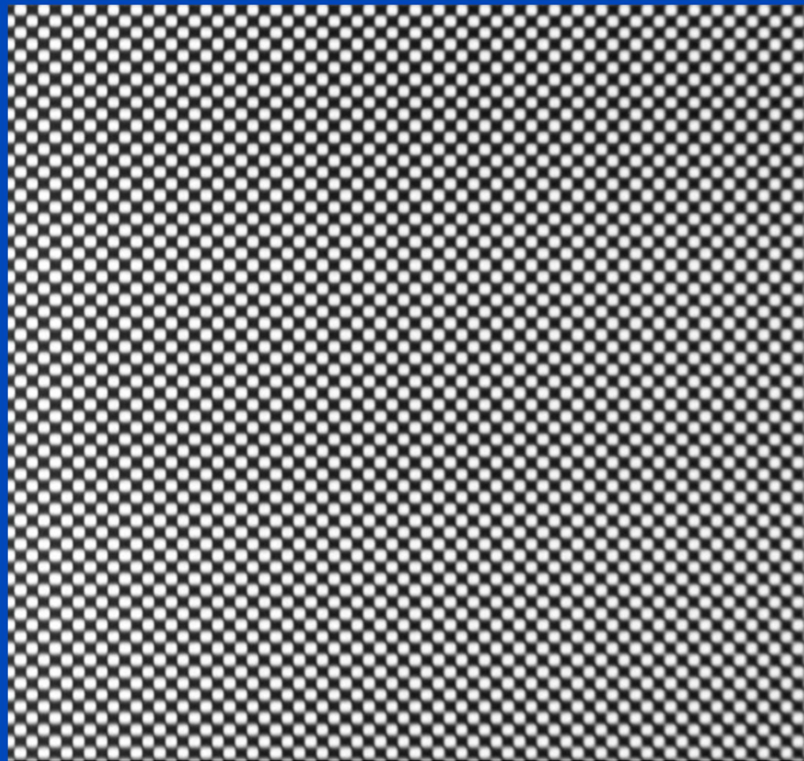

Projection image of the modulator

Primary Modulator Introduces Beam Hardening

- The primary modulator introduces high frequency variations of the incident x-ray spectrum.
- These variations show up as ring artifacts in the reconstructed images[1,2,3].

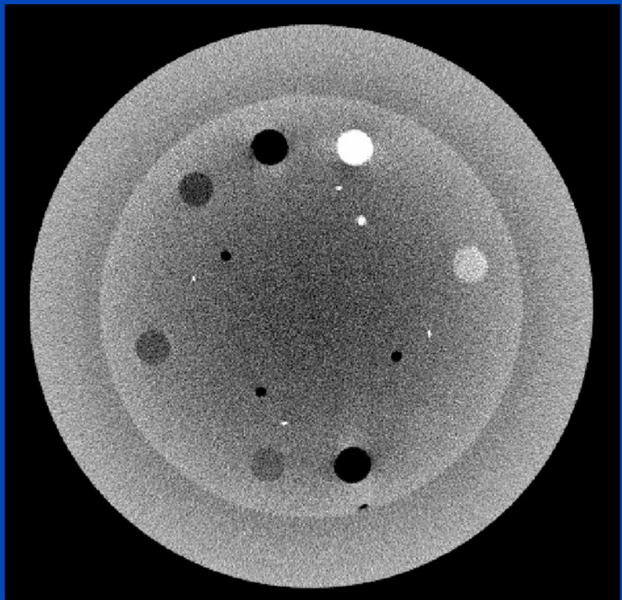

Scan without modulator, no scatter correction

(0 HU, 500 HU)

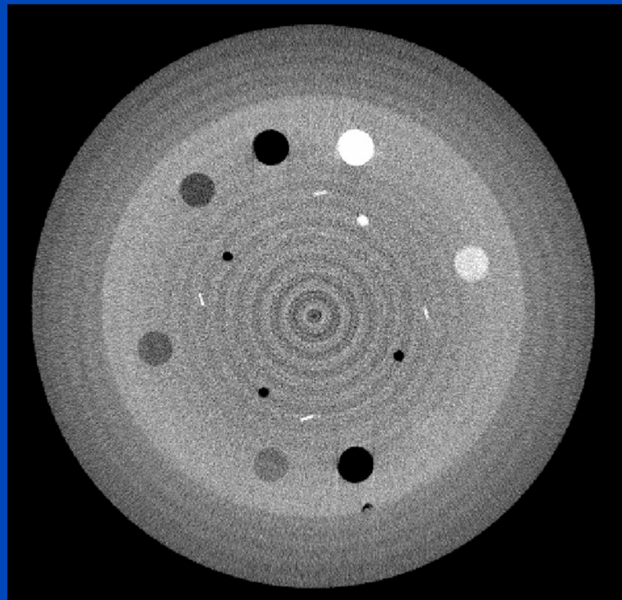

Scan with modulator, after PMSE correction

[1]Gao et al. MedPhys 37(2):934-946, 2010. [2]Gao et al. Proc. SPIE 7622, 2010. [3]Gao et al. MedPhys 37(8):4029-4037, 2010.

Catphan Phantom

Measurement without Modulator | Measurement with Modulator | ECCP–corrected

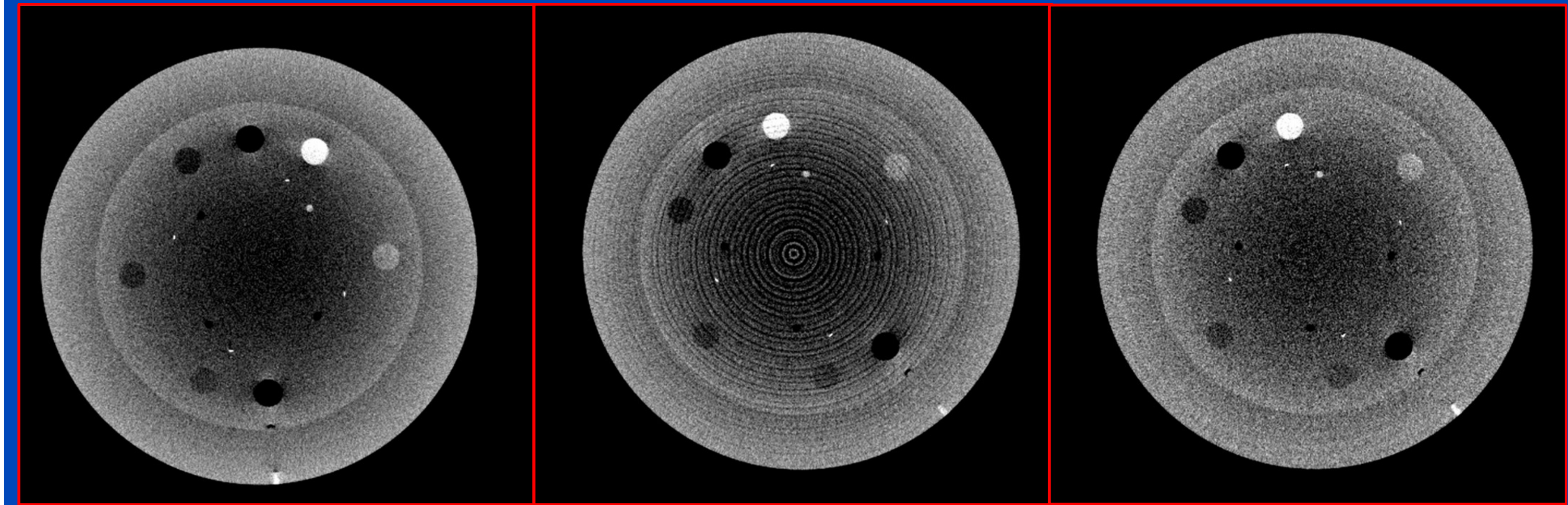

C = 0 HU, W = 500 HU

ECCP coefficients obtained from the water phantom calibration scan.

R. Grimmer, R. Fahrig, W. Hinshaw, H. Gao, and M. Kachelrieß, "Empirical cupping correction for CT scanners with primary modulation (ECCP)," Med. Phys. 39(2):825-831, February 2012.

Combined correction with PMSE and ECCP

Measurement without Modulator | PMSE+ECCP–corrected | Slitscan without modulator

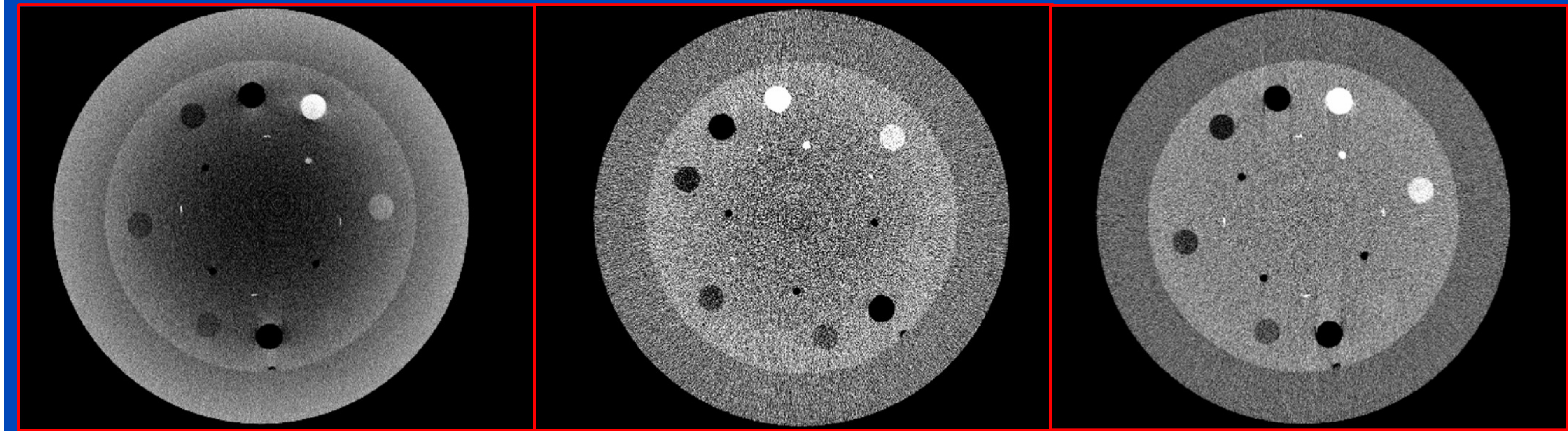

C = 0 HU, W = 500 HU

ECCP coefficients obtained from the PMSE-corrected water phantom calibration scan.

R. Grimmer, R. Fahrig, W. Hinshaw, H. Gao, and M. Kachelrieß, "Empirical cupping correction for CT scanners with primary modulation (ECCP)," Med. Phys. 39(2):825-831, February 2012.

Aim of iPMSE

Create a robust scatter estimation method which is able to estimate the scatter distribution with high accuracy using a modulator with an arbitrary high frequency pattern.

“Ideal” modulator (projection image of a copper modulator)

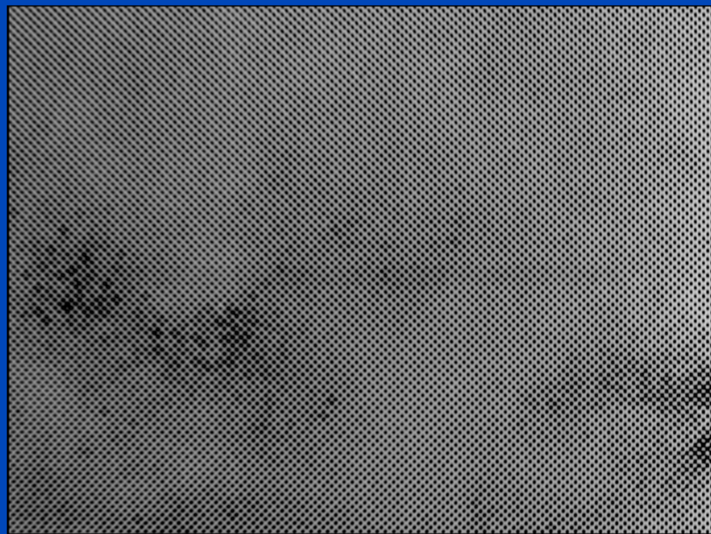

Non-ideal modulator (projection image of the erbium modulator)

L. Ritschl, R. Fahrig, M. Knaup, J. Maier, and M. Kachelrieß, “Robust primary modulation-based scatter estimation for cone-beam CT,” Med. Phys. 42(1):469-478, January 2015.

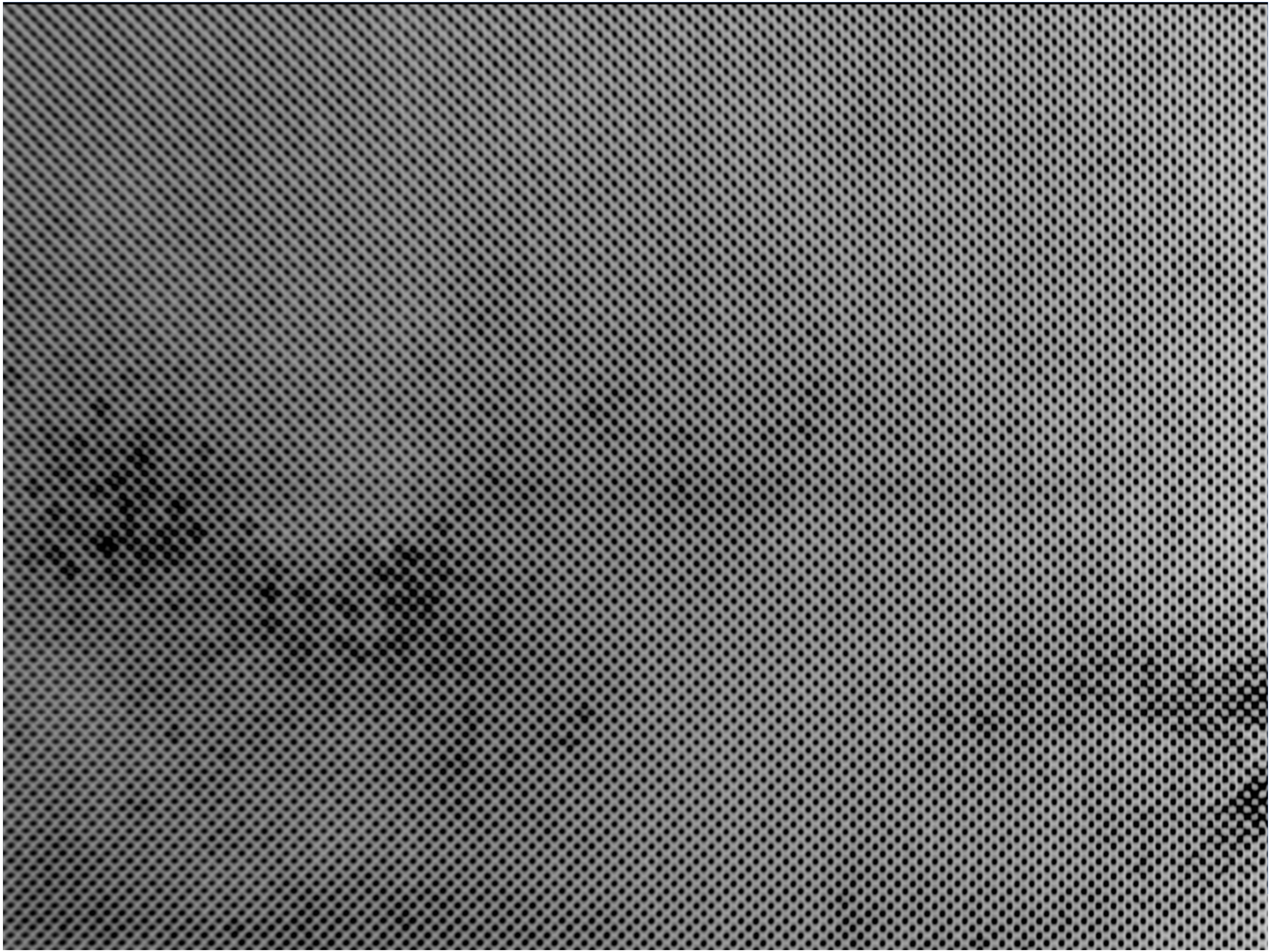

Modulation Process in the Rawdata Domain

Primary intensity

- **Measured data:** $$c_\mathrm{m} = M c_\mathrm{p} + c_\mathrm{s}$$

Measured intensity

Modulation pattern

Scatter intensity

- **Solving for the primary intensity:** $$c_\mathrm{p} = M^{-1}(c_\mathrm{m} - c_\mathrm{s})$$

- **Error of primary estimate:** $$\begin{aligned} c_\mathrm{p}^\mathrm{est} &= M^{-1}(c_\mathrm{m} - c_\mathrm{s}^\mathrm{est}) \\ &= c_\mathrm{p} + M^{-1}(c_\mathrm{s} - c_\mathrm{s}^\mathrm{est}) \end{aligned}$$

Scatter estimate error

The modulation pattern remains visible if the scatter estimate error is not zero.

L. Ritschl, R. Fahrig, M. Knaup, J. Maier, and M. Kachelrieß, "Robust primary modulation-based scatter estimation for cone-beam CT," Med. Phys. 42(1):469-478, January 2015.

iPSME

- **Subject to $H \cdot \boldsymbol{c}_\mathrm{s} = 0$ solve:**

$$C(\boldsymbol{c}_\mathrm{s}) = \|\nabla \cdot \boldsymbol{M}^{-1}(\boldsymbol{c}_\mathrm{m} - \boldsymbol{c}_\mathrm{s})\|_1$$

- **Assumption:**
  In a sufficiently small and sufficiently large sub image the constraint can be satisfied by assuming c_s = const.

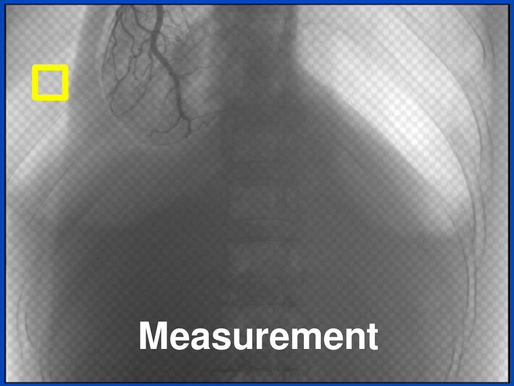

- **Solution:**
  Solve cost function for each possible sub image separately.

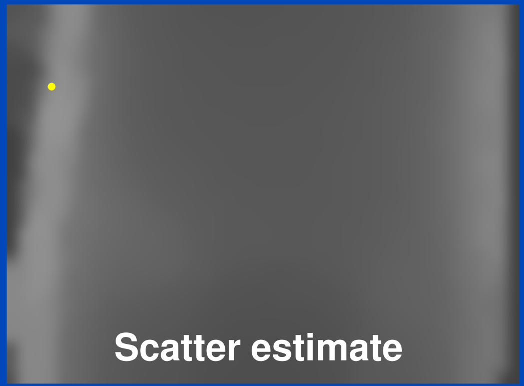

- **Finally do:**

$$\boldsymbol{c}_\mathrm{p} = \boldsymbol{M}^{-1}(\boldsymbol{c}_\mathrm{m} - \boldsymbol{c}_\mathrm{s})$$

Measured Intensity

L. Ritschl, R. Fahrig, M. Knaup, J. Maier, and M. Kachelrieß, "Robust primary modulation-based scatter estimation for cone-beam CT," Med. Phys. 42(1):469-478, January 2015.

iPMSE Estimation

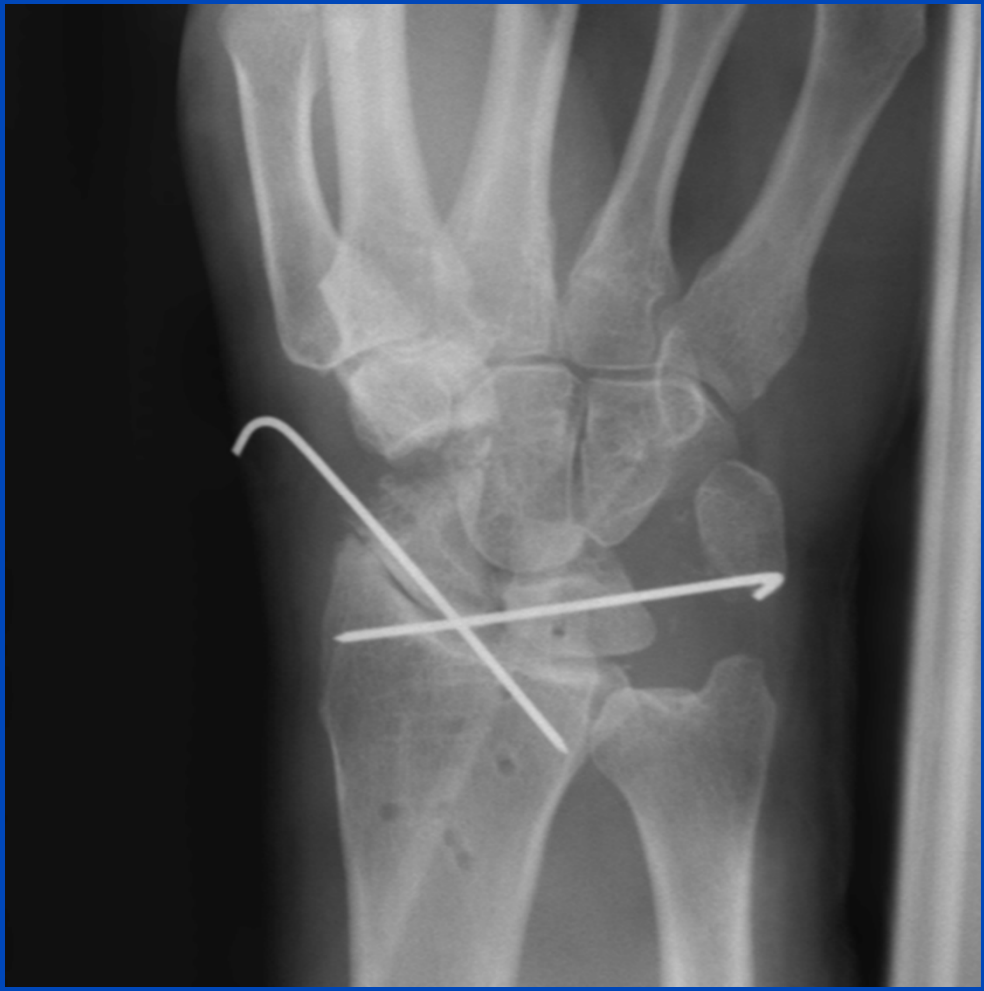

L. Ritschl, R. Fahrig, M. Knaup, J. Maier, and M. Kachelrieß, “Robust primary modulation-based scatter estimation for cone-beam CT,” Med. Phys. 42(1):469-478, January 2015.

Lung Phantom Scan

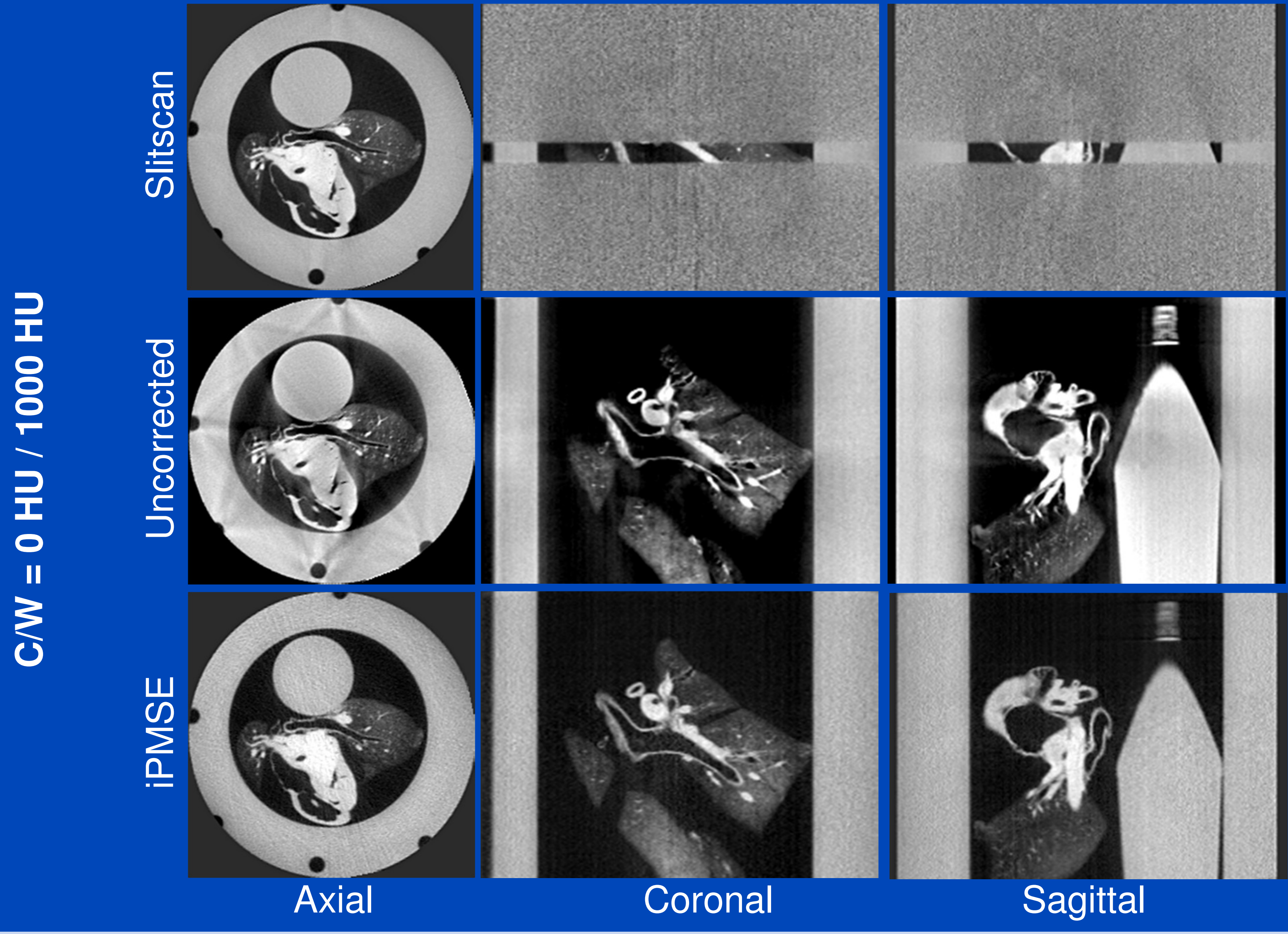

L. Ritschl, R. Fahrig, M. Knaup, J. Maier, and M. Kachelrieß, "Robust primary modulation-based scatter estimation for cone-beam CT," Med. Phys. 42(1):469-478, January 2015.

dkfz.

Metal Artifact Reduction (MAR)

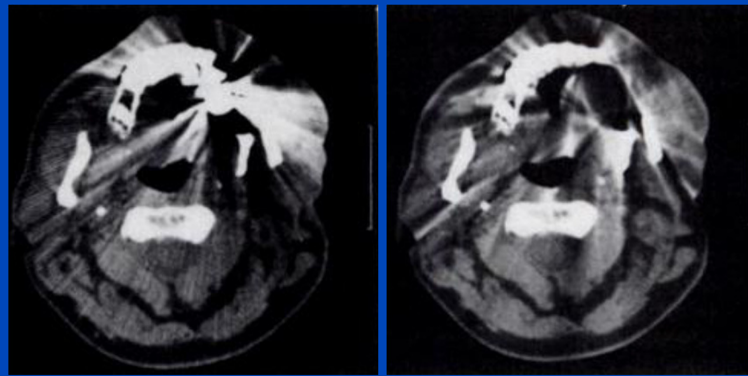

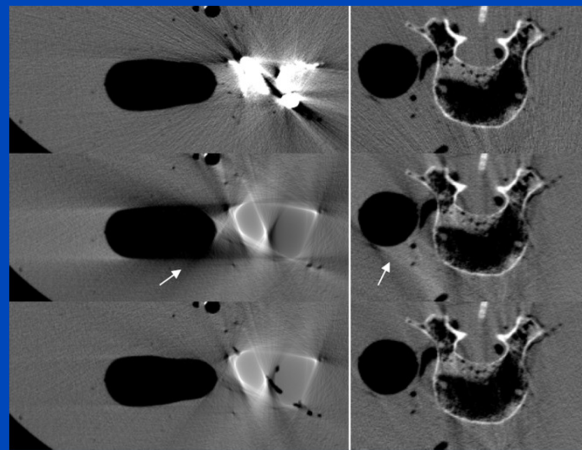

With linear interpolation (MAR1)

[1] W. A. Kalender, R. Hebel and J. Ebersberger, “Reduction of CT artifacts caused by metallic implants”, *Radiology,* vol. 164, no. 2, pp. 576-577, August 1987.

With simple length-normalization (MAR2)

[2] J. Müller and T. M. Buzug, “Spurious structures created by interpolation-based CT metal artifact reduction“, *SPIE Medical Imaging Proc.*, vol. 7258, no. 1, pp. 1Y1-1Y8, March 2009.

Our generalized normalization (NMAR)

[3] E. Meyer, F. Bergner, R. Raupach, and M. Kachelrieß. “Normalized metal artifact reduction (NMAR) in computed tomography”, *IEEE Medical Imaging Conference Record*, M09-206, October 2009.

MAR1

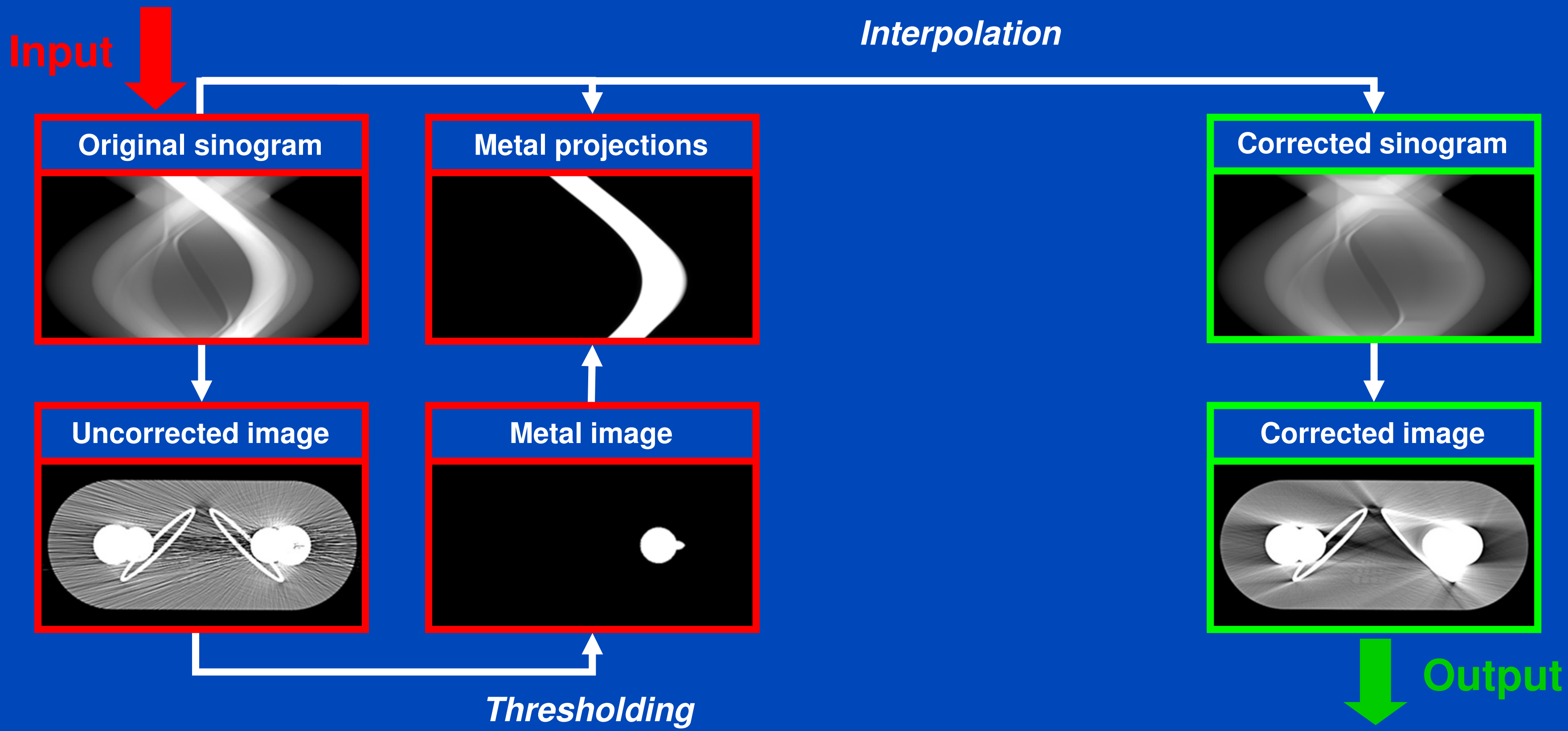

Input
Interpolation
Original sinogram
Metal projections
Corrected sinogram
Uncorrected image
Metal image
Corrected image
Thresholding
Output

Normalized MAR (NMAR)

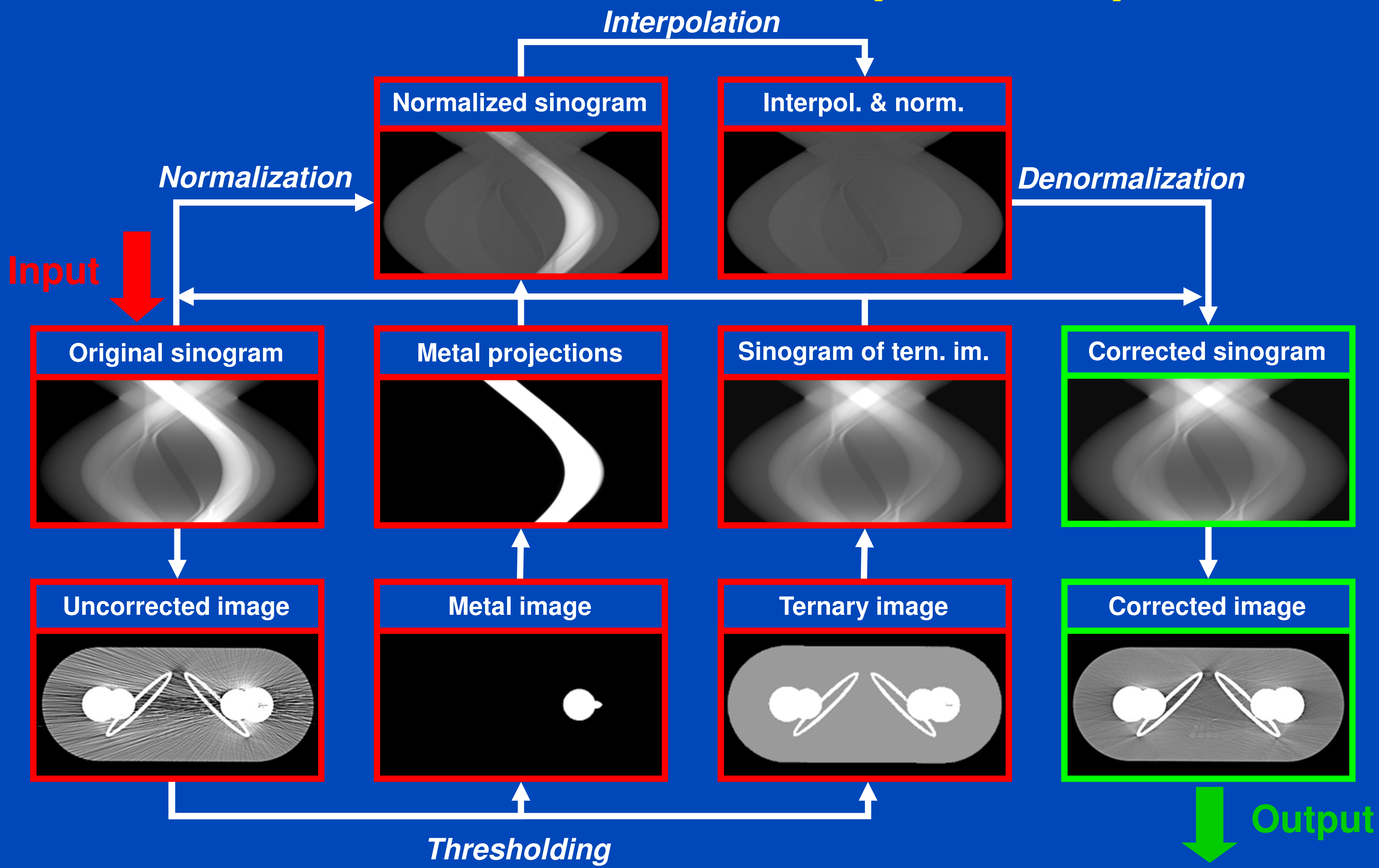

SIEMENS

Meyer, Raupach, Lell, Schmidt, and Kachelrieß, “Normalized metal artifact reduction (NMAR) in computed tomography”, Med. Phys. 37(10):5482-5493, 2012.

dkfz.

MAR1

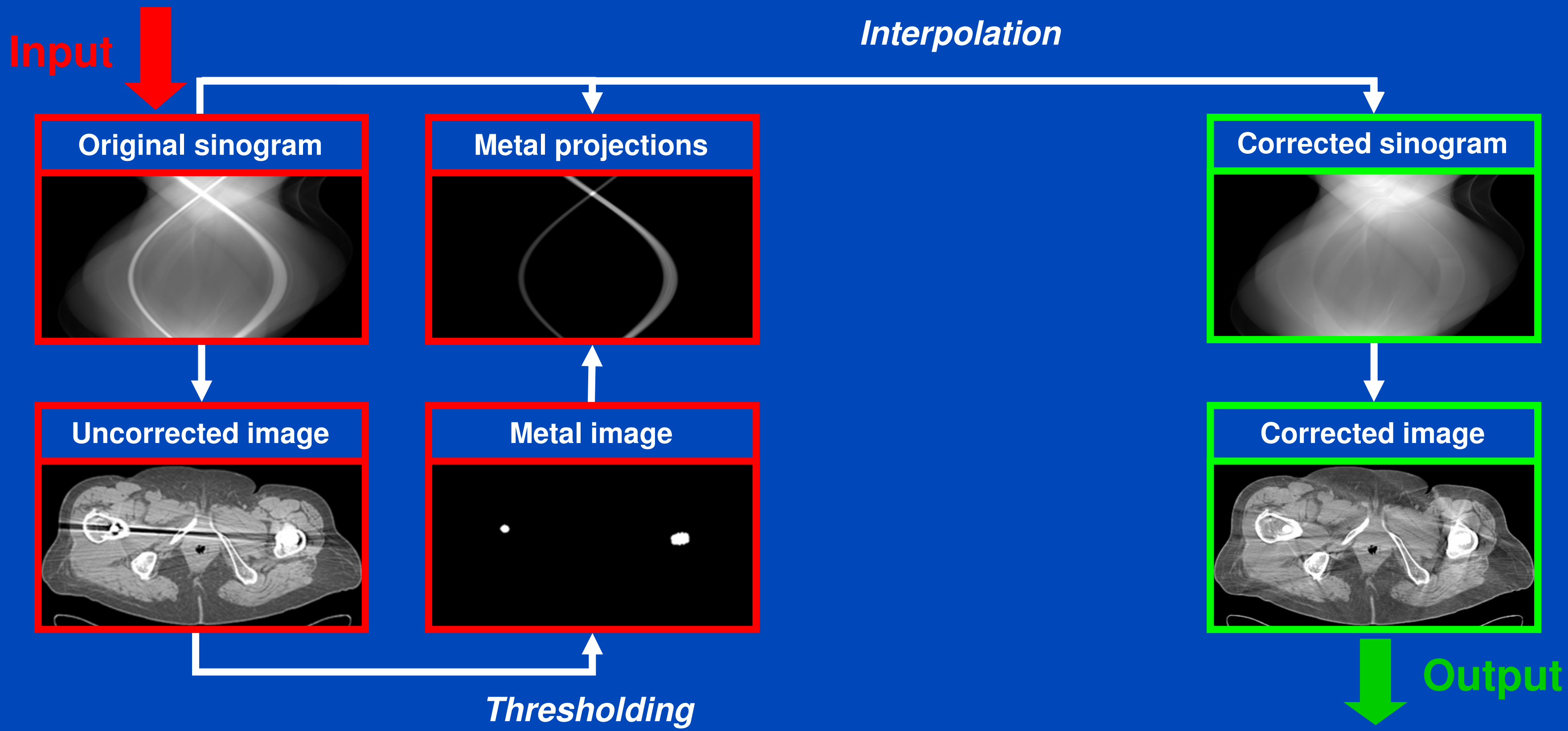
Input
Interpolation
Original sinogram
Metal projections
Corrected sinogram
Uncorrected image
Metal image
Corrected image
Thresholding
Output

Normalized MAR (NMAR)

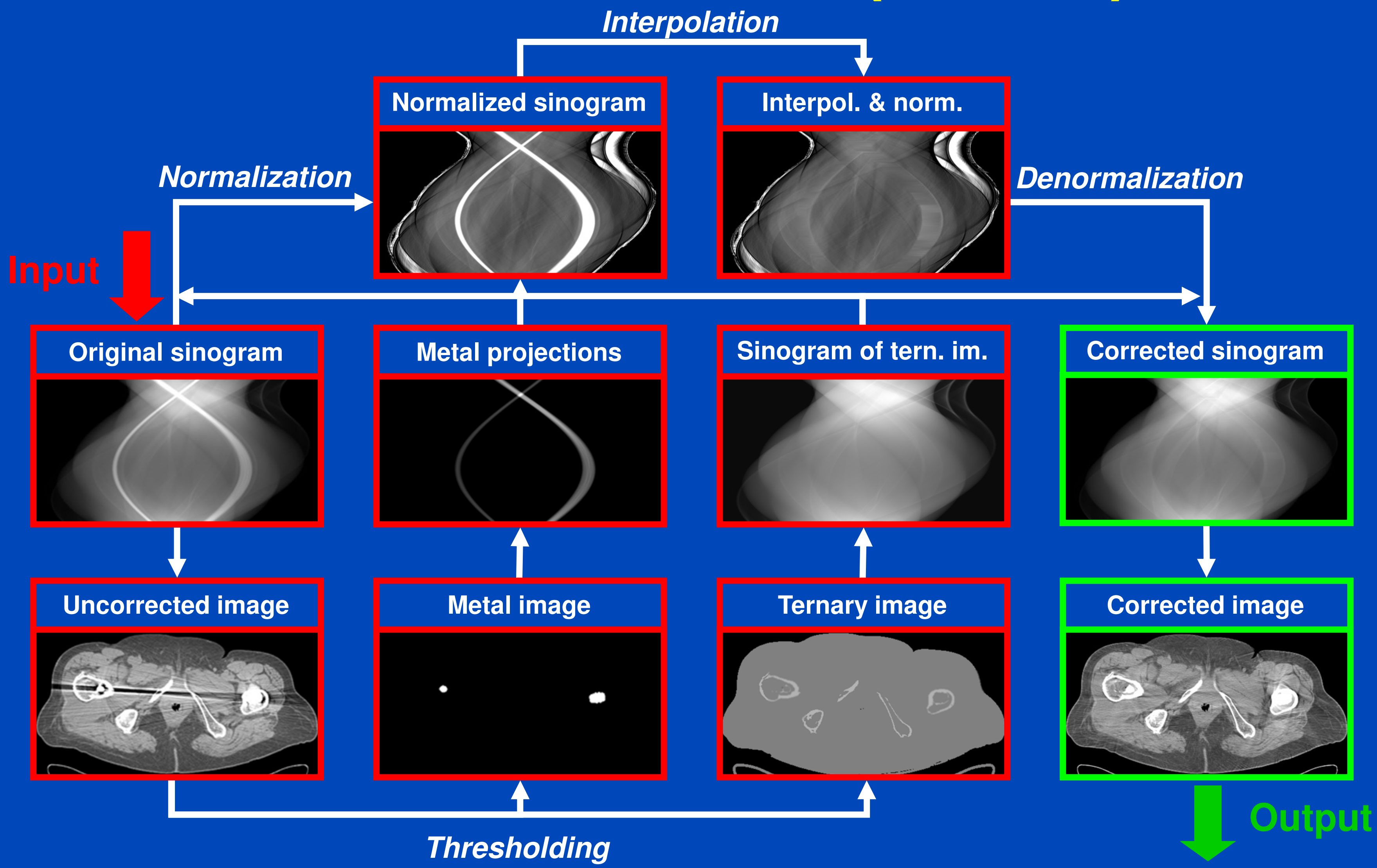

SIEMENS

Meyer, Raupach, Lell, Schmidt, and Kachelrieß, "Normalized metal artifact reduction (NMAR) in computed tomography", Med. Phys. 37(10):5482-5493, 2012.

dkfz.

Results and Comparison: Patient Data

Uncorrected

MAR1

MAR2

NMAR

Patient with hip implants, Sensation 16, 140 kV, (C=0/W=500)

SIEMENS

Meyer, Raupach, Lell, Schmidt, and Kachelrieß, "Normalized metal artifact reduction (NMAR) in computed tomography", Med. Phys. 37(10):5482-5493, 2012.

dkfz.

Results and Comparison: Patient Data

Uncorrected

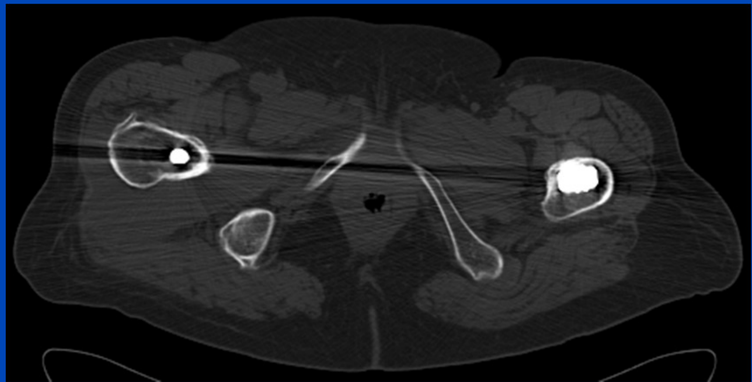

MAR1

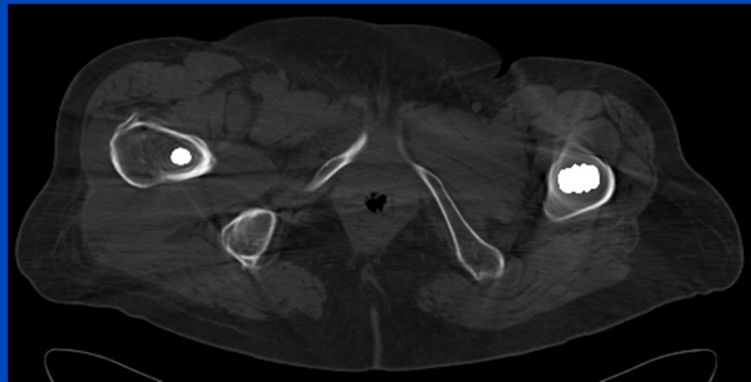

MAR2

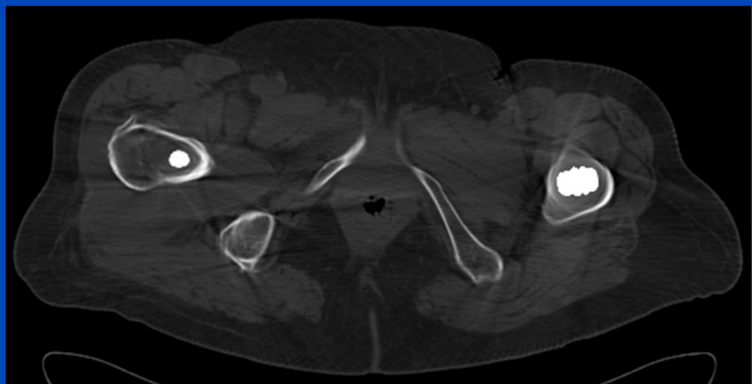

NMAR

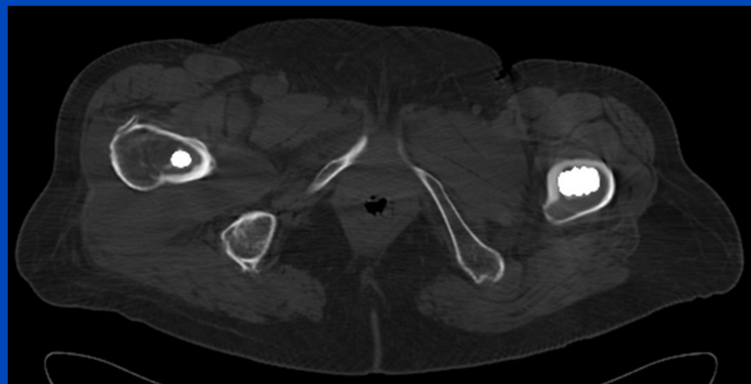

Patient with hip implants, Sensation 16, 140 kV, (C=500/W=1500)

Results and Comparison: Patient Data

Uncorrected | MAR1 | MAR2 | NMAR

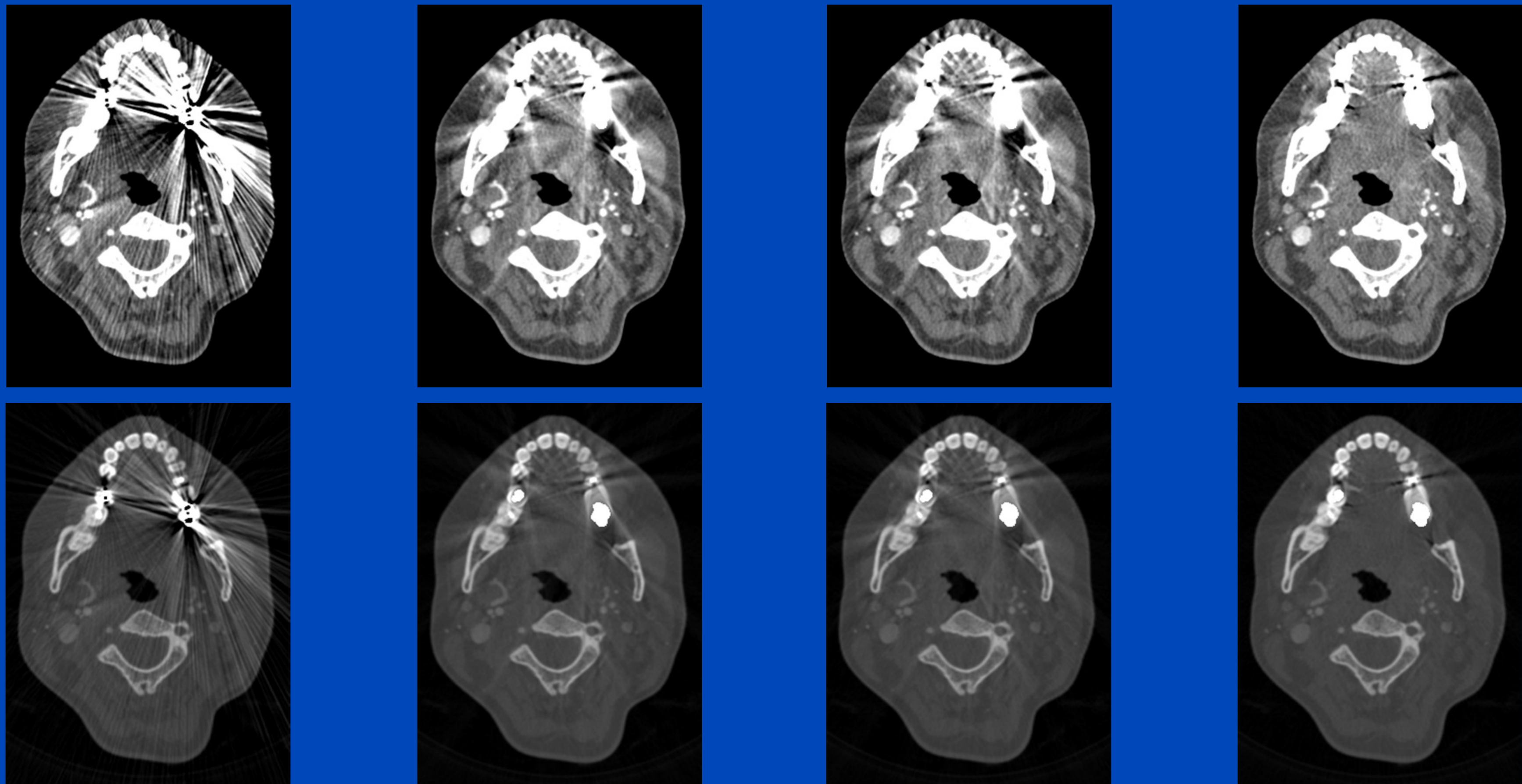

Patient dental fillings, slice 110, Somatom Definition Flash, pitch 0.9. Top and middle row: (C=100/W=750). Bottom row: (C=1000/W=4000)

Meyer, Raupach, Lell, Schmidt, and Kachelrieß, “Normalized metal artifact reduction (NMAR) in computed tomography”, Med. Phys. 37(10):5482-5493, 2012.

NMAR: Results

Uncorrected

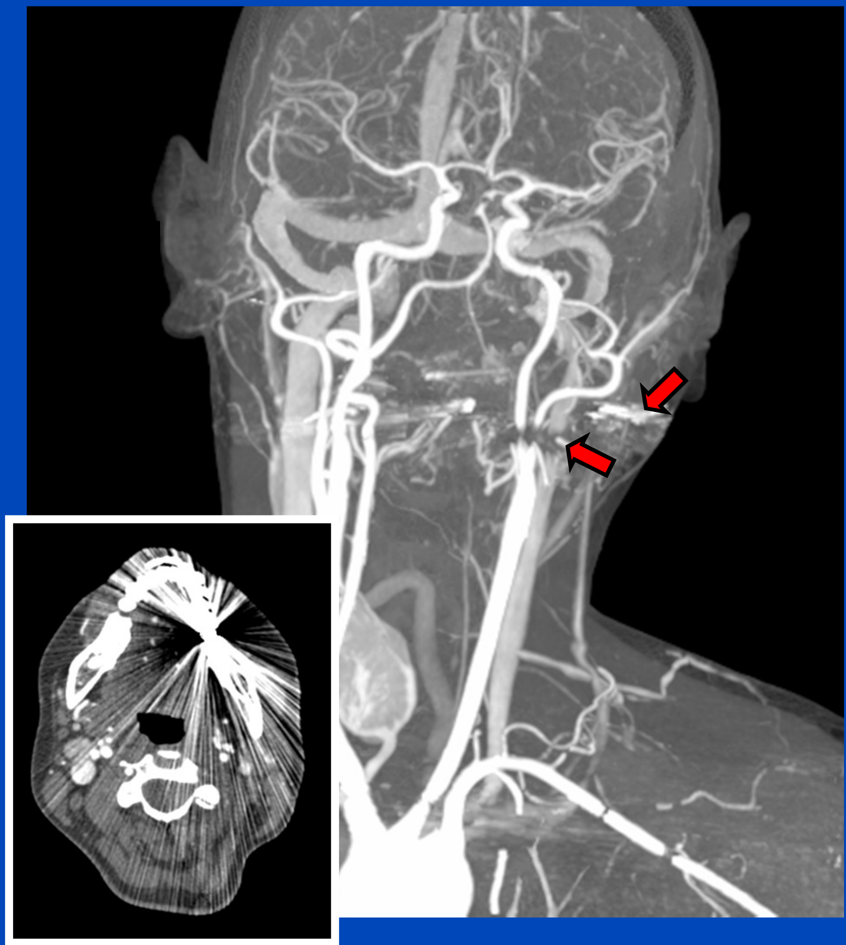

NMAR

Bone removal (with scanner software), (C=40/W=500).

Meyer, Raupach, Lell, Schmidt, and Kachelrieß, “Normalized metal artifact reduction (NMAR) in computed tomography”, Med. Phys. 37(10):5482-5493, 2012.

NMAR: Results

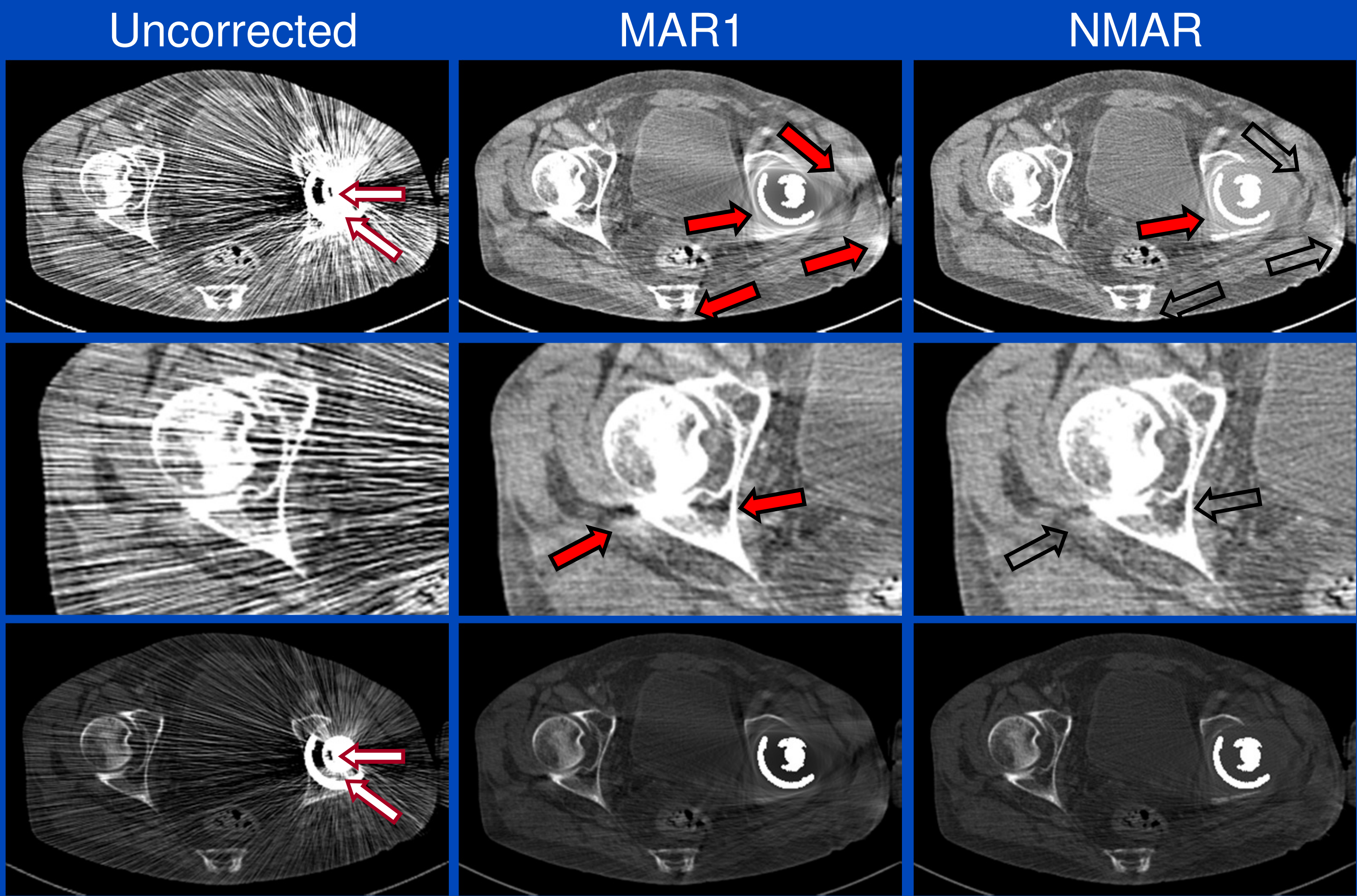

Patient with hip implant, Somatom Definition Flash, pitch 2.7.
Top and middle row: (C=0/W=500). Bottom row: (C=500/W=1500).

FSMAR: Scheme

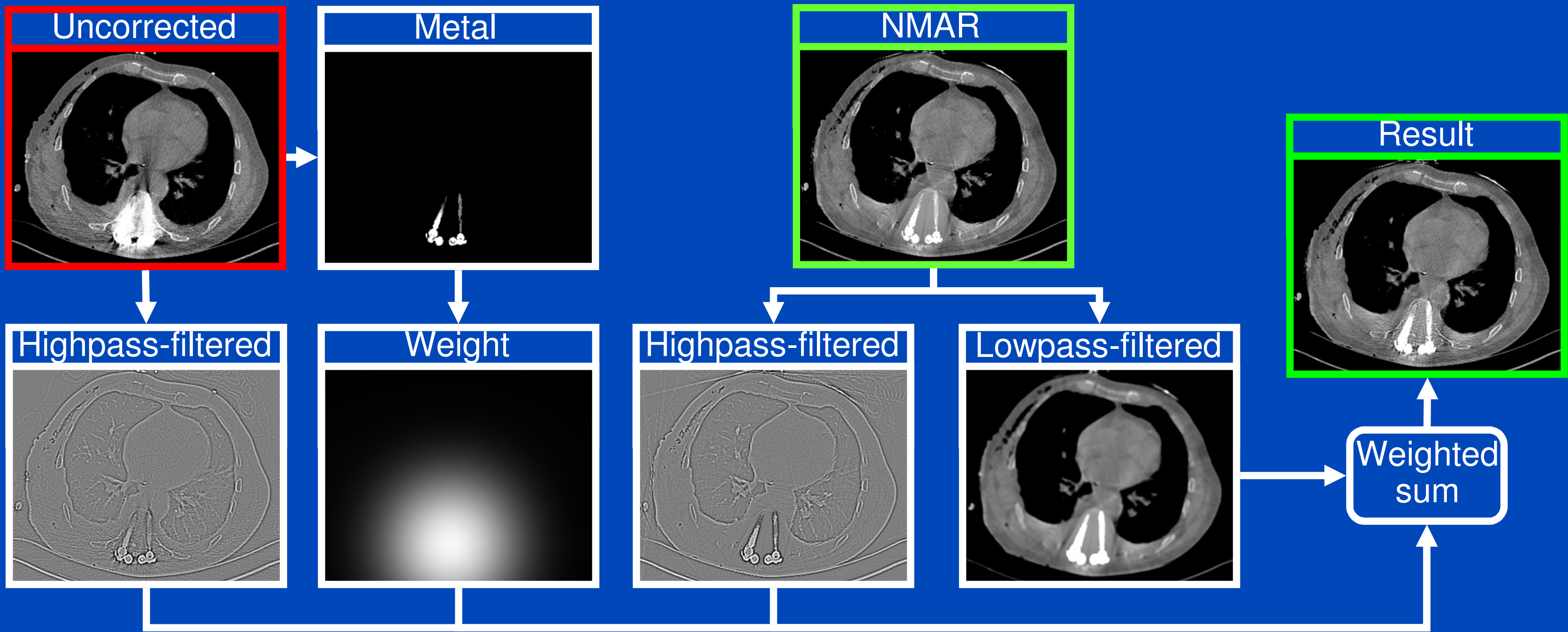

FSMAR: Results

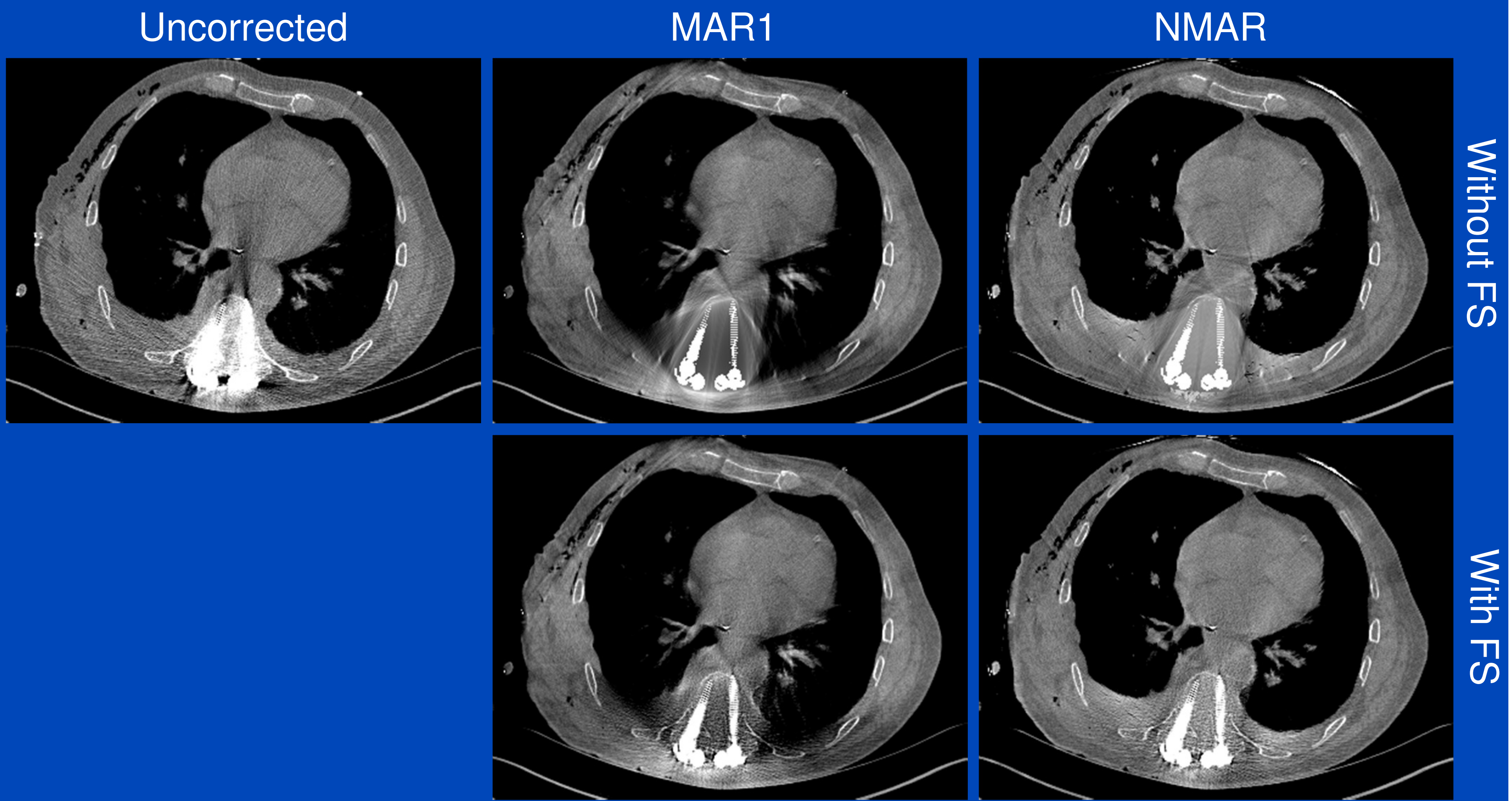

Patient with spine fixation, Somatom Definition, (C=100/W=1000).

SIEMENS

Meyer, Raupach, Lell, Schmidt, and Kachelrieß, “Frequency split metal artifact reduction (FSMAR) in computed tomography”, Med. Phys. 39(4):1904-1916, 2012.

dkfz.

FSMAR: Results

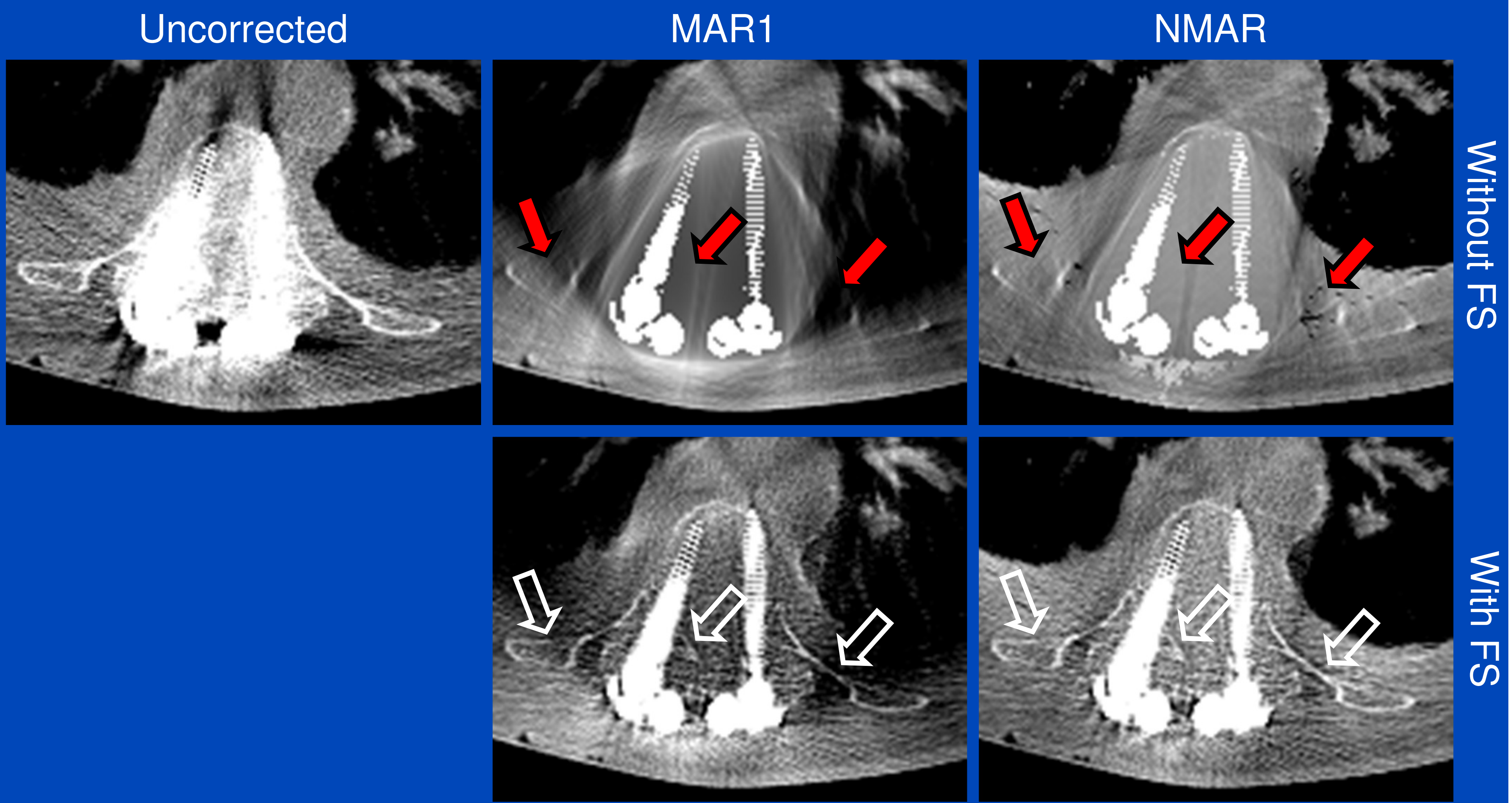

Patient with spine fixation, Somatom Definition, (C=100/W=1000).

FSMAR: Results

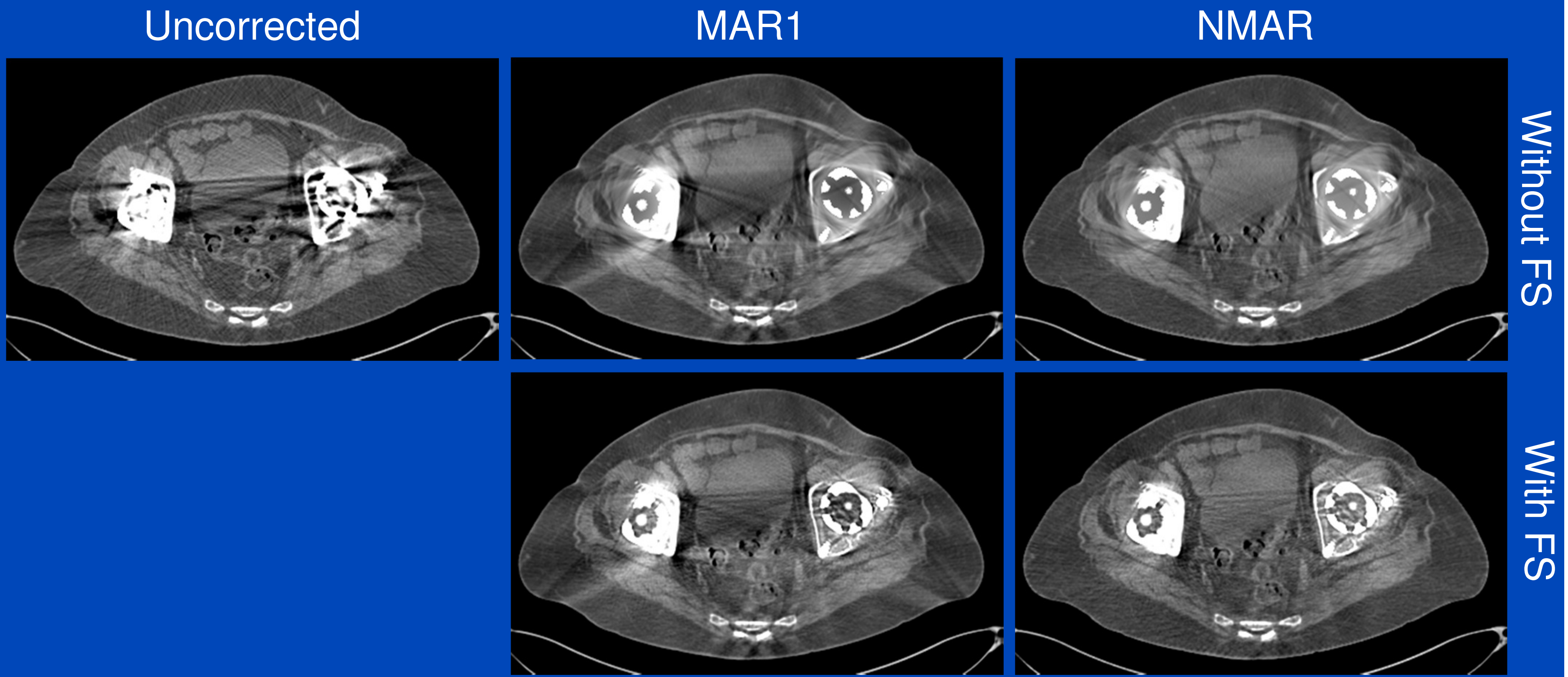

Patient with bilateral hip prosthesis, Somatom Definition Flash, (C=40/W=500).

FSMAR: Results

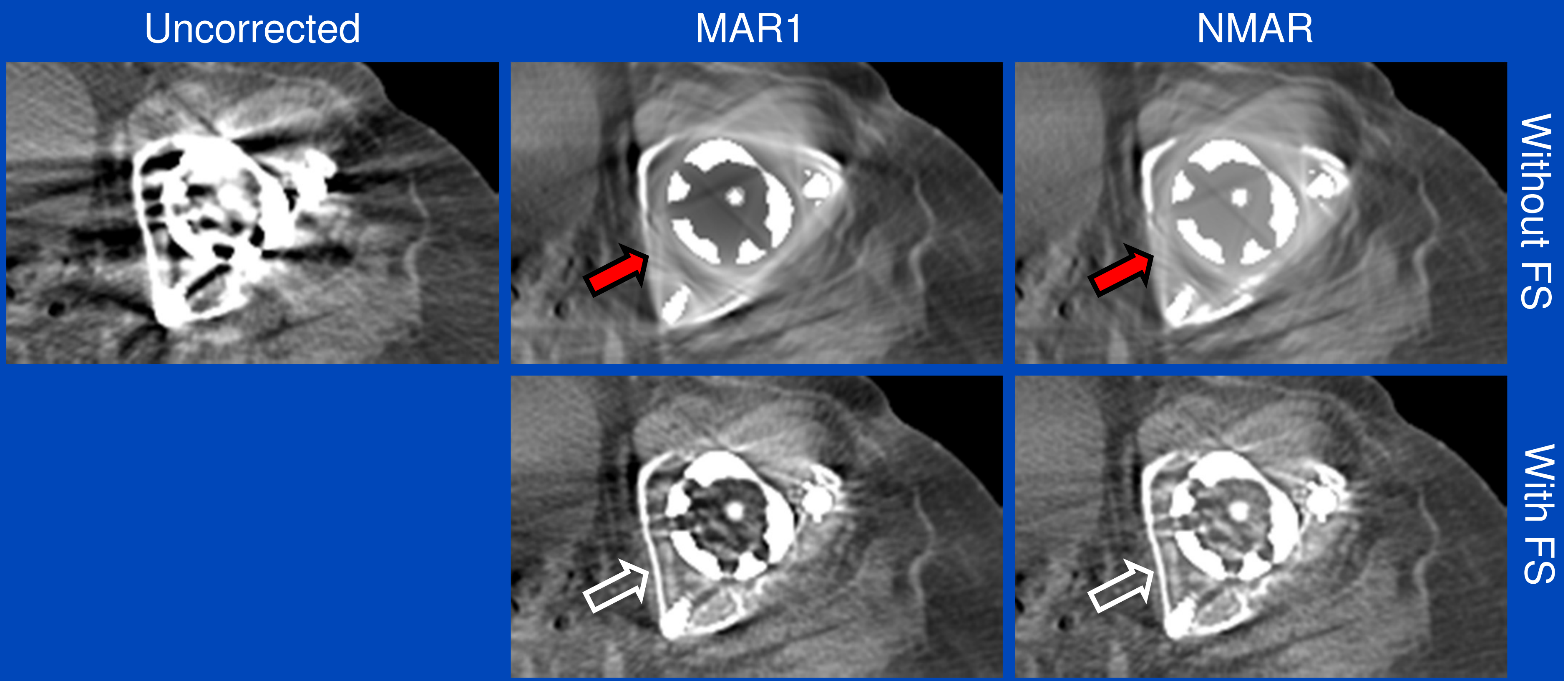

Patient with bilateral hip prosthesis, Somatom Definition Flash, (C=40/W=500).

Meyer, Raupach, Lell, Schmidt, and Kachelrieß, “Frequency split metal artifact reduction (FSMAR) in computed tomography”, Med. Phys. 39(4):1904-1916, 2012.

DECT Technology

- **In the clinic:**

– Multiple scans at different spectra	mid-range
– Dual source CT (DSCT), generations 2, and 3	high-end
– Fast tube voltage switching	high-end
– Dual layer sandwich detectors	high-end
– Split filter	mid-range

- **First prototypes:**

– Photon counting detectors (two or more energy bins)	high-end?

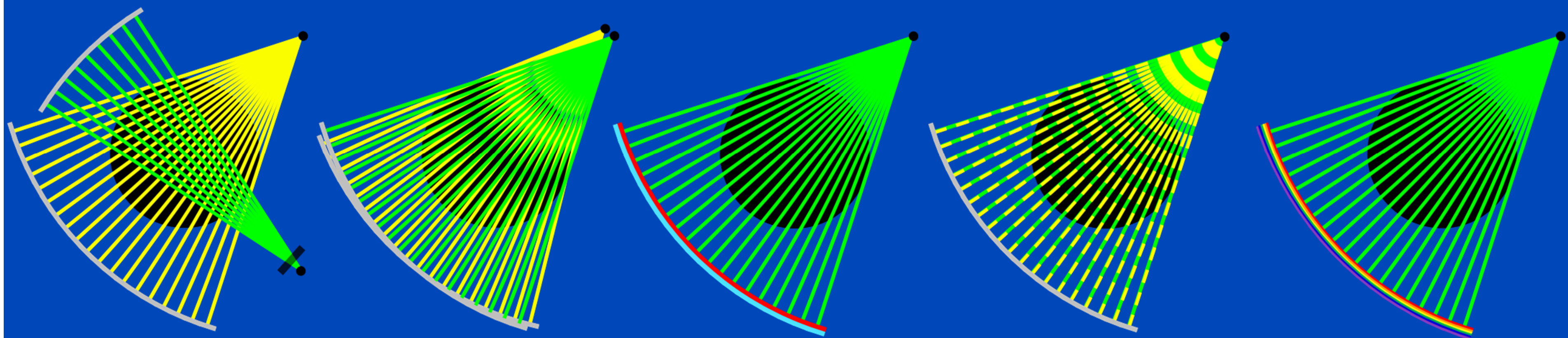

DECT Technology

- **DECT approaches in the clinic:**
  - **Dual source DECT (Siemens)**

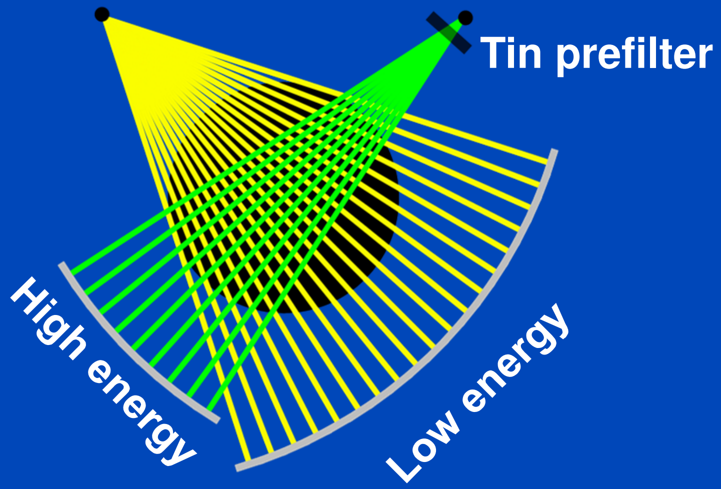

Siemens Somatom Force

DECT Technology

- **DECT approaches in the clinic:**
  - Dual source DECT (Siemens)
  - Fast tube voltage switching (GE)

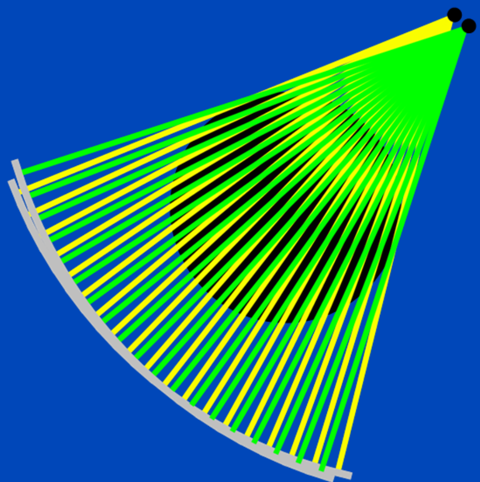

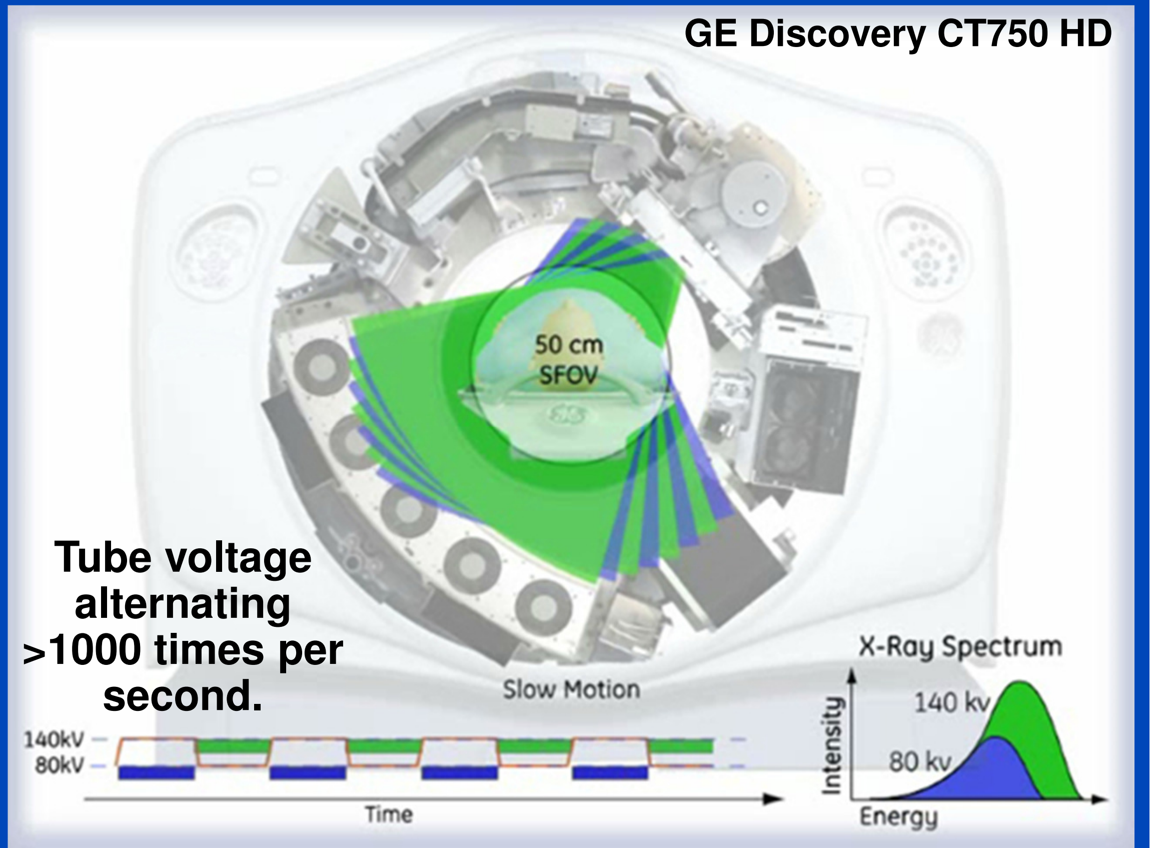

DECT Technology

- **DECT approaches in the clinic:**
  - Dual source DECT (Siemens)
  - Fast tube voltage switching (GE)

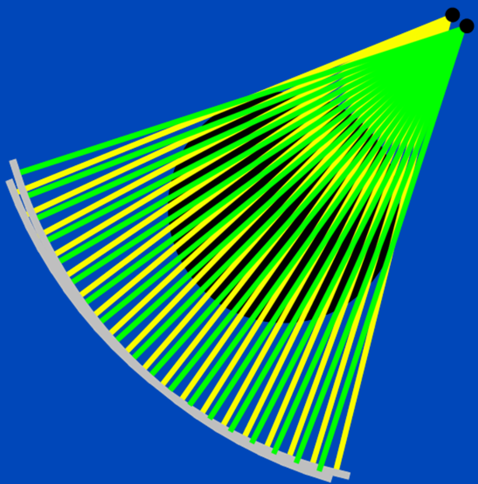

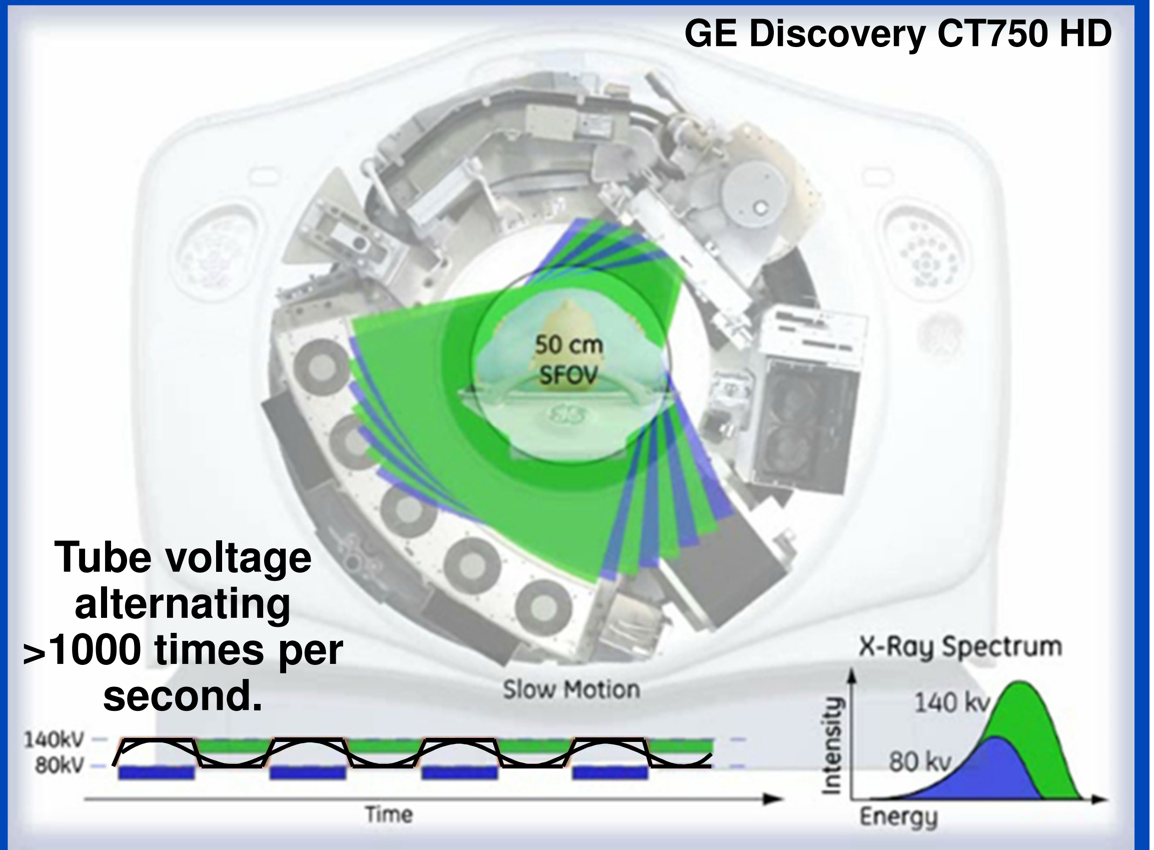

DECT Technology

- DECT approaches in the clinic:
  - Dual source DECT (Siemens)
  - Fast tube voltage switching (GE)
  - Dual layer (sandwich) detector (Philips)

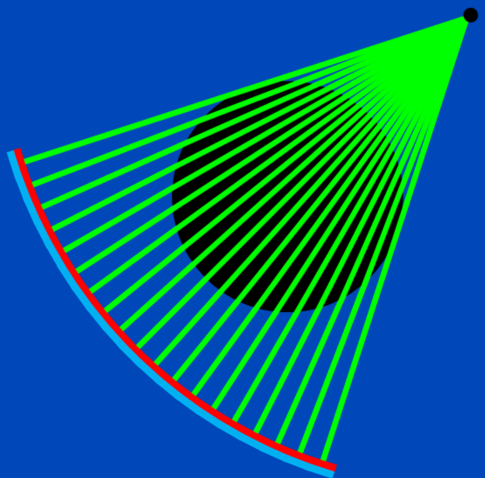

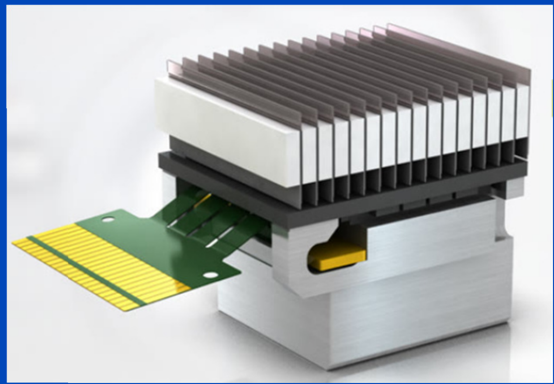

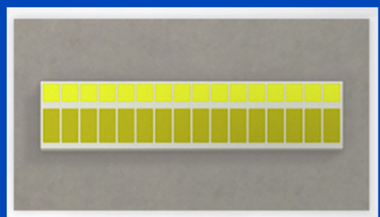

Philips IQon

DECT Technology

- **DECT approaches in the clinic:**
  - Dual source DECT (Siemens)
  - Fast tube voltage switching (GE)
  - Dual layer (sandwich) detector (Philips)
  - Split filter (Siemens)

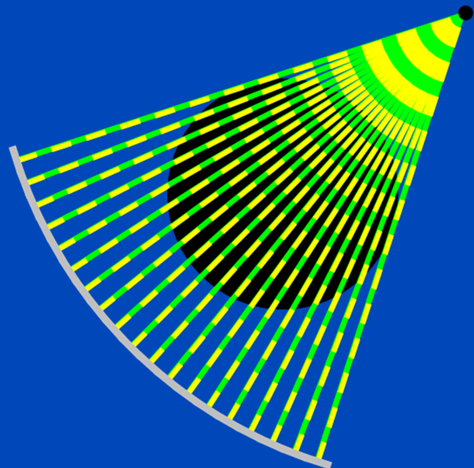

Siemens Definition Edge TwinBeam

DECT Technology

- **DECT approaches in the clinic:**
  - Dual source DECT (Siemens)
  - Fast tube voltage switching (GE)
  - Dual layer (sandwich) detector (Philips)
  - Split filter (Siemens)
- **First prototype systems**
  - Photon counting detector, multiple energy bins

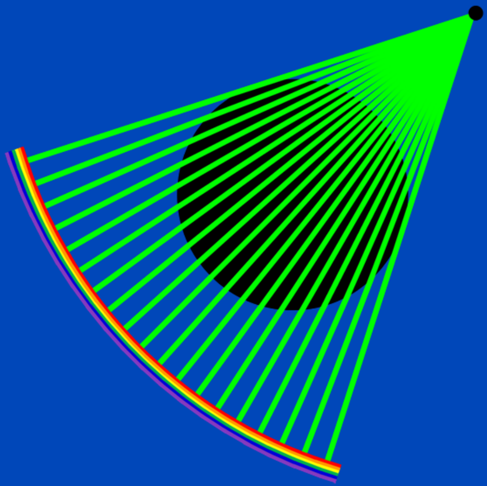

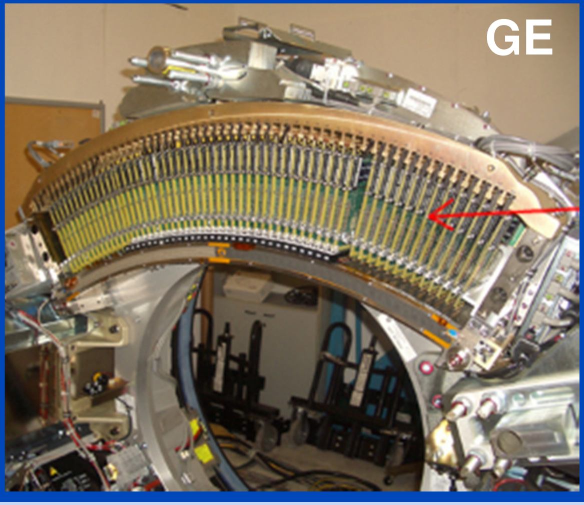

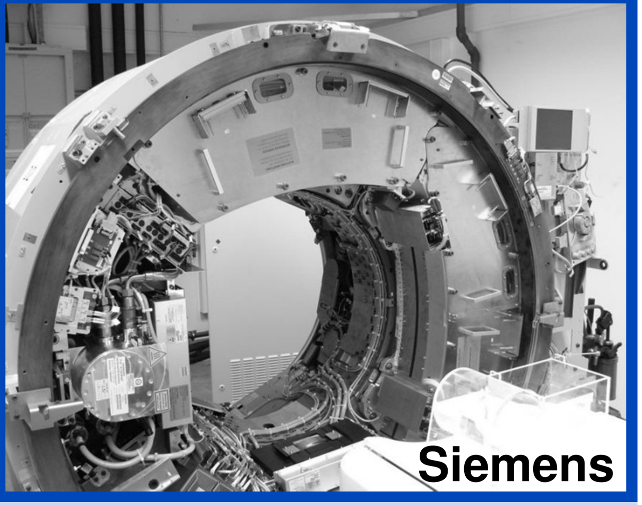

Examples

(Slide Courtesy of Siemens Healthcare)

DE bone removal

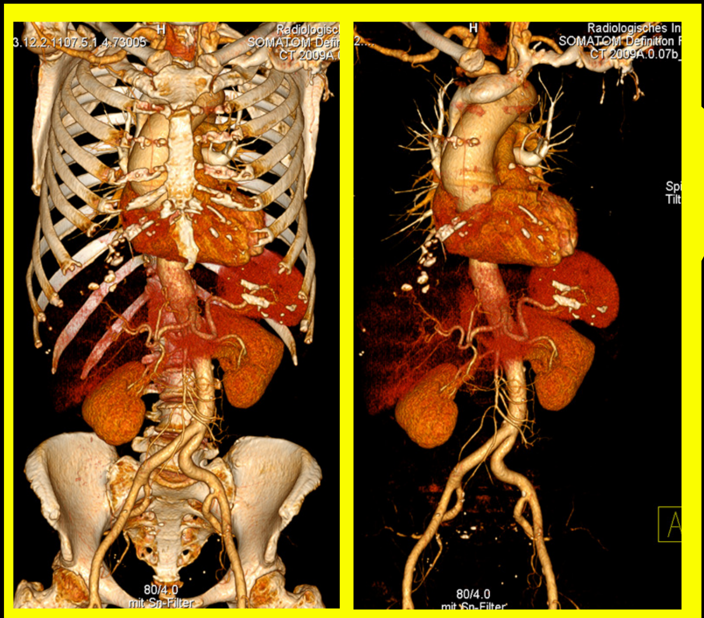

Single DECT Scan

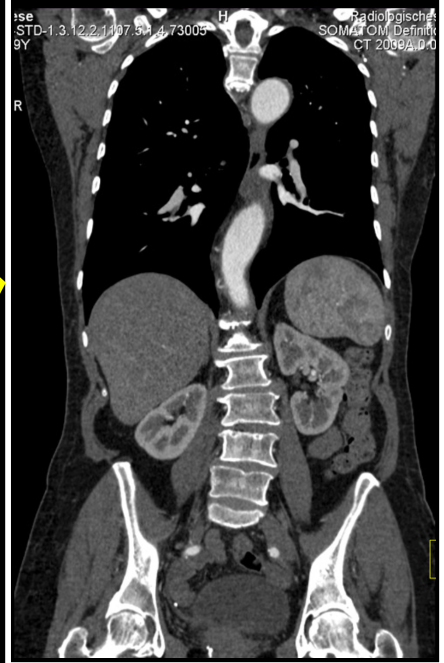

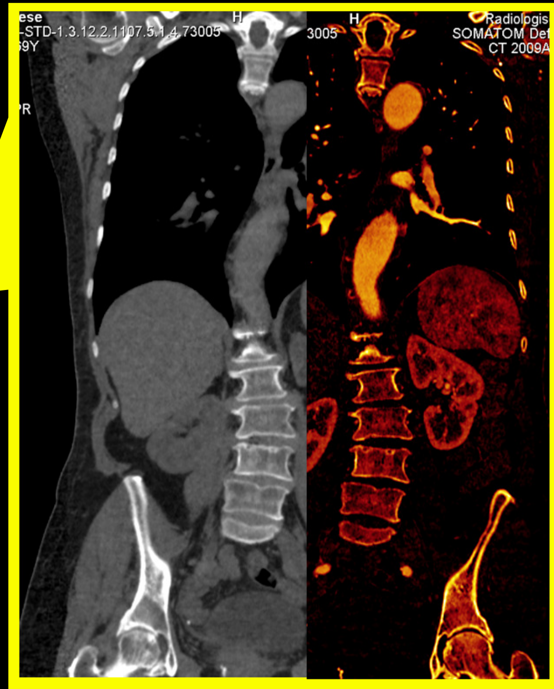

Virtual non-contrast and Iodine image

Dual Energy whole body CTA: 100/140 Sn kV @ 0.6mm

Courtesy of Friedrich-Alexander University Erlangen-Nürnberg

DECT Today: Widely Available via DSCT

(Slide Courtesy of Siemens Healthcare)

- **“Spectroscopy“: more specific tissue characterization**
  → Detection and visualization of calcium, iron, uric acid, …..

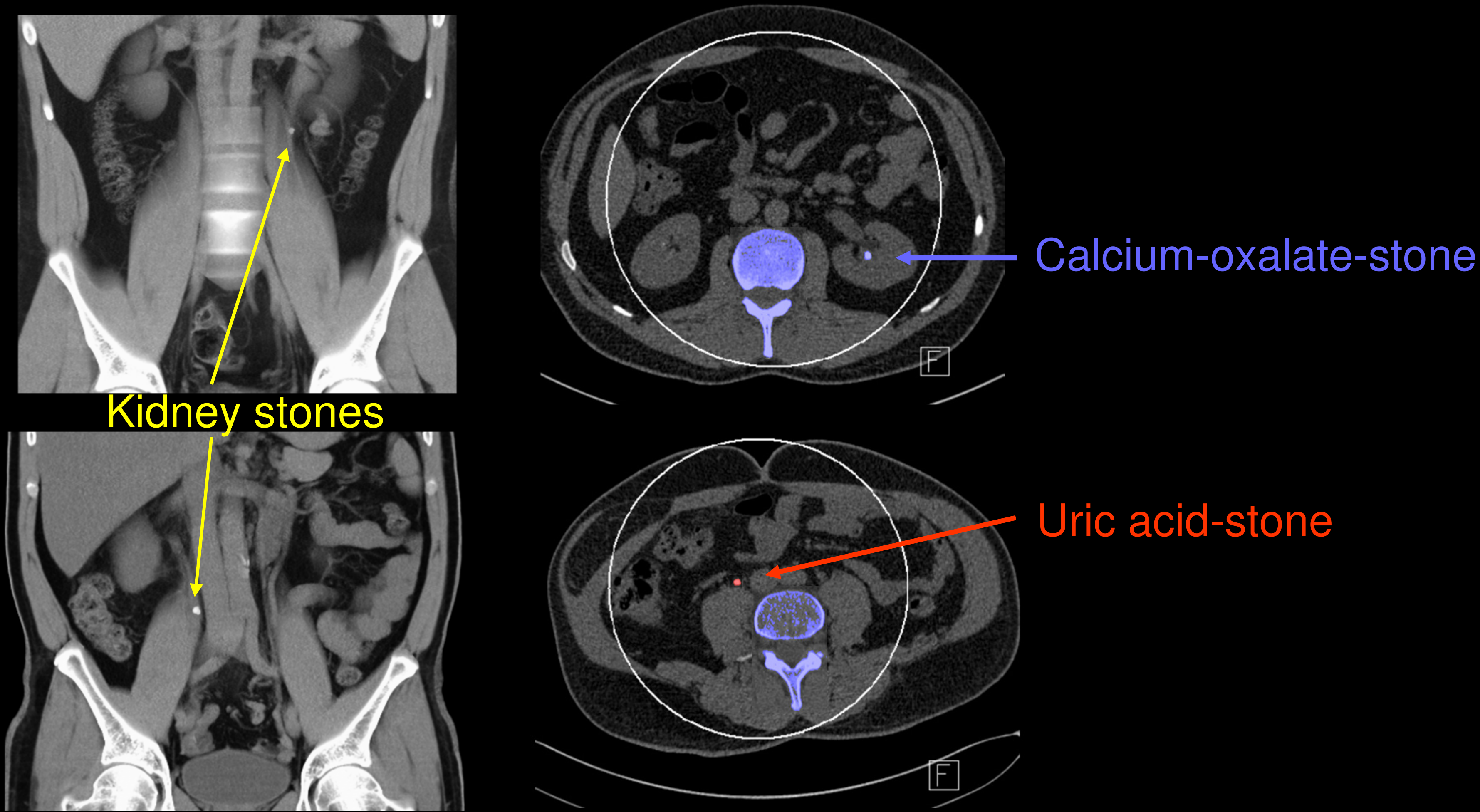

Courtesy of Klinikum Großhadern, LMU München

DECT Today: Widely Available via DSCT

(Slide Courtesy of Siemens Healthcare)

- **New approach: Detection, visualization and quantification of iodine**
  → Visualization of perfusion defects in the lung parenchyma

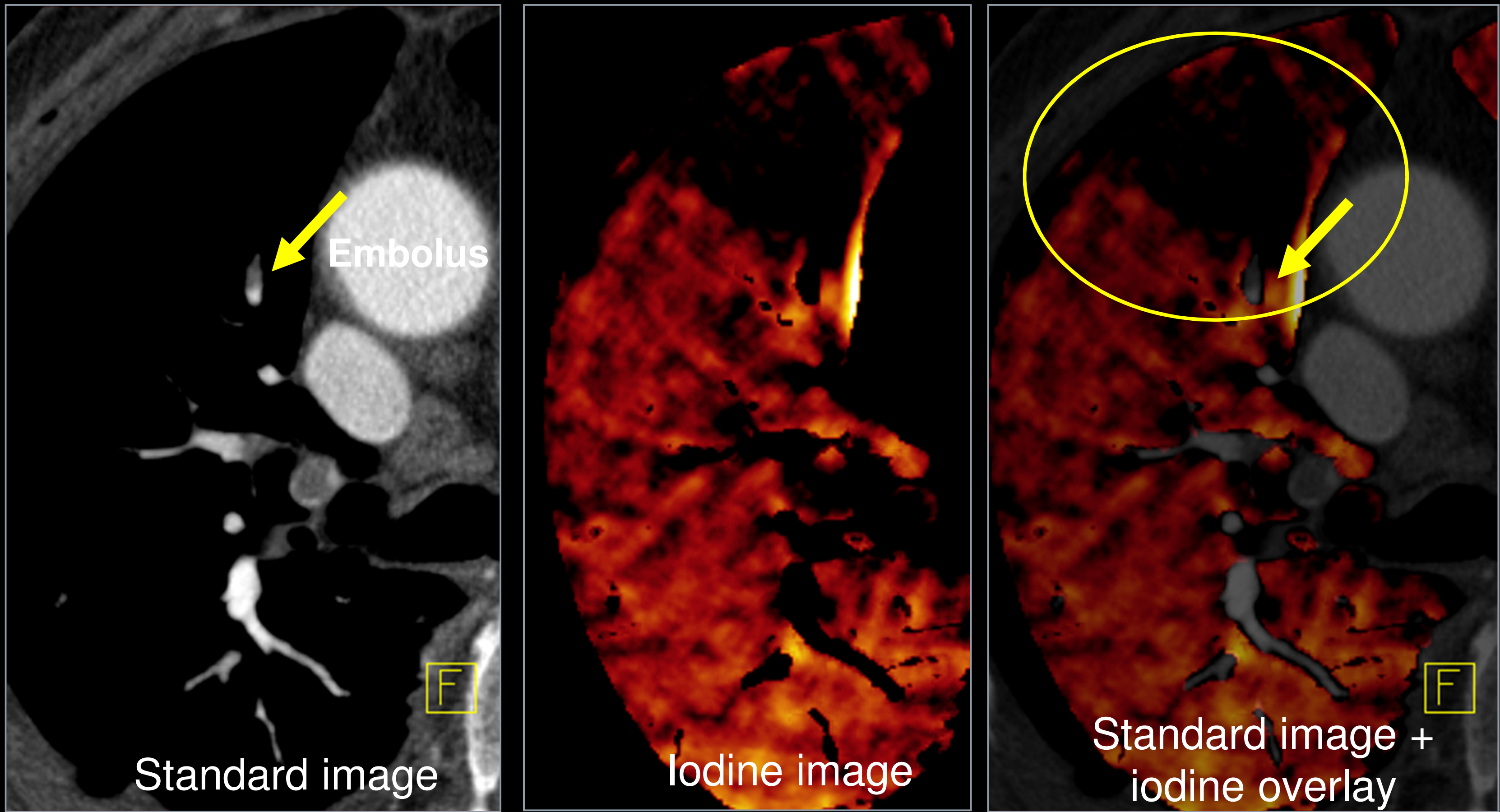

Courtesy of Hopital Calmette, Lille, France

Image-based Techniques
Mixed Image (Linear)

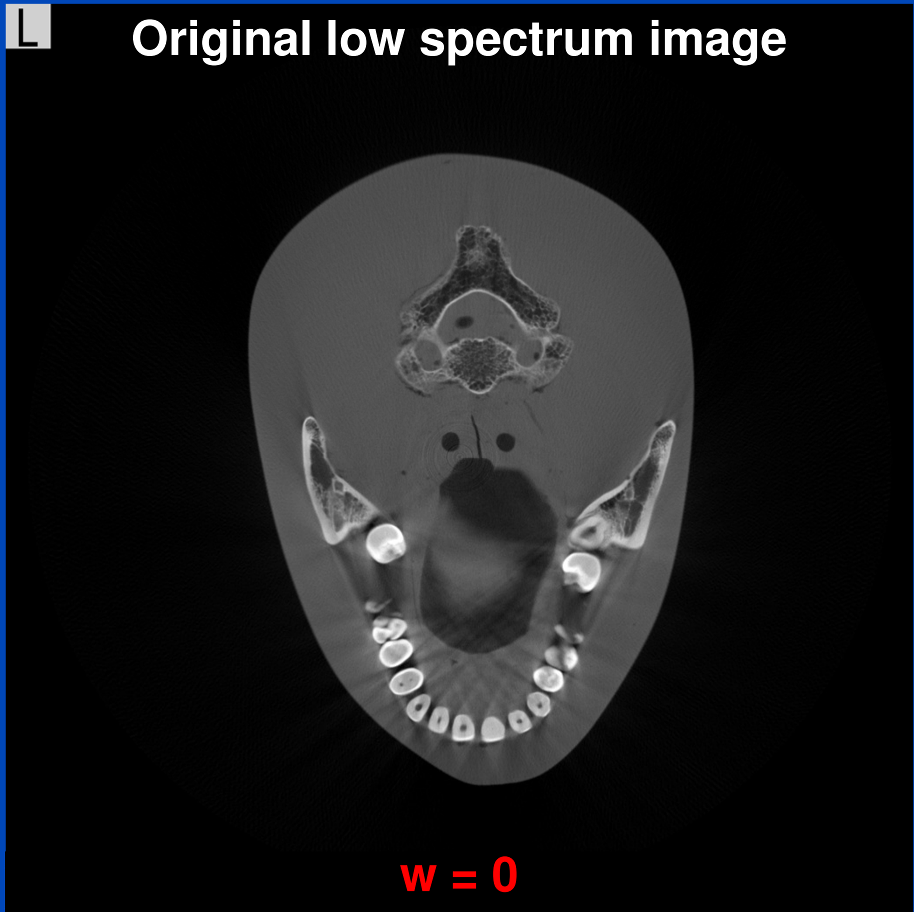

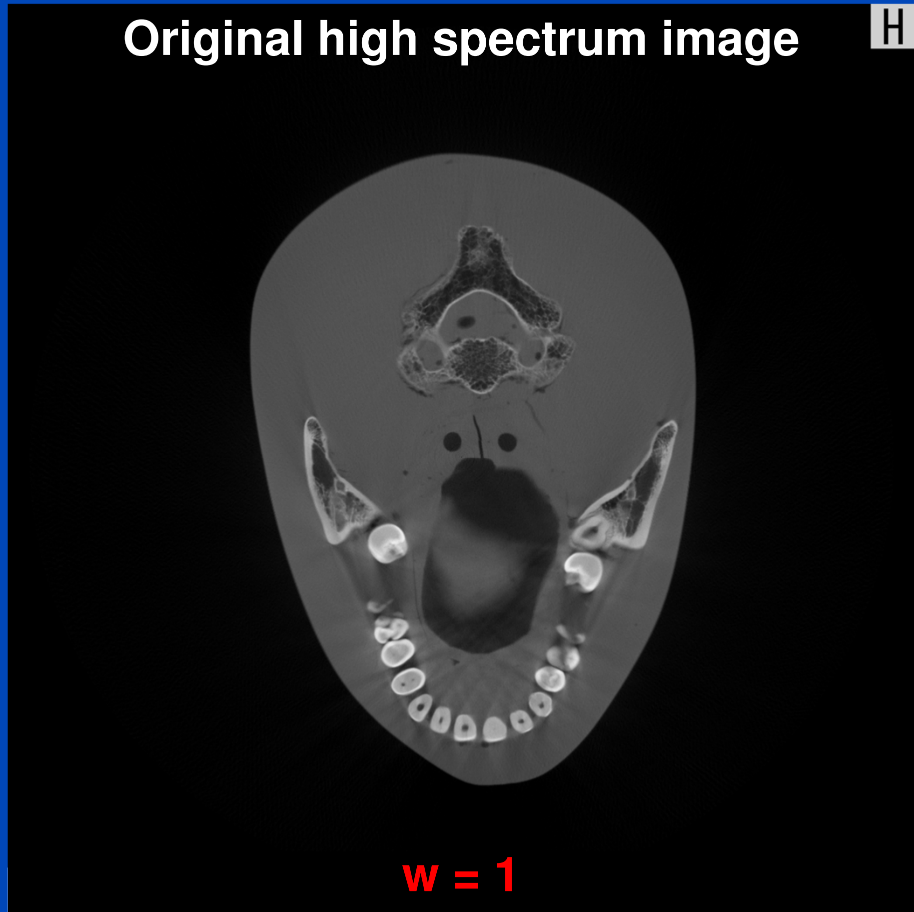

C/W: 500/3000 HU

Image-based Techniques
Mixed Image (Linear)

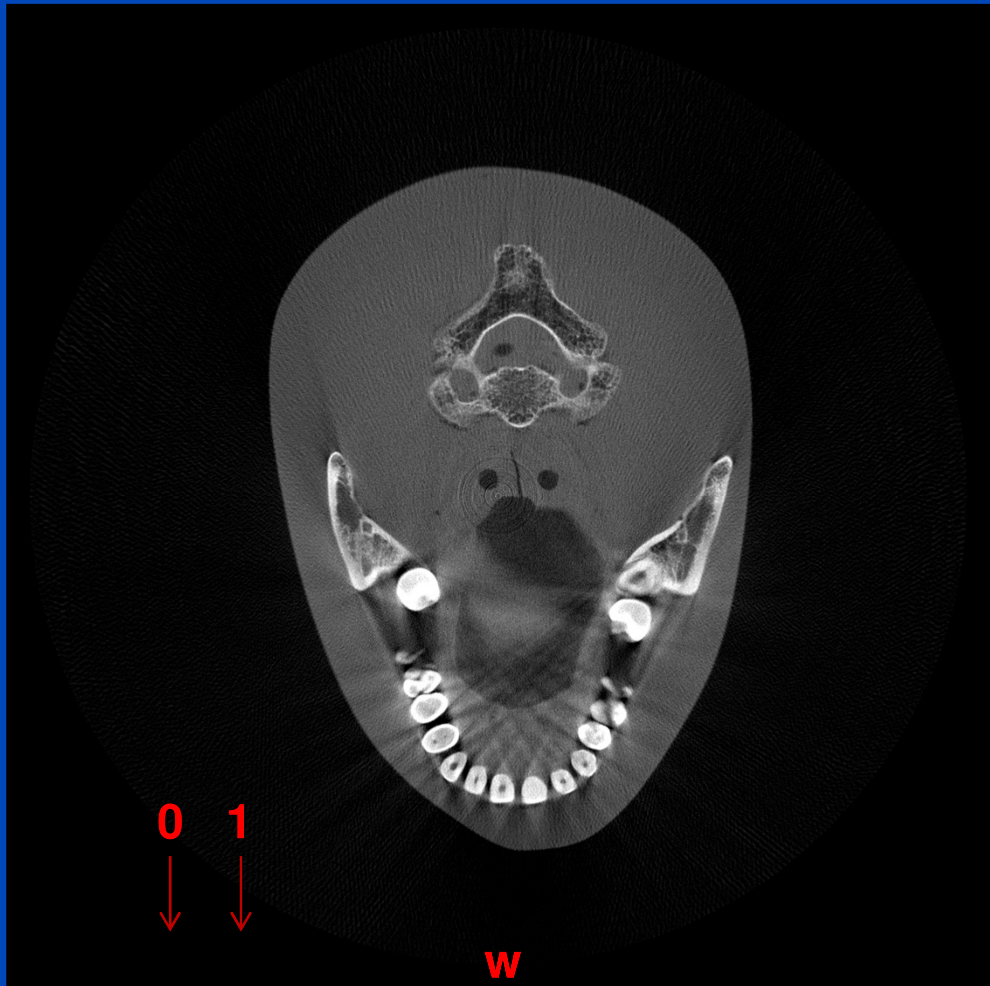

-2 w 10

Resulting mixed Image from low to high-energy image

dkfz.

DECT
and Pseudo Monochromatic Imaging

Pseudo monochromatic imaging is a linear combination of DECT f_L and f_H: $f_\alpha = (1-\alpha)\, f_L + \alpha\, f_H$

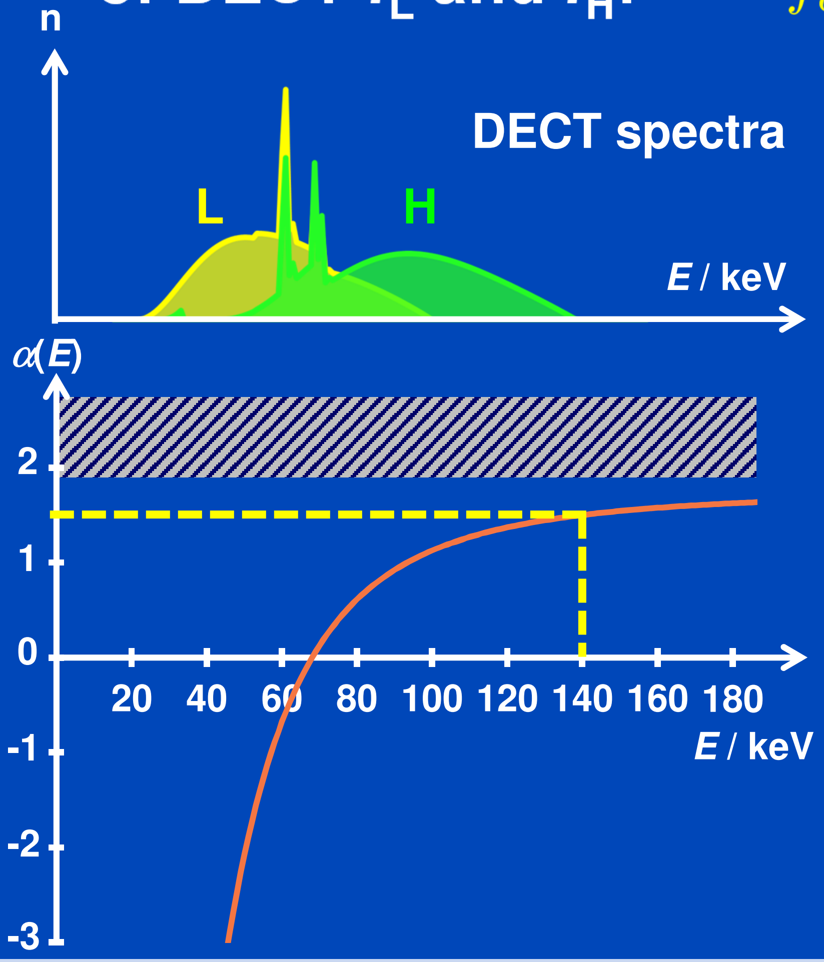

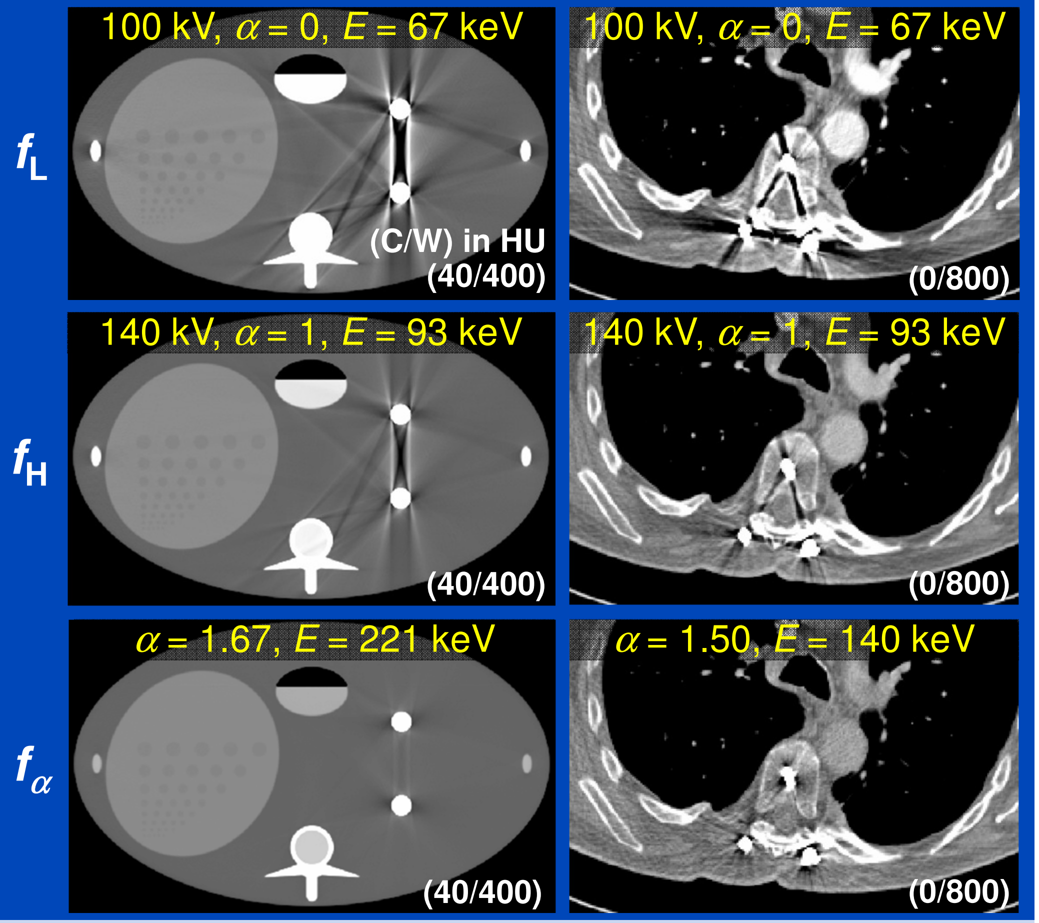

Monochromatic Imaging

- **Pseudo monochromatic imaging** $f_\alpha = (1-\alpha)\, f_\mathrm{L} + \alpha\, f_\mathrm{H}$
  - Image-based postprocessing
  - Provided in clinical DECT scanners
- **Virtual monochromatic imaging** $g_\alpha = (1-\alpha)\, g_\mathrm{L} + \alpha\, g_\mathrm{H}$
  - Rawdata-based preprocessing
  - Constraint on consistent rawdata
- **True monochromatic imaging**
  - Would require monochromatic x-rays – not applicable here

$$q_\mathrm{L} = -\ln \int dE\, w_\mathrm{L}(E)\, e^{-p_\mathrm{W}\mu_\mathrm{W}(E) - p_\mathrm{B}\mu_\mathrm{B}(E)}$$
$$q_\mathrm{H} = -\ln \int dE\, w_\mathrm{H}(E)\, e^{-p_\mathrm{W}\mu_\mathrm{W}(E) - p_\mathrm{B}\mu_\mathrm{B}(E)}$$

Series Expansion

- **Series expansion of the polychromatic attenuation:**

$$q_j = -\ln\int dE\, w_j(E)\, e^{-p_\mathrm{W}\mu_\mathrm{W}(E) - p_\mathrm{B}\mu_\mathrm{B}(E)} = \sum_{kl} c_{jkl} p_\mathrm{W}^k p_\mathrm{B}^l$$

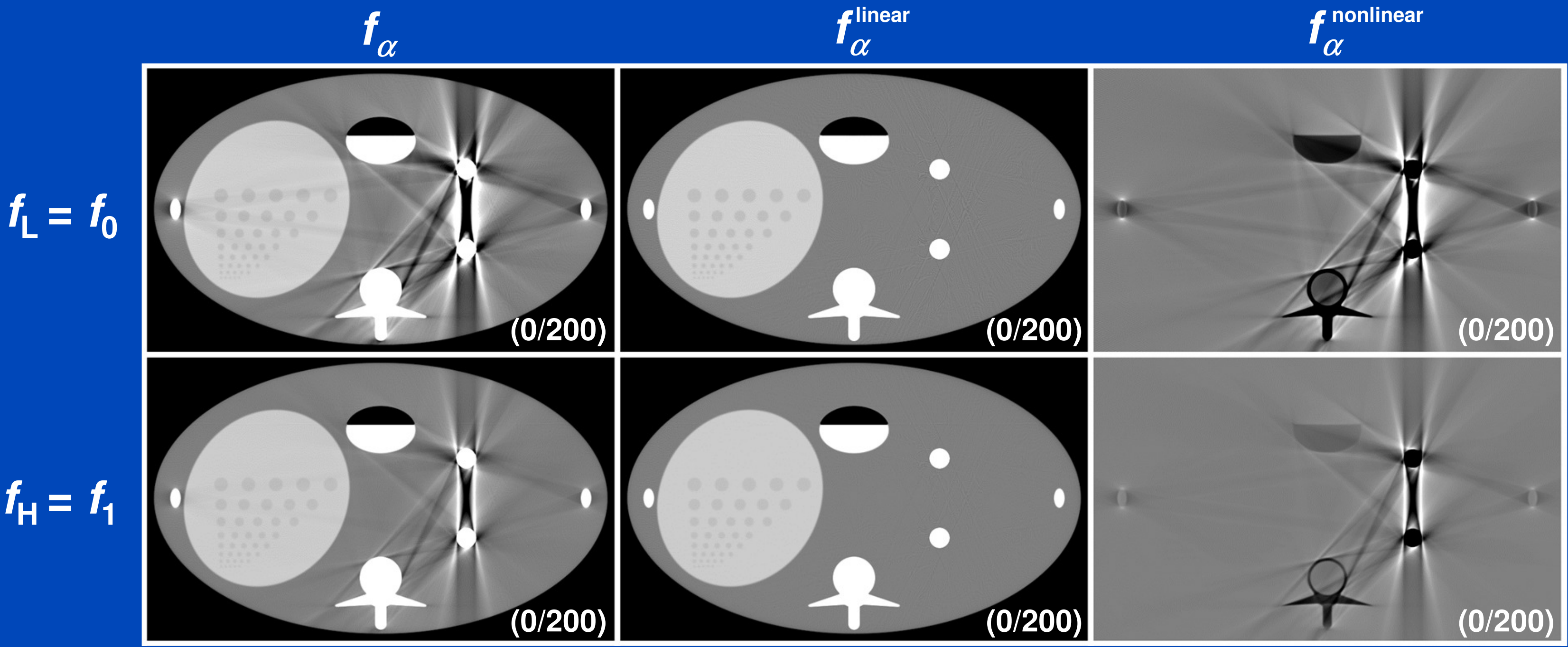

also reduces scatter artifacts →

pseudo monochromatic
image-based processing

virtual monochromatic
rawdata-based processing

← *works well in scatter-free situations*

$f_L = f_0$ (E = 67 keV)

maximum CNR

$f_H = f_1$ (E = 93 keV)

$f_{1.67}$ (E = 221 keV)

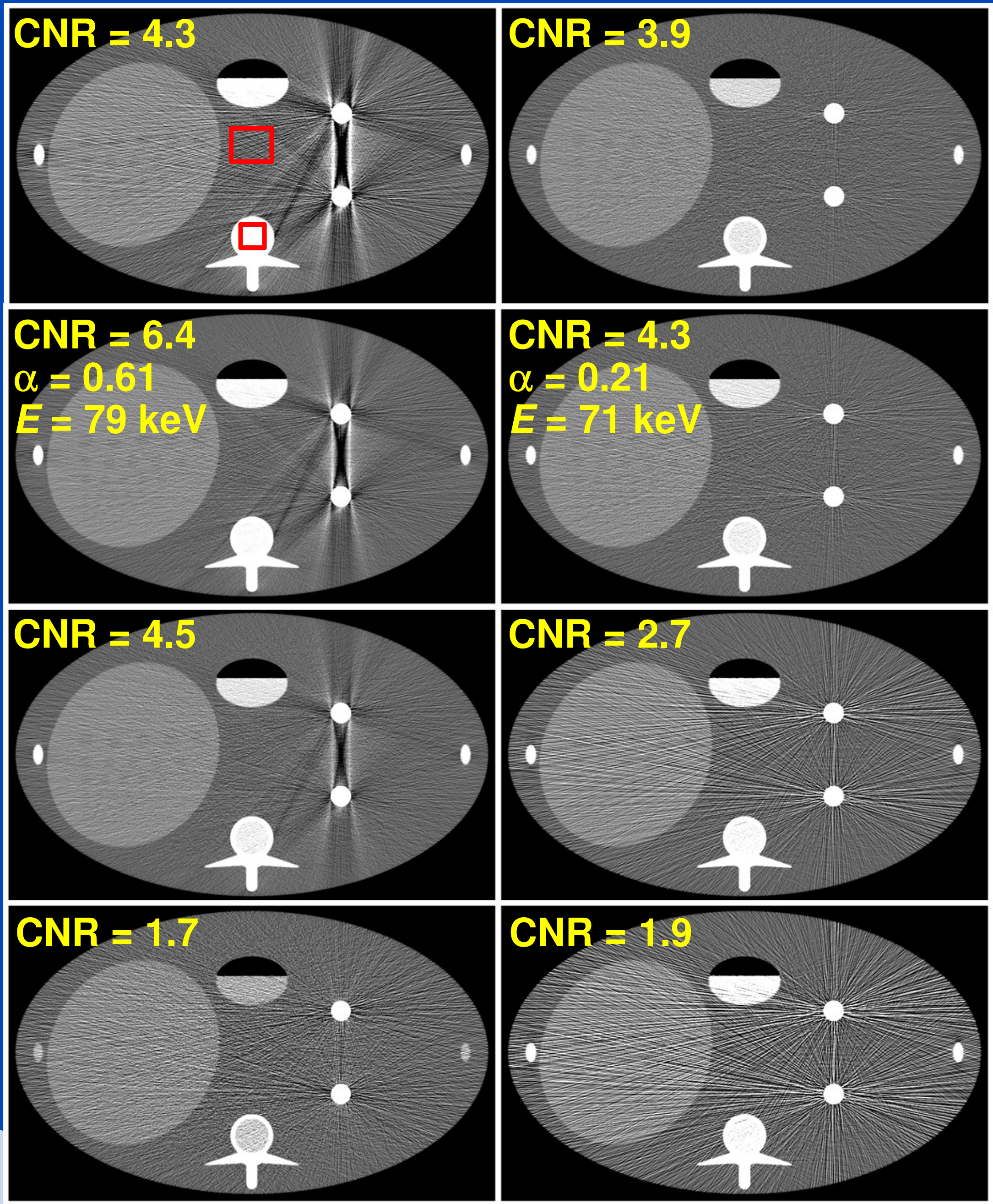

C = 40 HU, W = 400 HU

Patient Data Set – Pseudo Monochromatic Imaging

z = -723 mm　　z = -792 mm

$f_L = f_0$
(E = 67 keV)

$f_H = f_1$
(E = 93 keV)

$f_{1.55}$
(E = 154 keV)

$f_{2.00}$
(E = --- keV)

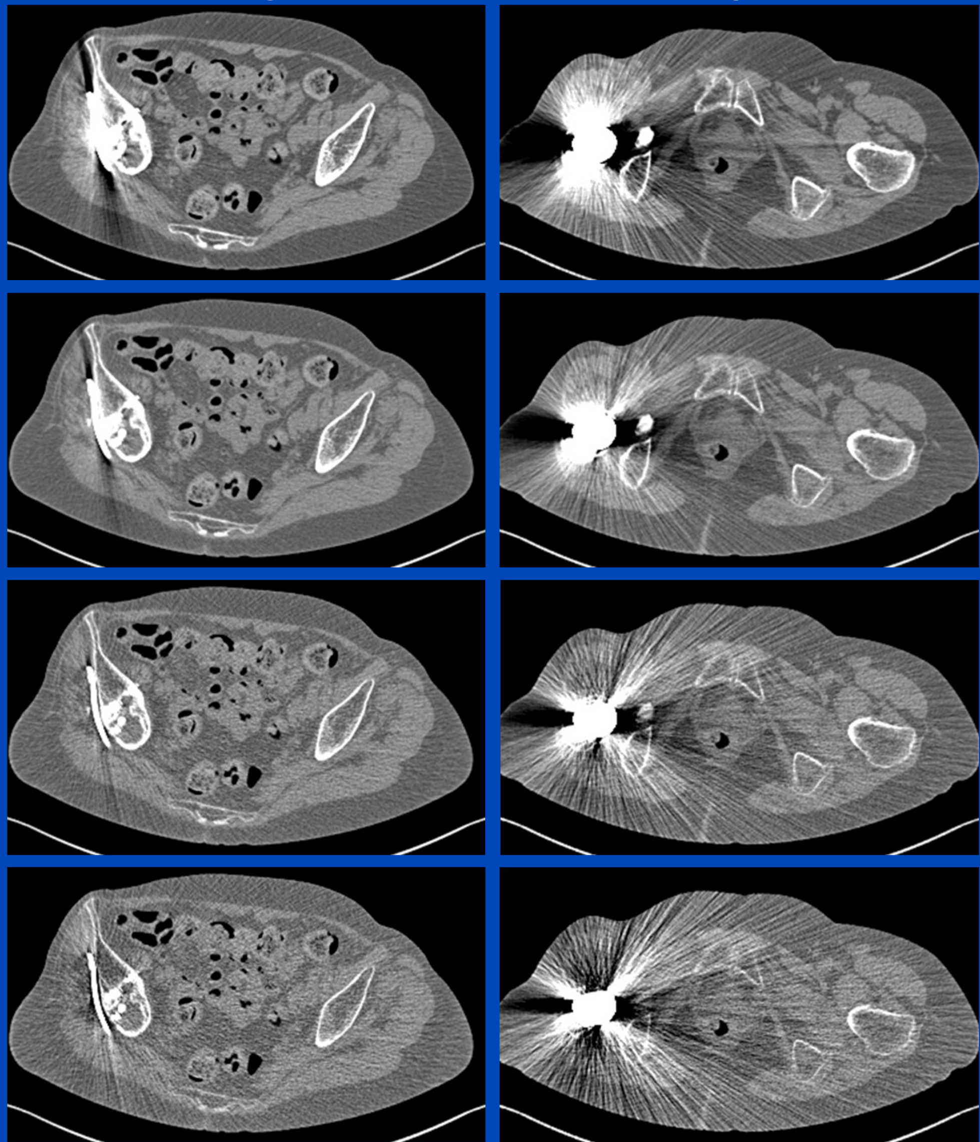

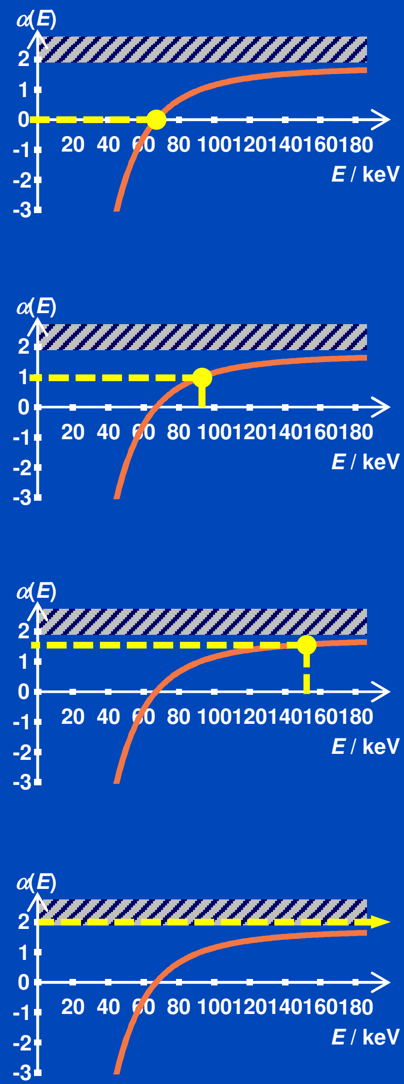

C = 0 HU, W = 800 HU

dkfz.

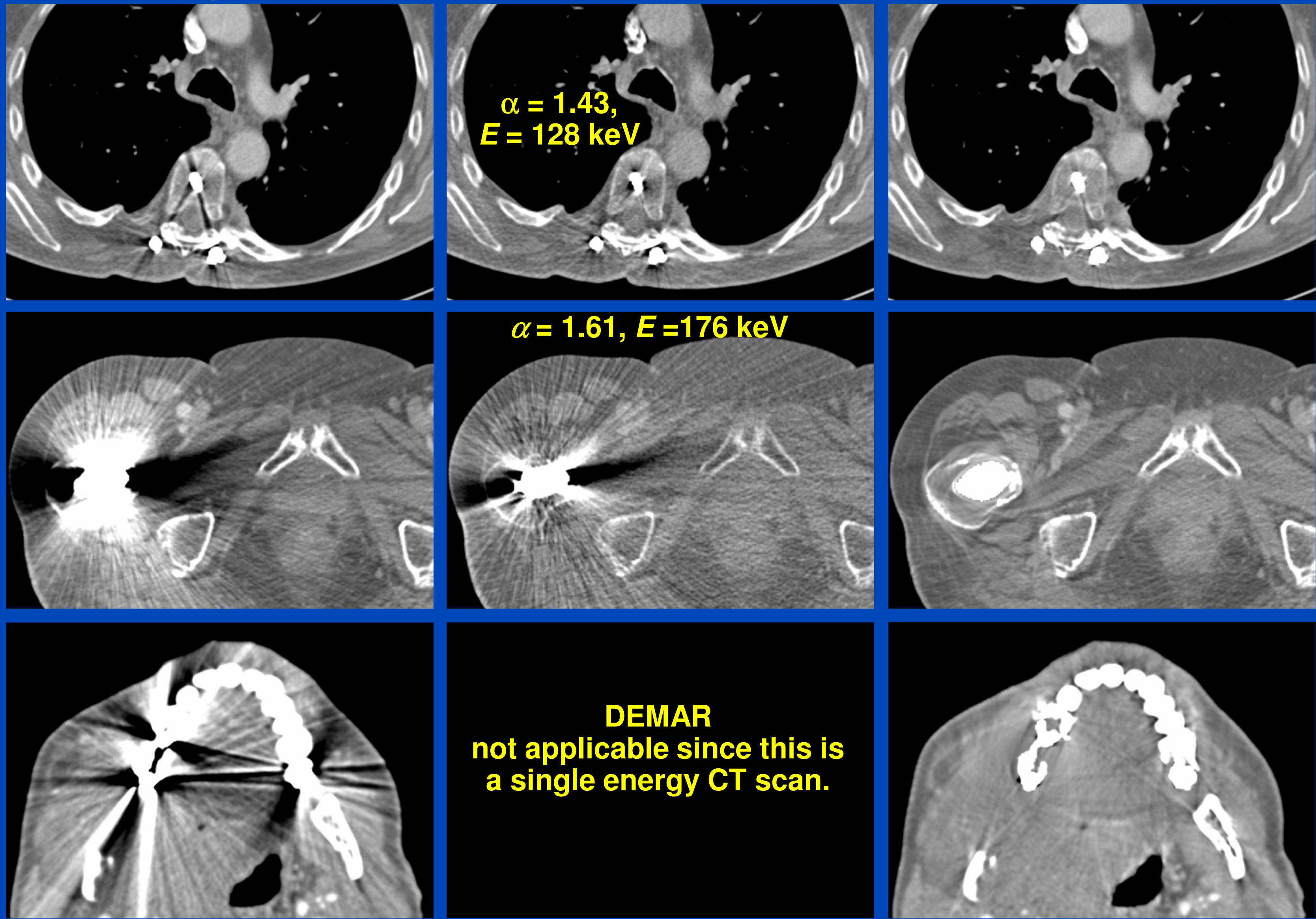

[1]Iterative metal artifact reduction (IMAR) is the Siemens product implementation of FSNMAR.

Conclusion

- Pseudo monochromatic imaging
  - cannot completely remove metal artifacts,
  - can sometimes reduce metal artifacts,
  - reduces CNR if used for metal artifact reduction.
- Rawdata-based methods should be preferred.
- The additional information available in DECT should be used for spectral imaging rather than for artifact reduction.

Image-Based DECT: Beyond Pseudo-Monochromatic Imaging?

- Pseudo monochromatic images may be used to reduce BH and metal artifacts. But there is only one pseudo monochromatic energy that minimizes the beam hardening and scatter artifacts.
- At this energy, the CNRD is low.
- Aim: find an image-based approach that yields high CNRD and low artifacts.

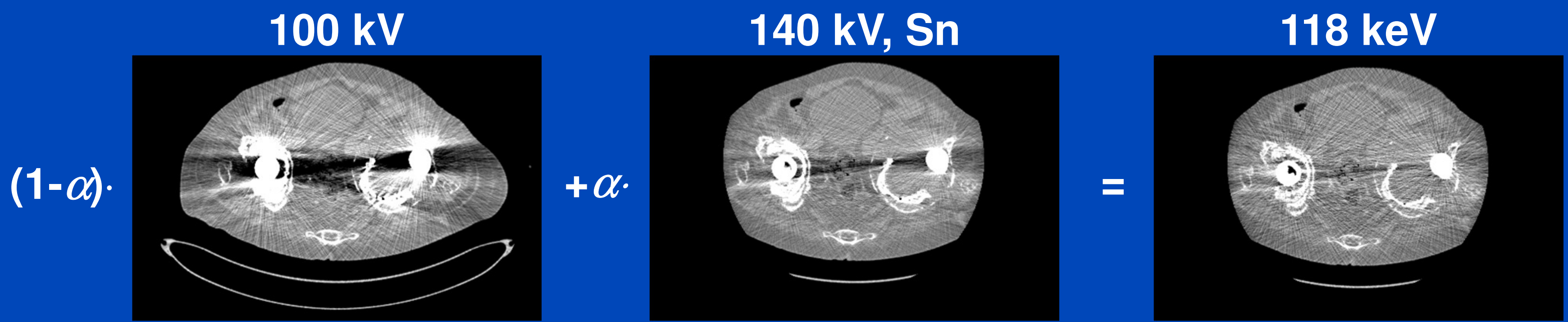

$$(1-\alpha)\cdot f_{\mathrm{Lo}} + \alpha \cdot f_{\mathrm{Hi}} = f_{\mathrm{Pseudo}}(\alpha)$$

EDEBHC

- Extend the simple α-blending by higher order terms:

$$f_{\text{EDEBHC}}(\boldsymbol{r}) = (1-\alpha)f_{10}(\boldsymbol{r}) + \alpha f_{01}(\boldsymbol{r}) + \sum_{ij} c_{\alpha ij} f_{ij}(\boldsymbol{r})$$

  with the basis images

$$f_{ij} = X^{-1} p_{\text{Lo}}^i p_{\text{Hi}}^j$$

  being the reconstruction of rawdata monomials.
- For a given value of α choose the $c_{\alpha ij}$ to minimize the artifact content in the resulting EDEBHC image.
- The α-value is constant during optimization and defines the desired contrast situation.

EDEBHC Cost Function

- **Artifacts in general, and beam hardening and scatter artifacts in particular, broaden the histogram peaks and thus increase the entropy of the image.**

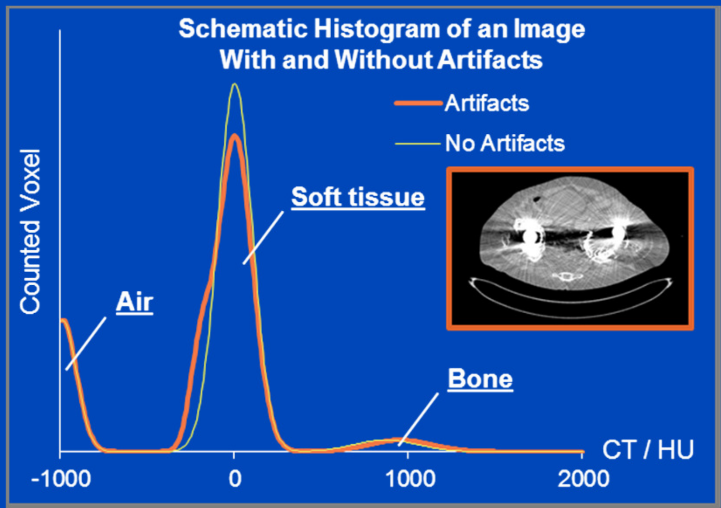

- **Thus, the image entropy *H***

$$H(f) = -\sum_b h_b(f) \ln h_b(f)$$

can be used as the EDEBHC cost function:

$$\boldsymbol{c}_\alpha = \arg\min_{\boldsymbol{c}} H\Big((1-\alpha) f_{10} + \alpha f_{01} + \sum_{ij} c_{ij} f_{ij}\Big)$$

EDEBHC Basis Images

Patient Measurement on a Siemens Definition Flash CT System

$$f_{ij} = X^{-1} p_{\mathrm{Lo}}^{i} p_{\mathrm{Hi}}^{j}$$

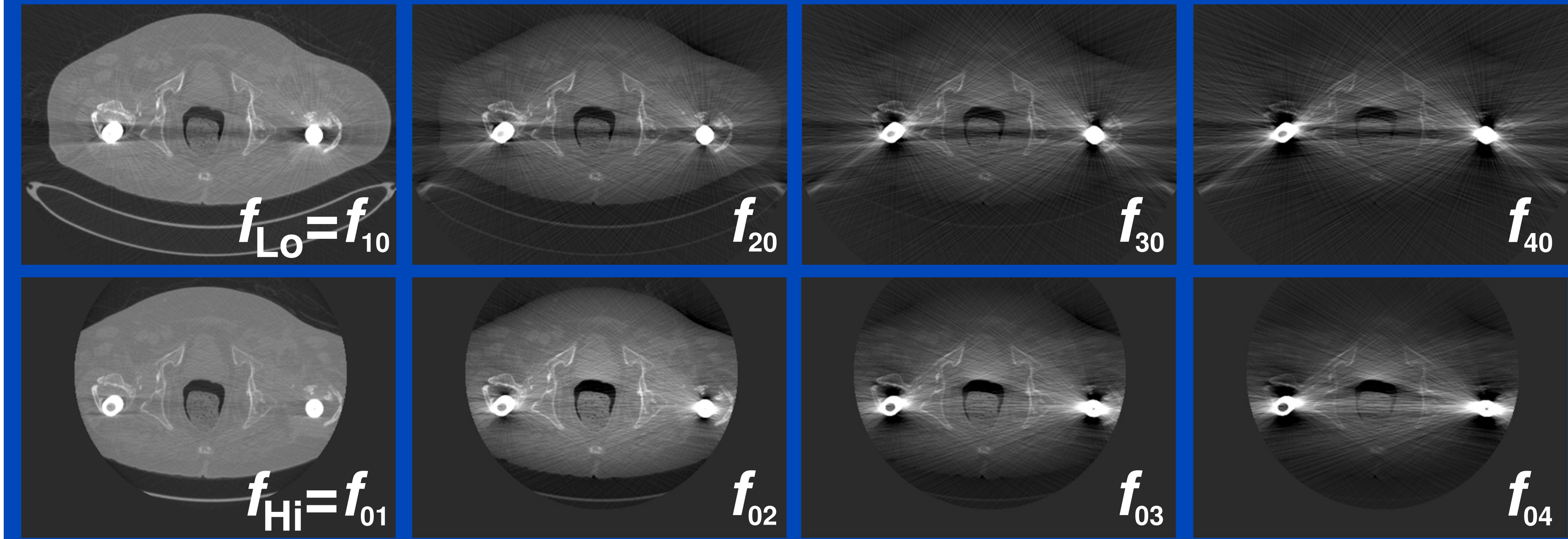

Only basis images without mixed terms are shown here.

C = 0 HU, W = 3000 HU

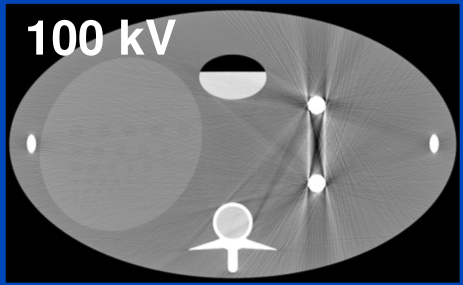

EDEBHC Results

Simulation of an Abdomen Phantom

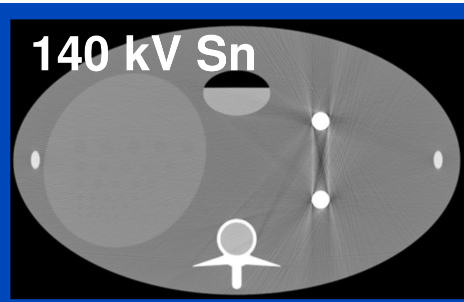

Pseudo-monochromatic Image
α = 1.6, CNR = 5.84

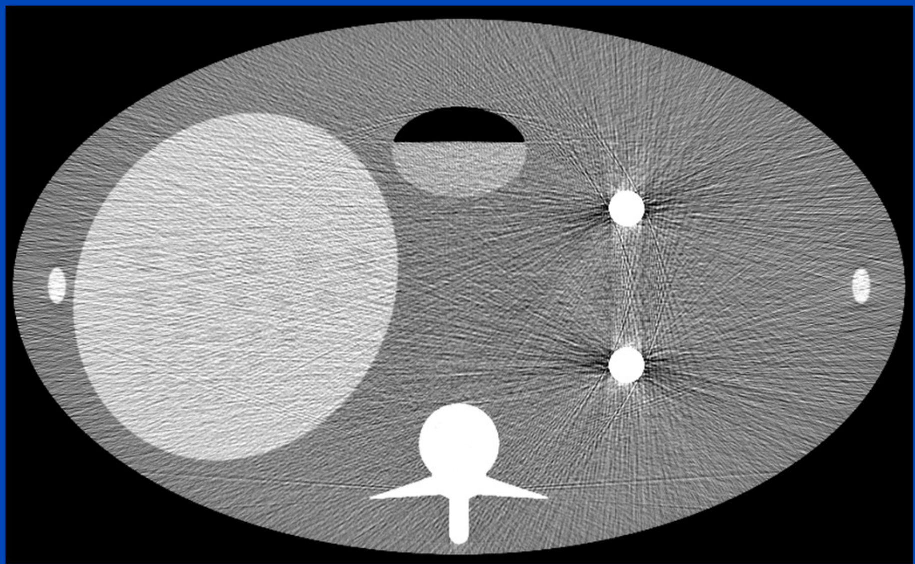

$$f_{\mathrm{Pseudo}}(\alpha) = (1-\alpha) f_{10} + \alpha f_{01}$$

EDEBHC Image
α = 1.6, CNR = 7.58

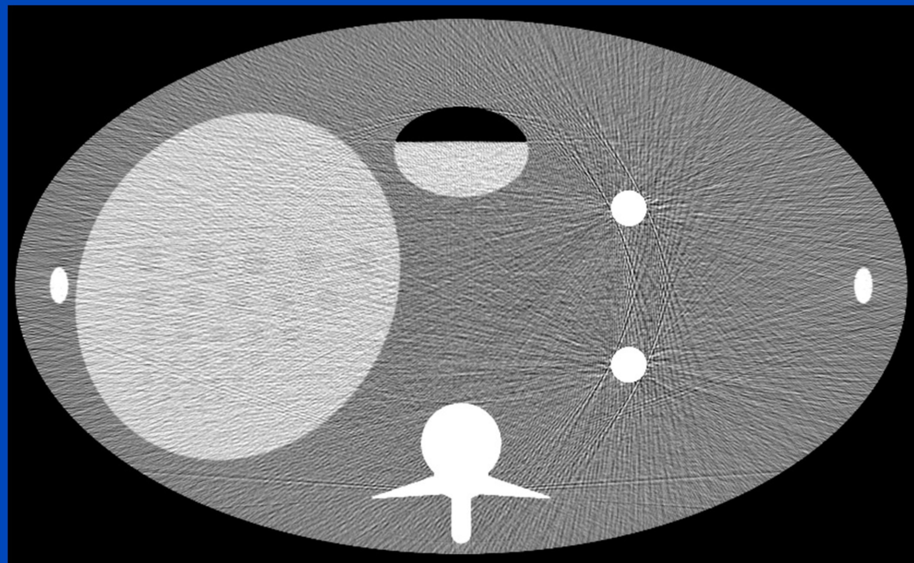

$$\begin{aligned} f_{\mathrm{EDEBHC}}(\alpha) &= (1-\alpha) f_{10} + \alpha f_{01} \\ &+ c_{20} f_{20} + c_{02} f_{02} + c_{30} f_{30} \\ &+ c_{03} f_{03} + c_{40} f_{40} + c_{04} f_{04} \end{aligned}$$

C **= 0 HU,** ***W*** **= 200 HU**

dkfz.

EDEBHC Results

Patient Measurement

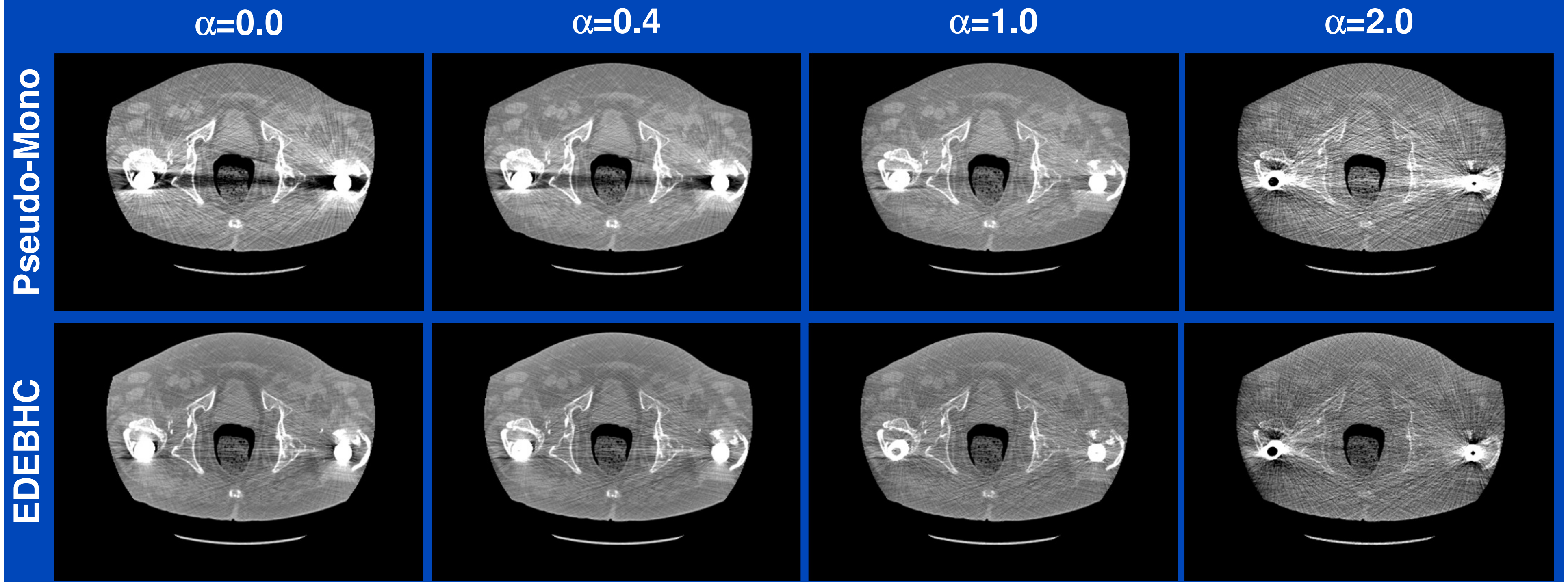

C = 0 HU; W = 1000 HU

dkfz.

Conclusion

- EDEBHC provides images with reduced beam hardening for an infinite number of contrast situations.
- Because EDEBHC uses both initial images (f_{Lo} and f_{Hi}) optimal for each chosen α-value, the CNR is increased compared to the same contrast situation in pseudo-monochromatic imaging.

Thank You!

The 4th International Conference on

Image Formation in X-Ray Computed Tomography

July 18 – July 22, 2016, Bamberg, Germany

www.ct-meeting.org

Conference Chair

Marc Kachelrieß, German Cancer Research Center (DKFZ), Heidelberg, Germany

This presentation will soon be available at www.dkfz.de/ct.
Parts of the reconstruction software were provided by RayConStruct® GmbH, Nürnberg, Germany.